Severe Autumn storms in Future Western Europe with a Warmer Atlantic Ocean

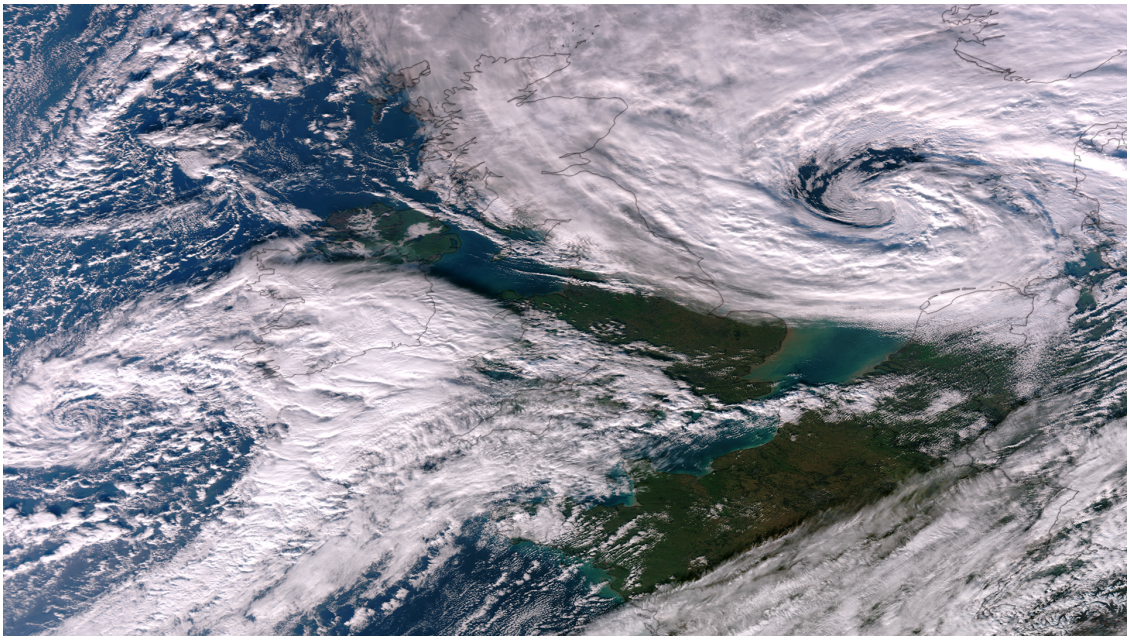

Michiel Baatsen

Supervisors
Reindert J. Haarsma (KNMI)
Aarnout J. van Delden (IMAU, UU)

KNMI - Utrecht University

Koninklijk Nederlands
Meteorologisch Instituut
Ministerie van Infrastructuur en Milieu

Abstract

Simulations with a very high resolution (∼25km) global climate model indicate that severe Autumn storms will impact Europe more often in a warmer future climate. The increase is mainly attributed to storms with a tropical origin, especially in the later part of the 21st century. As their genesis region expands and warms, tropical cyclones become more intense and have a higher chance of reaching Europe. This study focuses on the properties and evolution of such storms to clarify the occurring changes.

The studied tropical cyclones show a typical evolution of tropical development, extratropical transition and a final re-intensification. A reduction of the transit area separating the regions of baroclinic and tropical development allows more storms to cross and redevelop into powerful extratropical cyclones. Many of these modelled storms feature hybrid properties during a considerable part of their life cycle, exhibiting the hazards of both tropical and extratropical systems. In addition to tropical cyclones, cold core extratropical storms and tropical disturbances mainly originating over the Gulf Stream region also increasingly impact Western Europe. Despite of their different history, all of the studied storms have a striking similarity: the formation of a warm seclusion. Although their occurrence is rare in the studied region, observations confirm that the strongest Autumn storms in the present climate are indeed warm seclusion cyclones. Damaging winds associated with the occurrence of a sting jet are observed in a large portion of the storms. Baroclinic instability is of great importance during the re-intensification as is the presence of an atmospheric river. The latter provides the core with warm and most air that aids the intensification through latent heat release. Atmospheric rivers will considerably increase in strength towards the future, as will the associated flooding risks.

Acknowledgements

Before moving on, I would like to thank the KNMI for providing me with the opportunity to spend 8 months among them as part of my master's degree in meteorology. Their high quality data and skilled people enabled me to obtain some fascinating results but also to challenge myself and become a better scientist. Research is a shared effort and several people in particular should be accredited for their help. Primarily I want to mention Dr. Reindert J. Haarsma of the KNMI who has been my daily supervisor. Not only did he come up with the topic of this study, he also helped me a great deal getting to know the data and software and spent countless hours revising preliminary results and paving the way forward. Secondly, I should thank Dr. Aarnout J. van Delden of IMAU, Utrecht University of being my supervisor and helping me with a lot of practical matters. His knowledge and enthusiasm were a great addition and led to many good ideas which proved to be vital at times. Finally, Dr. Hylke de Vries also spent a lot of time helping me to succeed, especially with programming and visualising the results for which he has my sincere gratitude.

Maybe not mentioned as specifically but certainly not less important are the people surrounding you during the process. Most importantly I would like to thank Annelies Jonker for being there whenever I needed it and hearing my often too enthusiastic and endless talks. Additionally I want to mention my colleagues at the KNMI and fellow students for their feedback and critical view which is very important to improve the results. The great atmosphere and understanding at the KNMI also added significantly to my ability to successfully finish my thesis. Finally, the help and understanding of my parents was also critical, especially by enabling me to study meteorology which is and always will be my true passion.

Contents

Chapter 1

Introduction

Wind storms are a major weather hazard in Western Europe, capable of causing widespread damage and flooding (*Dorland et al.*, 1999). Currently, most of these storms occur during the winter season and it is important to assess possible changes in a future, warmer climate (*Schwierz et al.*, 2009). In general, global climate simulations predict a larger warming at the poles which reduces the meridional temperature gradient and thus the baroclinic instability which causes typical winter storms to form (*Gitelman et al.*, 1997). However, an increase in tropopause height and latent heat release related to the warming atmosphere tends to intensify storms (*Lorentz and De Weaver*, 2007). Both effects counteract each other and will probably result in a nearly unchanged number and frequency of mid-latitude storms (*Lambert and Fyfe*, 2006; *Bengtsson et al.*, 2006, 2009; *Leckebusch and Ulbrich*, 2004; *Loptien et al.*, 2008; *Ulbrich et al.*, 2008).

Occasionally, tropical cyclones reach the mid-latitudes and re-intensify into powerful storms after transitioning into an extratropical system (Figure 1.1), such as Hurricane Irene of 1999 (*Agusti-Panareda et al.*, 2004). Since their genesis region expands as sea surface temperatures (SSTs) rise, these storms may impact Western Europe more frequently in the future. Especially the eastward expansion of the Atlantic warm pool causes tropical storms to form further to the east making it more likely for them to curve towards Europe in the mid-latitude westerlies. Before, global climate models have been unable to adequately reproduce these small scale tropical cyclones making it impossible to validate the assumptions above. Now, using EC-Earth (*Hazeleger*, 2010) at a very high resolution (25km), future changes in storminess over western Europe can be studied with the influences of tropical cyclones taken into account. As it was pointed out in a recent research (*Haarsma et al.*, 2013), the most significant changes take place in Autumn so the focus of this research will lie on the months August through November.

First, the model will be presented briefly and its set-up for both present and future weather simulations. To get an impression of the model performance, a case study of one specific storm is treated which also serves as an example of a severe future storm impacting Europe. The aim is to get a better understanding of the processes that govern the evolution of the studied cyclones, their characteristics and possible impacts throughout the 21st century. Therefore, a climatology is made with information about their tracks, intensity and general properties such as the thermal nature of the core. In addition, mean fields of all of the storms are studied to get more insight in their overall structure. Finally, the evolution is looked at in more detail with special focus on the different forcings that are at work during a possible re-intensification at the end of a storm's life cycle.

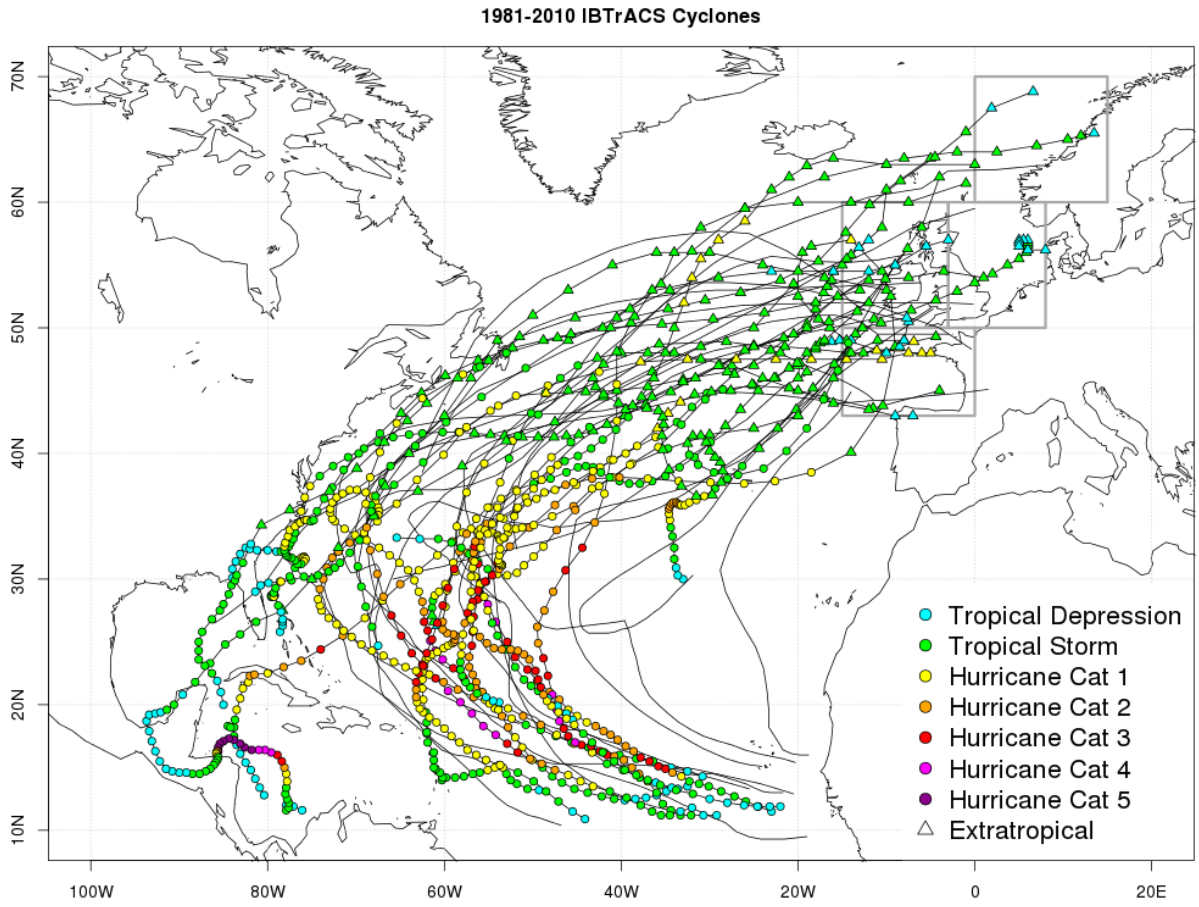

Figure 1.1: Storm tracks using the IBTrACS database (http://www.ncdc.noaa.gov/ibtracs/index.php) and only selecting the storms that reach Western Europe (specific regions are further specified below and indicated by the gray boxes). Tracks represented just by black lines depict storms occurring before 1981.

Chapter 2

Model and experimental set-up

For this study, only the atmospheric component of EC-Earth is run with forced SSTs at a resolution of T799 L91 which was used for the operational model predictions at ECMWF from February 2006 until January 2010. Three sets of simulations are performed representing the present (2002-2006), near future (2030-2034) and future (2094-2098) climate. For each period, a 10 year spin-up was created at a low resolution (T159) preceding a full resolution 9 month period. By taking the first six days of October as initial conditions, a six member ensemble was generated for the three different periods resulting into data sets representing 30 years each. For the present, daily SSTs from NASA observations were used of the respective period which are available at a resolution of 0.25°(http://www.ncdc.noaa.gov/oa/climate/research/sst/oi-daily.php). For both other periods, SSTs were estimated by adding the predicted (low resolution) change to (high resolution) observations. The applied changes are taken from the ensemble mean calculated in the ESSENCE project (*Sterl et al.*, 2008) using the ECHAM5/MPI-OM model with the A1B scenario which is compatible with the RCP4.5 scenario (*van Vuuren* (2011), Figure 2.1). Finally, observed concentrations of greenhouse gases and aerosols where used for the present simulations while those derived from the RCP4.5 were applied for the other periods.

To detect severe wind storms impacting Western European coastal regions, a certain wind criterion was applied to four different areas. These cover of the Gulf of Biscay (40°N-50°N, 0°W-15°W), Norway (60°N-70°N, 0°E-15°E), the North Sea (50°N-60°N, 3°W-8°E) and western UK (50°N-60°N, 3°W-15°W), respectively. Whenever the 3-hourly averaged 10m wind speed exceeds Beaufort 11 (28.4 m/s) a severe wind event is registered. Subsequently, the events are linked to nearby cyclones which are tracked back in time as long as 10m wind speeds exceed the tropical depression threshold (13.9 m/s). This results in a set of storms for each period that will be examined and compared to detect possible changes.

The total amount of data generated in the simulations is quite vast; 90 years, 3-hourly at high resolution. For this data set, only five pressure levels are extracted from the original output and stored at 6 hour intervals: 850, 700, 500, 300 and 200hPa. In addition, surface fields and fluxes are stored 3-hourly at full horizontal resolution (the latter also holds for the 6-hourly data). For one specific storm, all data is stored to allow for a thorough investigation of its properties.

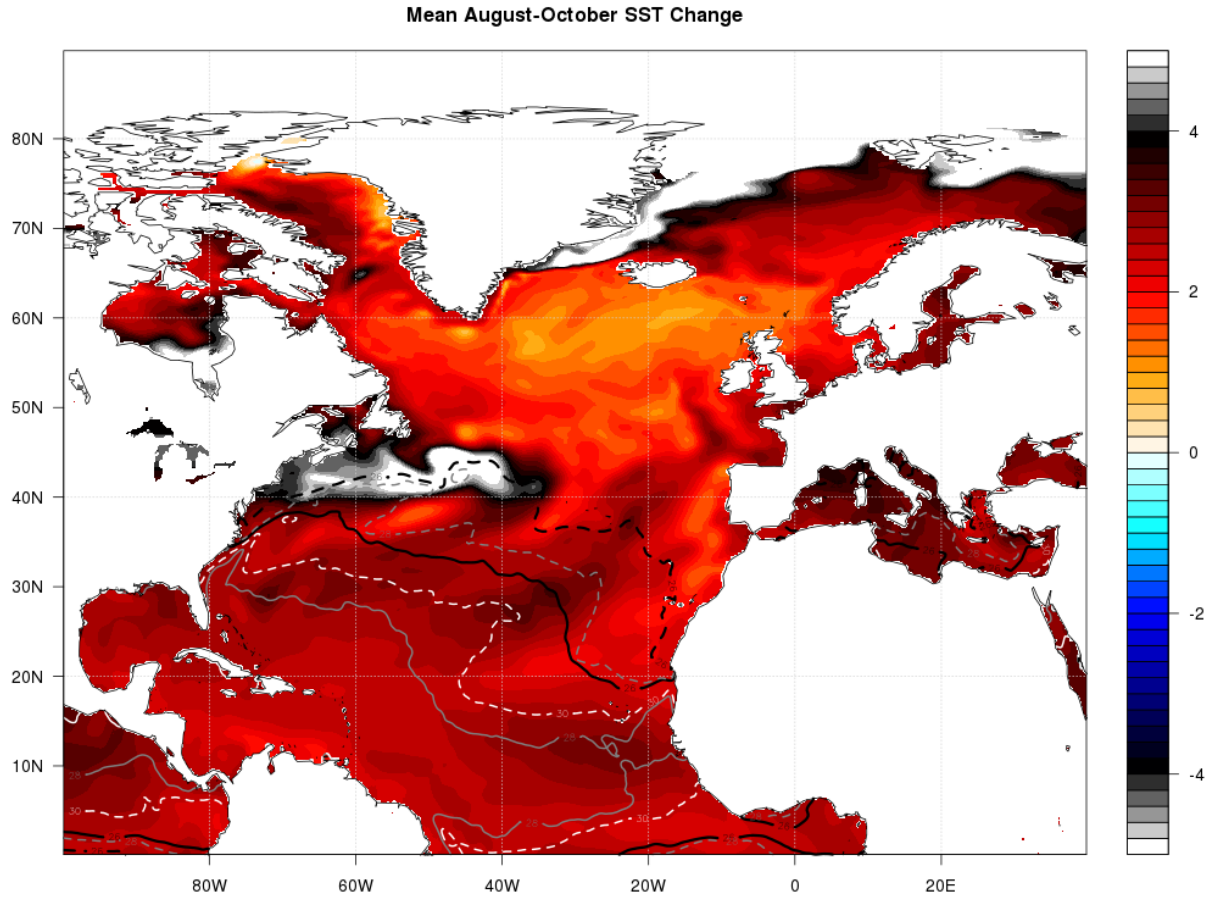

Figure 2.1: Predicted SST changes (°C, shading) between the present and future climate. Contours indicate the respective August-October mean SST fields in the present (solid) and future (dashed). In black is the 26°C isotherm whereas gray represents that of 28°C and white shows the one at 30°C.

Chapter 3

Case study: Storm Amy

To gain insight in the quality of the model output and study the properties of a specific storm in more detail, the data at full vertical and horizontal resolution of a future cyclone are considered. This is achieved by repeating the calculations for a specific period while conserving all of the generated data. A simulated storm called Amy was chosen which would impact the North Sea region on 7 October 2097. The selected period includes the first 15 days of October; time indications are expressed in hours starting at 0:00 UTC on 1 October 2097.

3.1 Life cycle

Amy is a classical example of how future tropical cyclones can impact Western Europe. The system emerges as a tropical wave off the East African coast and intensifies into a tropical storm over the Atlantic Ocean. The storm steadily strengthens over warm SST's and reaches its peak intensity after about 4 days (96h, Figure 3.1). Shortly after, the cyclone crosses the critical 26°C isotherm impeding the support of its tropical characteristics. Indeed, a weakening is observed during the fifth and sixth day suggesting that the storm undergoes extratropical transition (ETT). At first, only the maximum wind speeds decrease but then also the central pressure starts to rise. This phase is followed by a short but fierce re-intensification resulting in wind speeds well over hurricane force and a central MSLP below that of the previous minimum (before ETT). When comparing the SST values to those in the present (Figure 2.1), it is clear that global warming plays a significant role in the history of this cyclone. While surface waters are a warm 28-29°C in the future case, they are only marginally favourable for tropical development in the present situation.

A closer look into the surrounding weather pattern is needed to explain the observed path and intensity changes of Amy. Therefore, a composite of MSLP, wind speed, geopotential height, energy fluxes, total column water vapour and 850hPa equivalent potential temperature (EPT) is generated for t = 78h (Figure 3.2), 126h (Figure 3.3), 144h (Figure 3.4) and 162h (Figure 3.5) marking some distinct phases in the storm's evolution. Wind speed and MSLP are indicative for the general circulation pattern and are useful to discern extratropical from tropical cyclones as the latter are much smaller in size. Additionally, geopotential heights at 500hPa and 300hPa show the tilted structure of extratropical cyclones (the upper level trough lies west of the surface low) and the jet stream location as a tight gradient (mainly at 300hPa). Furthermore, heat fluxes (determined by the sum of the latent heat flux (LHF) and sensible heat flux (SHF) at the surface upwards) are important for cyclones and reveal relatively warm

and cold areas as well as energy sources. Finally, water vapour but especially EPT depict the presence of warm and moist tropical air (high EPT) in contrast to cold and dry arctic air (low EPT). Here, EPT (θ_e) is calculated as (*Bolton*, 1980):

$$\theta_e = T \left(\frac{p_{ref}}{p} \right)^{\kappa} \exp \left(\frac{L_v r_s}{c_p T} \right), \tag{3.1}$$

where T is the temperature in K, p_{ref} is a reference pressure (usually 1000hPa), p is the actual pressure in hPa, $\kappa = R/c_p$ with R the universal gas constant (8.314 J/molK) and c_p the heat capacity of dry air (taken to be 1005 J/kgK), L_v is the latent heat of evaporation of water ($2.5 \cdot 10^6$ J/kg) and r_s is the saturation mixing ratio (kg/kg).

3.1.1 Tropical phase

The first snapshot (Figure 3.2) shows Amy as an intense tropical cyclone over the northern Atlantic Ocean. The weather pattern in Europe is dominated by a vast low pressure area located over southern Scandinavia. The warm sector of this extratropical cyclone is well indicated by the region of higher EPT stretching from Spain to Finland and carrying warm, moist air to high latitudes. The warm sector is marked by a cold front to its west, accompanied by lower EPT and a shift in wind direction. Cold, polar air behind the front flows over the North Sea which is relatively warm, resulting in large upward latent heat fluxes. The difference in size between the tropical and extratropical cyclone can be seen in the wind field as the latter has an expansive area of high wind speeds located away from its centre. The tropical cyclone can be further distinguished by its warm core which is depicted by the high EPT and symmetrical latent heat fluxes supporting the associated deep convection. Bands of high EPT air wrap into the centre of the cyclone and help to sustain its warm core. Generally, the EPT reveals tight flows and distinct interfaces between different air types. This can only be reproduced by high resolution models and is consistent with the concept of atmospheric rivers described in *Zhu and Newell* (1998). The location of the jet stream is revealed by a tight gradient in 300hPa geopotential height around 50°N. Furthermore, a local amplification called a jet streak is present over Western Europe where the gradient is stronger. The expansive low pressure area is located at the left exit region of this feature which is supportive for cyclogenesis (*Newton*, 1954). Finally, a baroclinically unstable wave is present near the coast of Greenland, characterised by a strong tilt with height i.e. the pressure minimum at the surface lies downstream of the trough at 500hPa (*Hoskins et al.*, 1997). This is not the case for the Scandinavian cyclone as it is a mature system that has lost its tilt during its evolution (*Hoskins*, 1990).

3.1.2 Extratropical transition

Two days later at t = 126h (Figure 3.3), Amy has moved to a region of high wind shear (underneath the jet stream) and lower SSTs. The system is undergoing extratropical transition (ETT), characterised by some profound structural changes (*Jones*, 2003). The wind pattern has become asymmetrical, less intense and is characterised by two frontal regions. Sharp transitions in wind speed can be identified south-west and north-east of the centre, located at roughly (45°N, 20°W). The latter is also well visible in the EPT pattern and marks a warm front ahead of the cyclone, separating the remnant warm core from the polar air it is moving into. The other structure is a cold front marking the western boundary of an atmospheric river accompanying the storm. Polar air is not only present to the north but has also started to wrap around the centre as being indicated by the asymmetric structure of the energy fluxes. In general, during ETT the cyclone expands in size while becoming asymmetric and less intense. The

baroclinically unstable wave formerly located near Greenland has travelled south-east and now lies close to Ireland. It has developed into an extratropical cyclone with a closed circulation and is located at the left exit region of another jet streak, exhibiting a strongly tilted structure. The newly formed extratropical cyclone has an EPT signature that is consistent with the one described by the Norwegian model (*Bjerknes*, 1919; *Bjerknes and Solberg*, 1922). The warm sector is located south-east of the centre and has a reversed V-shape. A small curl is present to its north marking the presence of an occluded front where the cold front has overtaken the warm front to its east. This is also the region where locally the highest surface wind speeds occur.

3.1.3 Merging

About 12 hours after the situation described above, Amy completes its ETT and reaches a relative minimum in intensity (Figure 3.1b). At the same time, it starts to merge with the developing extratropical cyclone located to its north of which the situation is shown another 6 hours later (Figure 3.4). The remnant warm core of the formerly tropical cyclone becomes incorporated in the warm sector of the other cyclone, of which the cold core is located just north of Ireland. Associated with the latter is an occluded front which is still generating a strong wind field to the west. Again clearly visible in the EPT pattern are a warm front north of the cyclone and a cold front to the south-west as well as an atmospheric river of tropical air. The latter is part of a vast warm sector over the European mainland while cold air flows south over the Atlantic Ocean, associated with large latent heat fluxes. At this point, all of the ingredients for explosive cyclogenesis are present: a strong EPT gradient, a baroclinically unstable wave and the left exit region of a jet streak.

3.1.4 Re-intensification

Following the merging of both cyclones is a quick re-intensification during which the central pressure drops 20 hPa in 15 hours. The maximum intensity is reached at t = 156h, with a central pressure of 939 hPa, but the situation 6 hours later is more interesting to look at (Figure 3.5). At the final stage of its evolution, Amy is a large and powerful extratropical storm. The highest wind speeds are present just south of its centre accompanied by a sharp pressure gradient and strong latent heat fluxes over the north sea. The 500 and 300hPa geopotential heights indicate that the storm is still located at the left exit region of a jet streak but has lost its tilt, in resemblance to the extratropical cyclone in Figure 3.2. There is, however, a major difference between both storms: a region of (potentially) warmer air is present in the centre of Amy. The structure of this storm is consistent with that of a warm seclusion as described by *Shapiro and Keyser* (1990). Instead of having an occluded front (which was present but has dissipated), the cold front moves perpendicular to the warm front (frontal breaking). The latter subsequently wraps around the centre to form a back-bent front while isolating a region of warm air that makes up the warm seclusion (Figure 3.6). These storms generally form as cold core systems in which cold air quickly encircles a portion of warmer air from the warm conveyor belt. In this case, latent heat release in the core helps the intensification similar to how it does in the warm core of a tropical cyclone. Meanwhile, the storm is still extratropical in nature and intensifies through baroclinic processes. Consequently, warm seclusion cyclones can deepen at an extraordinary rate and are among the strongest cyclones that are observed on earth (*Maue*, 2010).

3.2 Sting jet

Warm seclusion cyclones differ from typical other extratropical cyclones through the presence of a shallow warm core. Not only do they possess an expansive wind field typical for extratropical storms but also a smaller area of strong winds that is located close to the centre. This secondary wind field is associated with the strong pressure gradient marking the warm core. In addition, the generally eastward motion of these storms generates an isallobaric wind component which further increases wind speeds mainly south of the centre. An example of an intense warm seclusion cyclone is given in Figure 3.7, showing a hindcast using WRF 9km by *Maue* (2010).

While the reasoning above can illustrate the approximate pattern of the wind field brought forth by a warm seclusion storm quite well, very high wind speeds have been measured in such systems (e.g. Great Storm of 1987, *Browning* (2004)) that cannot be explained yet. The formation of a warm seclusion is sometimes accompanied by that of a sting jet (Grønås, 1995). Such a feature develops at the end of the back bent front to the south-east of the centre. Wrapping around the warm core is a flow of cold, stratospheric air with a generally downward movement. This downward movement is enhanced by the secondary, thermally direct circulation around the core which is analogous to that of a tropical cyclone and driven by latent heat release. The air flow around the centre is as such compressed as long as it moves along the back bent front, increasing the wind speed with a maximum at its end (*Baker* (2009), Figure 3.8).

Another effect adding to the wind speed is the presence of a nearby jet streak, which is mostly the case for rapidly deepening extratropical cyclones. Strong upper level flow is then directed north-eastward parallel to the cold front, just east of the centre (from the left bottom to (40°N,170°W) in Figure 3.7). When the set-up is right, horizontal wind can become aligned throughout most of the troposphere and the downward motion can transfer momentum from the jet stream towards the surface. Such a downward extension of the jet stream can be observed in the cyclone that was shown in Figure 3.7 (Figure 3.9). The corresponding EPT fields nicely show the warm core encircled by colder air and the warm sector to the east and south. The sting jet occurs just south of this warm core, in agreement with the theory. Another notable observation is the qualitative difference with the wind field that is present around 170°W associated with the cold front. Although the latter is stronger overall, high winds are not present below 900hPa while they are in the sting jet. This is a good indication of the downward motion which is causing a wind maximum to occur close to the surface.

3.3 Wind field and thermal structure

Previous results suggested that Amy evolves into a warm seclusion cyclone, it is therefore interesting to study its wind field and especially whether a sting jet is present. As they provide a great inside into the structure of the storm, cross sections similar to those shown in Figure 3.9 where made for Amy through the location of minimum MSLP.

The first image (Figure 3.10) again shows Amy as a tropical cyclone (but at t = 84h instead of 78h). The structure of the system exhibits a tight and symmetric warm core with high EPT values surrounded by high wind speeds. The latter are strongest in the eastern part of the storm as they are increased by its northward motion. A decrease with height is observed, which is consistent with the presence of a warm

core through the thermal wind balance ($\frac{\partial u}{\partial z} \sim -\frac{\partial T}{\partial y}; \frac{\partial v}{\partial z} \sim \frac{\partial T}{\partial x}$).

During its extratropical transition, Amy moves underneath the jet stream which is present between 300 and 200hPa (Figure 3.11). Especially the northern part of the wind field is disrupted by the wind shear while the other part expands resulting in an asymmetric picture. Colder polar air approaches the warm core from the north-west, forming the frontal boundary that was seen in Figure 3.3. A peculiar feature in this image is the atmospheric river just east of the centre, having a distinct vertical structure that extends high into the troposphere.

At the end of the ETT, the storm still exhibits some properties of a remnant warm core which is being incorporated into the warm sector of another cyclone. The wind field has become completely asymmetrical and features an increase with height towards a jet streak that is located south-east of the centre (Figure 3.12). The atmospheric river can still be identified as a narrow band of moist air to its east. Polar air has started to wrap around the core forming a warm seclusion and is visible to the south (Figure 3.12c). A cold front is also starting to become visible, marking the northern and western edge of the warm conveyor belt.

After merging with an extratropical cyclone, Amy re-intensifies into a strong warm seclusion storm (Figure 3.13). The warm core is completely surrounded by colder air making the general structure profoundly different to that of an actual tropical cyclone. Similar to the EPT cross section in Figure 3.9, the warm sector is clearly evident to the east of the centre. The only difference is the absence of high wind speeds along the cold front, which is much weaker in this case. Near the centre is once again a narrow vertical wind-free region resembling the eye in Figure 3.10. Furthermore, the wind speed just south of this region clearly decreases with height, suggesting the existence of a shallow warm core. To make a better comparison between the wind field of Amy and that of the warm seclusion storm shown in Figures 3.7 and 3.9, the weather pattern is shown in more detail (Figure 3.14) and another cross section is made 1.25°south of the centre (Figure 3.15).

The weather pattern shows a small region of higher 850hPa EPT values over the North Sea, indicating the location of the shallow warm core. This area is surrounded by a back bent front and nearby high wind speeds to the south where the strongest pressure gradient is present. Further east, another wind speed maximum can be detected in a region with weaker pressure gradients that coincides with the end of the back bent front. This occurs where the horizontal flow becomes vertically aligned which is evident in Figure 3.5. Slightly enhanced wind speeds are also present along the trailing cold front over Western Europe but are much weaker than those near the centre of the storm. Apart from the absence of such high wind speeds associated with the cold front, the vertical structure shown in Figure 3.15 is quite similar to the one of Figure 3.9. The warm core appears to be even stronger in the case of Amy, possibly due to the incorporation of tropical air carried by the tropical cyclone remnants and the associated atmospheric river. High wind speeds are brought down from the jet stream and the generally downward motion in the cold conveyor belt results in a wind maximum close to the surface. The occurrence of such a feature in the results is not straightforward as a hydrostatic model was used in which vertical motion is not solved explicitly.

3.4 Precipitation

To further clarify the structure of Amy and its possible impacts on Western Europe, the associated precipitation is looked at briefly. During the tropical phase (Figure 3.16), large amounts of convective precipitation fall in a relatively small area surrounding the core. Thanks to the high resolution, some of the characteristic rain bands are also visible further away. Over Scandinavia, the large extratropical system is also producing precipitation but far less intensely. When Amy is undergoing ETT (Figure 3.17), an active warm front forms to its north that induces large rainfall amounts. In contrast, the trailing cold front is associated with only minor amounts of rain. Most of the nearby precipitation is in fact caused by slanted upward motion in the warm conveyor belt.

Despite having a weaker appearance in the MSLP pattern, the newly forming extratropical cyclone is also causing considerable amounts of rain, especially where the occlusion is taking place. Although the remnant warm core is rapidly dissipating when both cyclones merge (Figure 3.18), the warm front to the north greatly expands and activates. A newly formed feature is the back bent front that wraps around the warmer air separating it from the former cold core of the extratropical system. The latter can still be identified by a weakening occluded front located to the west that coincides with high wind speeds observed in Figure 3.4a. Large amounts of rain fall near the center of the storm which favours the development of a warm seclusion as the associated latent heat release helps to sustain a shallow warm core.

After re-intensifying (Figure 3.19), the precipitation pattern is dominated by the back bent warm front and the now weakening warm front north of the centre. Some convection is also occurring in the cold air flowing over relatively warm water in the North Sea. Enhanced rainfall can be observed over Scandinavia but this is mainly due to orographic lifting of moist air. When comparing this system to the extratropical cyclone in Figure 3.16, there are some subtle differences. There is no significant precipitation along the cold front but the overall pattern looks more intense. This suggests that the incorporation of a post-tropical cyclone leads to higher precipitation amounts, mainly near the centre of the storm.

As a final addition to this section, the total precipitation during Amy's existence is studied (Figure 3.20). The effects of the cyclone are well represented by a continuous path stretching from its genesis region all the way across Scandinavia. At first, the precipitation path is narrow and intense as a result of the tight tropical cyclone structure. Somewhat surprisingly, the pattern intensifies during ETT due to enhanced convection in the cloud head that marks the end of the warm conveyor belt. This is consistent with the ETT of for instance typhoon Forest of 1989 that was discussed in *Maue* (2010). During this stage, Amy drops over 300mm of rain in less than 24 hours over an area north of the Cape Verde Islands. This shows that precipitation in the warm front is one of the main hazards of transitioning tropical cyclones in mid latitude regions. During ETT, the precipitation pattern gradually weakens but greatly expands and intensifies again when the other cyclone forms and both systems start to merge. The effects of the vast and active warm front as well as the back bent front are clearly visible over the North Sea and the Northern British Isles. Most of the UK receives 50-100mm of rain with local amounts approaching 200mm. Finally, Southern Scandinavia picks up similar amounts of rain with locally even higher peaks in mountainous regions. For this region, however, precipitation from the first storm also makes up a considerable part of the totals. Nevertheless, a major part of Europe receives an amount of rain over several days that would probably result in large scale flooding events leaving soils already saturated at the start of the stormy winter season.

3.5 Potential Vorticity

3.5.1 Definition and calculation

To conclude the chapter on storm Amy, potential vorticity (PV) is considered as a good indication of some important forces acting on the system. Here, the quantity is used as it was defined by Hans Ertel:

$$PV = \frac{1}{\rho}\zeta^a \cdot \nabla\theta, \tag{3.2}$$

where ρ is the air density (kg/m^3), $\zeta^a = \zeta + f = \frac{\partial v}{\partial x} - \frac{\partial u}{\partial y} + f$ with $\zeta = \frac{\partial v}{\partial x} - \frac{\partial u}{\partial y}$ the relative vorticity, $f = \Omega \sin\phi$ the Coriolis parameter, calculated from the inertial frequency Ω (7.292 $\cdot 10^{-5}$ s^{-1}) and the latitude angle ϕ. θ represents potential temperature, calculated as: $\theta = T\left(\frac{p_{ref}}{p}\right)^{\kappa}$, analogous to Equation 3.1 but without the moisture term.

For general atmospheric conditions, horizontal temperature gradients are much smaller than vertical ones and can be neglected resulting in the following simplification:

$$PV = -g(\zeta + f)\frac{\partial\theta}{\partial p}, \tag{3.3}$$

using the hydrostatic balance ($\frac{\partial p}{\partial z} = -\rho g$) to eliminate density while converting the equation to pressure coordinates.

The model data is calculated and stored on hybrid sigma levels that can easily be extrapolated onto pressure levels. The 91 model levels are subsequently converted to 86 equidistant pressure levels between 1000 and 150hPa with a 10hPa interval. The horizontal latitude-longitude grid is adopted from the model without changes for the current analysis. On the resulting discrete 3-dimensional grid, the potential vorticity at each point (i, j, k) is calculated using finite differences:

$$PV_{i,j,k} \cong -g\left(\frac{v_{i+1,j,k} - v_{i-1,j,k}}{\Delta x_{i,j,k}} - \frac{u_{i,j+1,k} - u_{i,j-1,k}}{\Delta y_{i,j,k}} + f_{i,j,k}\right)\frac{\theta_{i,j,k+1} - \theta_{i,j,k-1}}{p_{i,j,k+1} - p_{i,j,k-1}}, \tag{3.4}$$

where:

- $\Delta x_{i,j,k} = \frac{2\pi R_E}{360}\cos\phi_j \cdot (\vartheta_{i+1} - \vartheta_{i-1})$ the zonal distance;
- $\Delta y_{i,j,k} = \frac{2\pi R_E}{360} \cdot (\phi_{j+1} - \phi_{j-1})$ the meridional distance;
- $f_{i,j,k} = 2\Omega\cos\phi_j$,

with $R_E = 6.371 \cdot 10^6$m the Earth's radius, ϕ_j the latitudinal and ϑ_i the longitudinal coordinate of the considered grid point (i, j).

3.5.2 Results

Both horizontal fields and vertical cross sections of PV are made during different stages of Amy's evolution. Horizontal fields are calculated at 250hPa to show the different processes taking place in the vicinity of the polar jet stream. Vertical cross sections are made through the location of minimum pressure as they were earlier on for the wind and EPT in Section 3.3.

Horizontal fields

The first PV field shows Amy as a tropical cyclone in the central Northern Atlantic and the extratropical low pressure system over Scandinavia (3.21). The former has a small and intense structure while the latter is very expansive. Both systems are characterised by high PV values but for a different reason. The small and intense wind field of a TC is accompanied by high relative vorticity (ζ) and PV is generated at lower levels through latent heat release (causing an increase in $-\frac{\partial\theta}{\partial p}$). The extratropical system, on the other hand, is located at a higher latitude thus having a higher planetary vorticity (f) and accompanied by high PV stratospheric air in the cold conveyor belt. The downward motion surrounding the tropical cyclone due to its outflow can also be observed through filaments of higher PV. Further northward, the jet stream is present and accompanied by a downward fold of the tropopause to its north which is again marked by higher PV values.

The ETT of Amy is accompanied by the interaction with a PV filament to its west from a southern branch of the jet stream (Figure 3.22). A dip in the tropopause can be seen as a filament of high PV to the south-west associated with the trailing cold front. This shape is characteristic of an LC1 cyclone as described in *Shapiro* (1999), in contrast to the occluded cyclone over Scandinavia which is of the LC2 type (resembling the one described by the Norwegian model). A trough in the jet stream pattern was already present earlier on just east of Greenland but it is now accompanied by a new jet streak and amplifying. This is probably due to the outflow of the transitioning TC which tends to stretch the vorticity pattern in the meridional while contracting it in the zonal direction. Due to the enhanced meridional gradients, the jet stream accelerates, forming a jet streak or amplifying an existing one. It is therefore no coincidence that the nearby trough intensifies along with the formation of a jet streak and an associated low pressure area. This phenomenon has been described in *Orlanski and Sheldon* (1995) and is referred to as downstream development.

The small filament of PV interacts with Amy and tends to form a smaller version of the dry intrusion pattern seen in the extratropical cyclone in Figure 3.21. This interaction weakens as the filament deteriorates and is replaced by the influence of the large baroclinic wave to the north (Figure 3.23). The air flow around the cyclone is now strongly affecting the jet stream pattern and has caused the jet streak to split up. The northern PV filament is being stretched further by the outflow which takes on the typical shape of a cloud head in a developing cyclone. To the south, a new jet streak is forming that marks the boundary between cold stratospheric air being advected southwards and warm tropical air in the warm conveyor belt. The associated hook in the PV pattern along the trailing cold front is typical for a cyclone as described by the conceptual model of *Shapiro and Keyser* (1990).

Due to its own influence and the interaction with the baroclinic wave to the west, the storm now lies in both the left exit and the right entrance region of a jet streak. This favours its intensification, resulting in a fast development with the warm and cold conveyor belt twisting into each other (Figure 3.24). The two air types are well distinguished by their PV signature related to different origins. At this point, cold stratospheric air is approaching the centre of the cyclone which evolves into a mature, occluded state. The general picture accordingly resembles that of the extratropical cyclone in Figure 3.21 quite well.

Vertical cross sections

In accordance to the wind speed pattern (Figure 3.10), the PV column of Amy has a tight and intense structure which is typical for a tropical cyclone (Figure 3.25). Here, the cross section is drawn at t = 96h (12 hours later) as the PV structure is still solid and the approaching jet stream can already be spotted to the north. As was seen in the horizontal fields (Figures 3.21-3.24), the jet stream is accompanied by a downward fold in the tropopause to its north. The PV column of a TC reaches high into the troposphere (up to 150hPa), hence it could still be detected at 250hPa.

The ETT of a tropical cyclone is characterised by 2 major changes of the vertical PV structure: an overall deterioration, mainly at the upper levels and a tilt with height. Both can be observed in Figure 3.26 and especially the latter is important for the system to become baroclinically unstable and re-intensify. A strong stratospheric intrusion along the jet streak can be observed to the north. This is the descending cold air that is encircling the cyclone's centre in Figure 3.3. To its south, the formation of a new jet streak has begun which was also observed previously (Figure 3.23). This secondary maximum is indicative for the transition of the warm core into a cold core as winds are now partially increasing with height.

The local wind maximum near the surface eventually dissipates marking the completion of the ETT as only the PV core remains (Figure 3.27). In addition to the TC remnants, the developing cold core cyclone can be observed to the north as a strongly tilted but weaker PV column. Both systems are now adjacent to an equally strong jet streak located between 300 and 200hPa. The dry intrusion associated with the large baroclinic wave to the north-west is wrapping around Amy's core which is mainly visible to the west.

Both PV columns merge into one system that intensifies again in this favourable location with respect to the jet streaks (Figure 3.28). The southern jet streak has further strengthened and the dry intrusion has almost fully wrapped around the core. Most notable is the formation of a PV maximum near the surface which is indicating the generation of PV through diabatic heating and the formation of a shallow warm core. The latter is supported by the decreasing winds with height near the centre. Another striking evolution is the renewed upright position of the PV column. Its structure somewhat resembles that of the tropical cyclone in Figure 3.25 but is weaker and does not reach quite as high. This shows that the storm can actually be considered as a shallow warm core system embedded into a large extratropical cyclone.

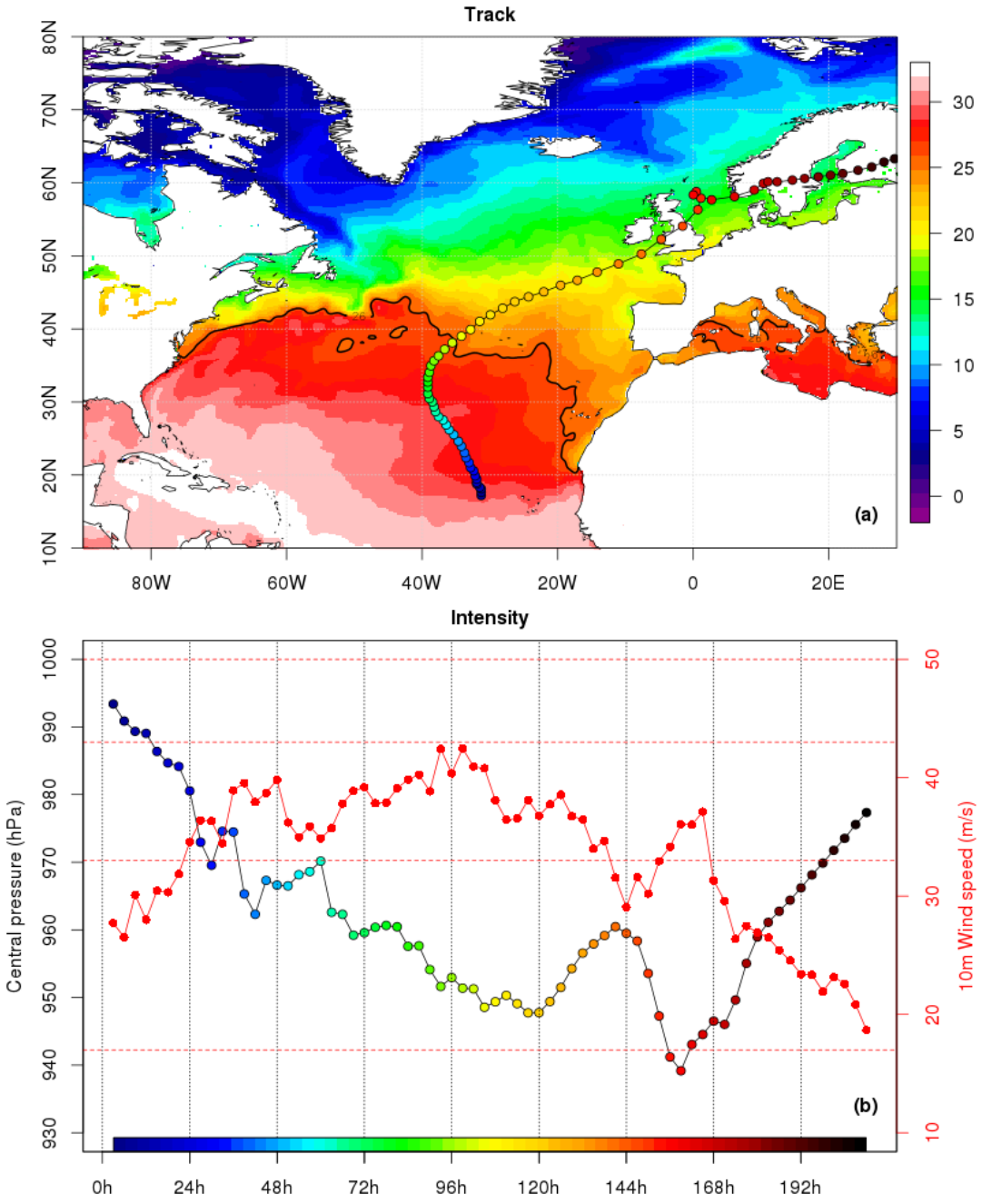

Figure 3.1: Track (a) and Intensity (b) of Amy throughout its life cycle. Background colours in (a) depict the SST (°C) at the time of the storm's occurrence, marker colours indicate time as shown by the colour bar in (b). The lower panel shows minimum MSLP (black, colour filled) and maximum 3-hourly mean 10m wind speed within a 5°radius.

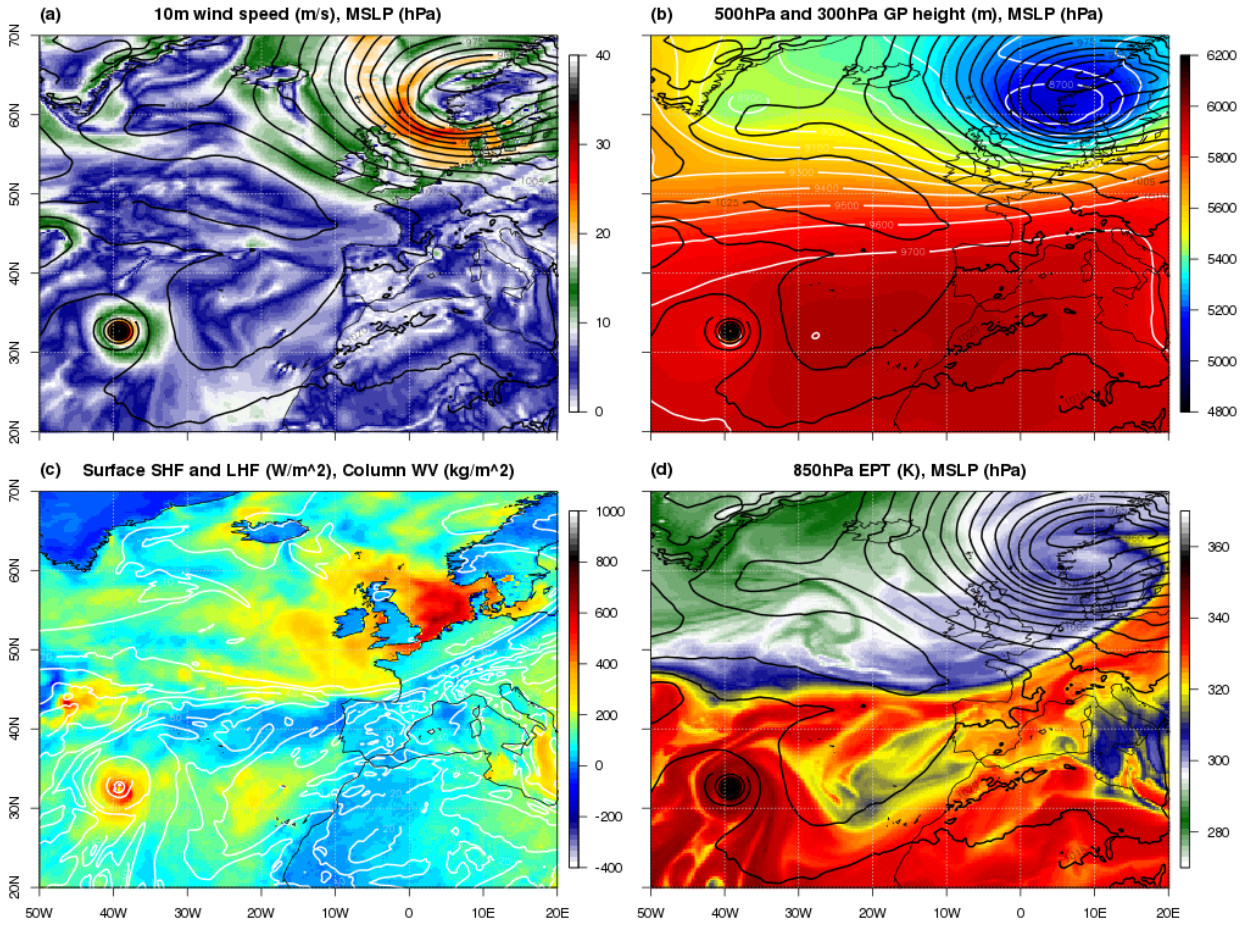

Figure 3.2: Composite illustrating the weather pattern surrounding storm Amy at t = 78h, showing 3-hourly 10m wind speed (a), geopotential height (shading: 500hPa and white: 300hPa, b), heat fluxes (shading) and column water vapour (white contours, c) and equivalent potential temperature (d). All panels except (c) also contain MSLP as black contours.

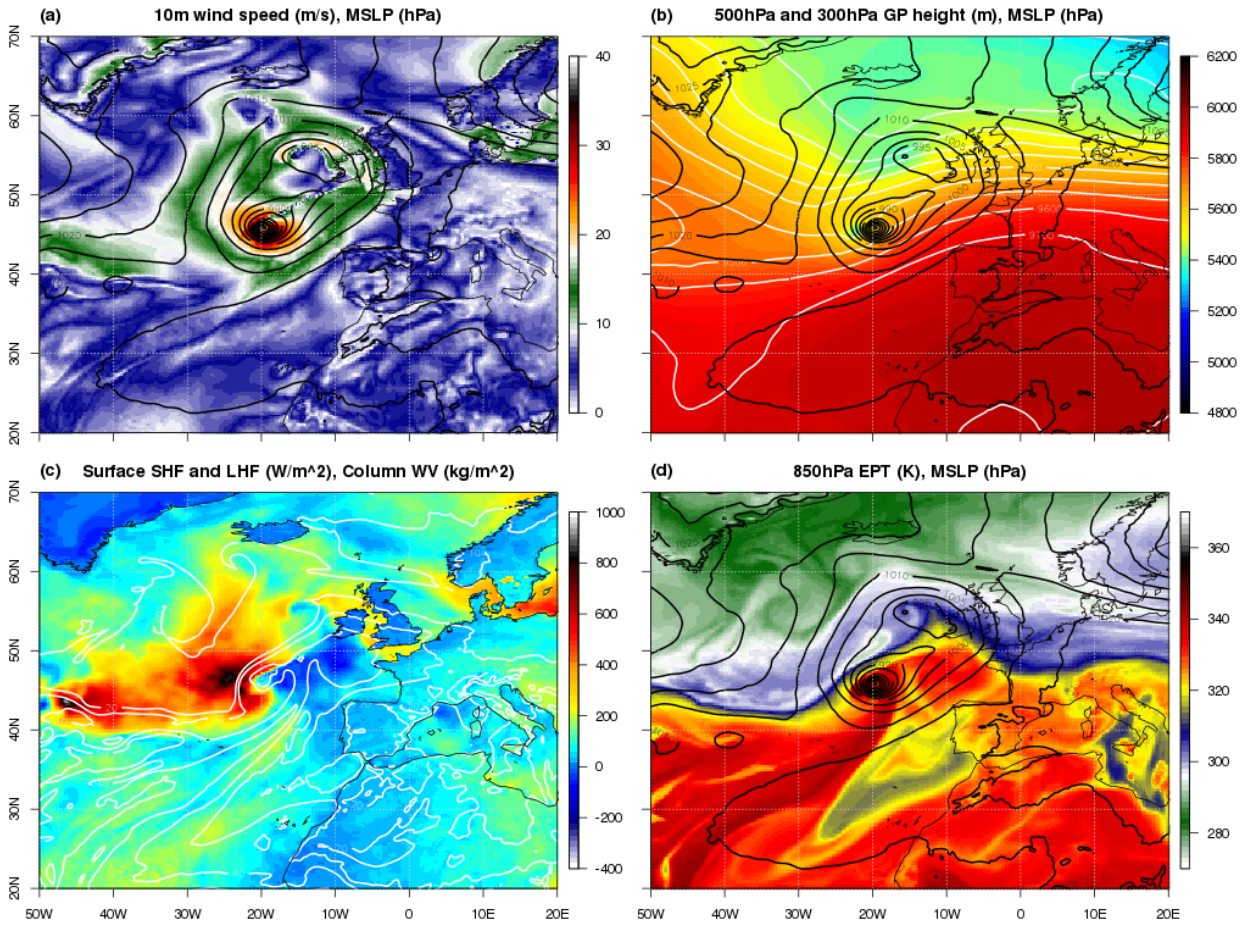

Figure 3.3: Same as in Figure 3.2 but for t = 126h.

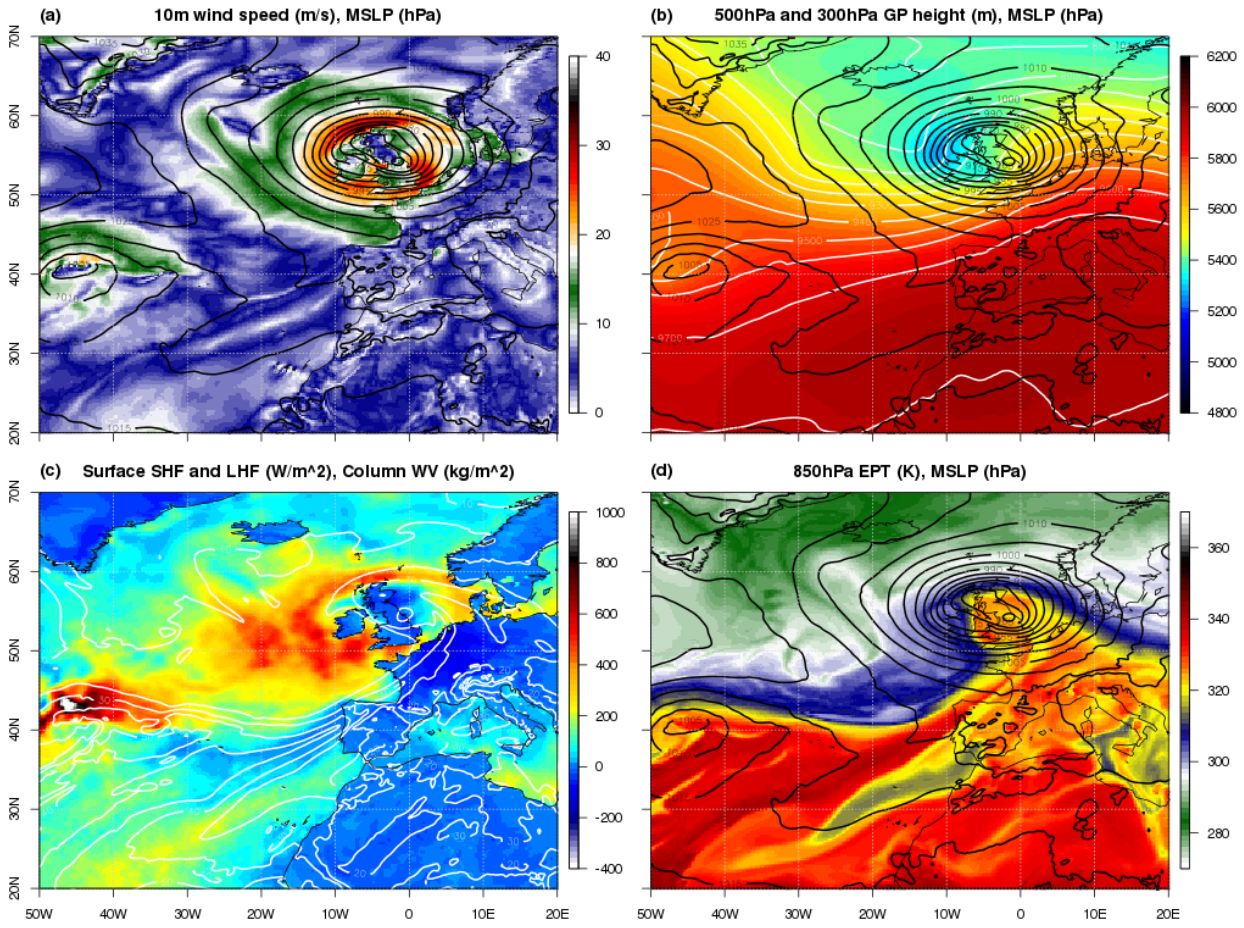

Figure 3.4: Same as in Figure 3.2 but for t = 144h.

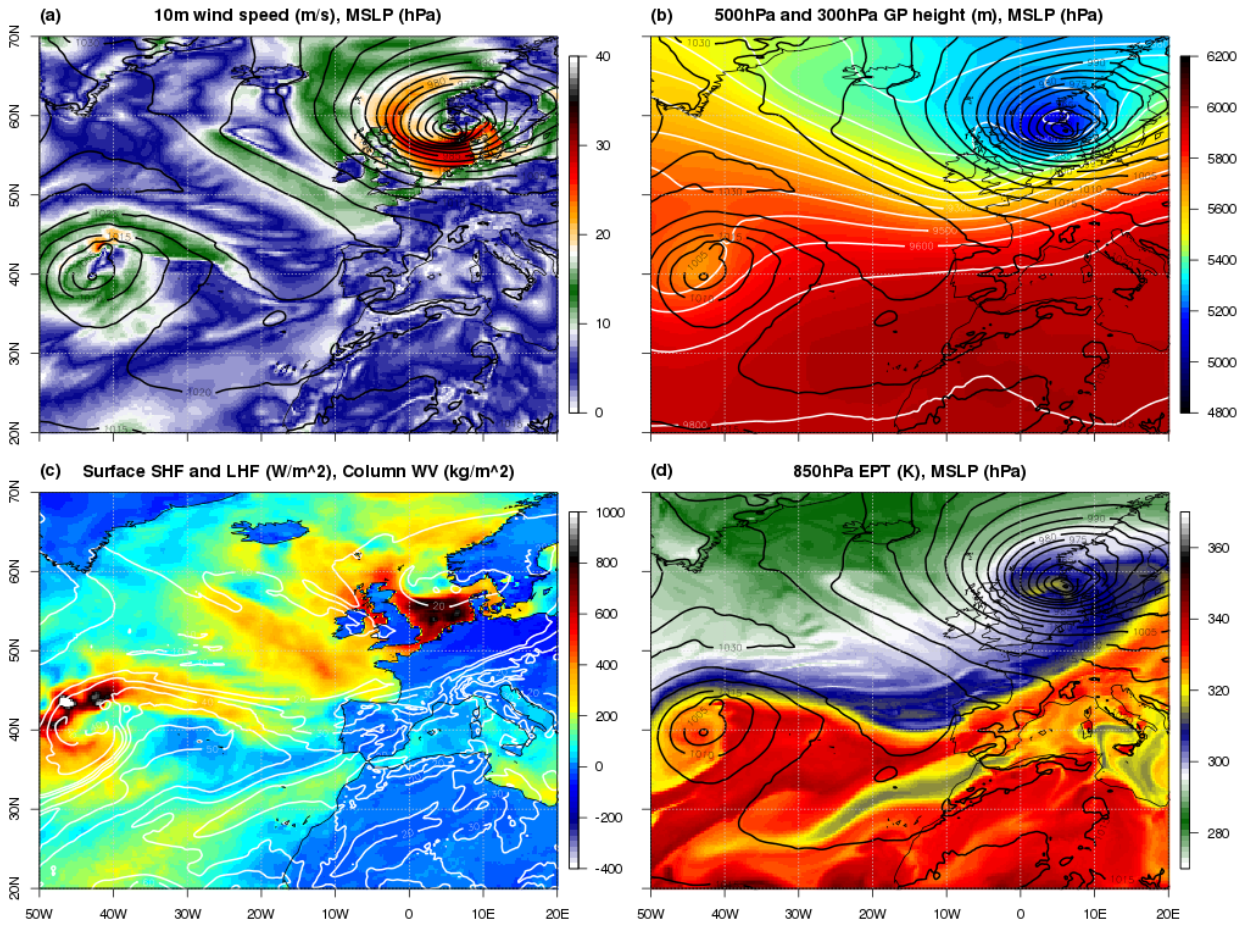

Figure 3.5: Same as in Figure 3.2 but for t = 162h.

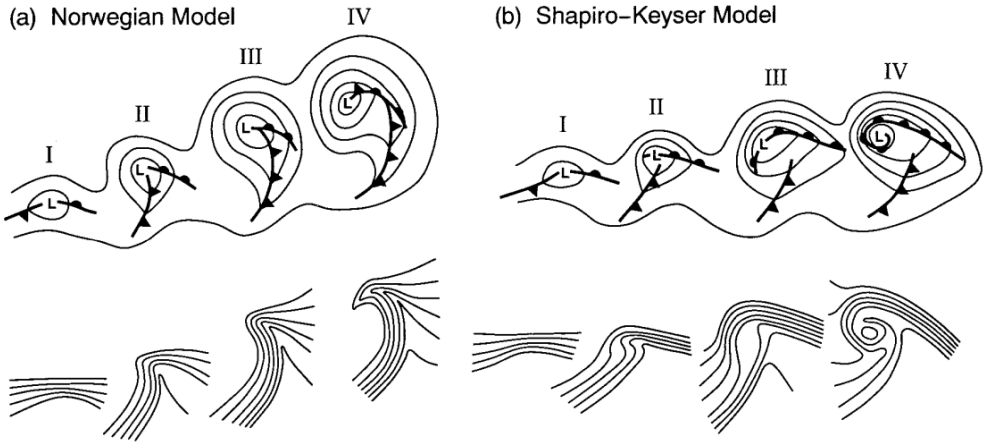

Figure 3.6: Comparison of the Norwegian model and the one presented by *Shapiro and Keyser* (1990). Upper panels show MSLP and fronts while the lower ones depict EPT, from *Schultz et al.* (1998).

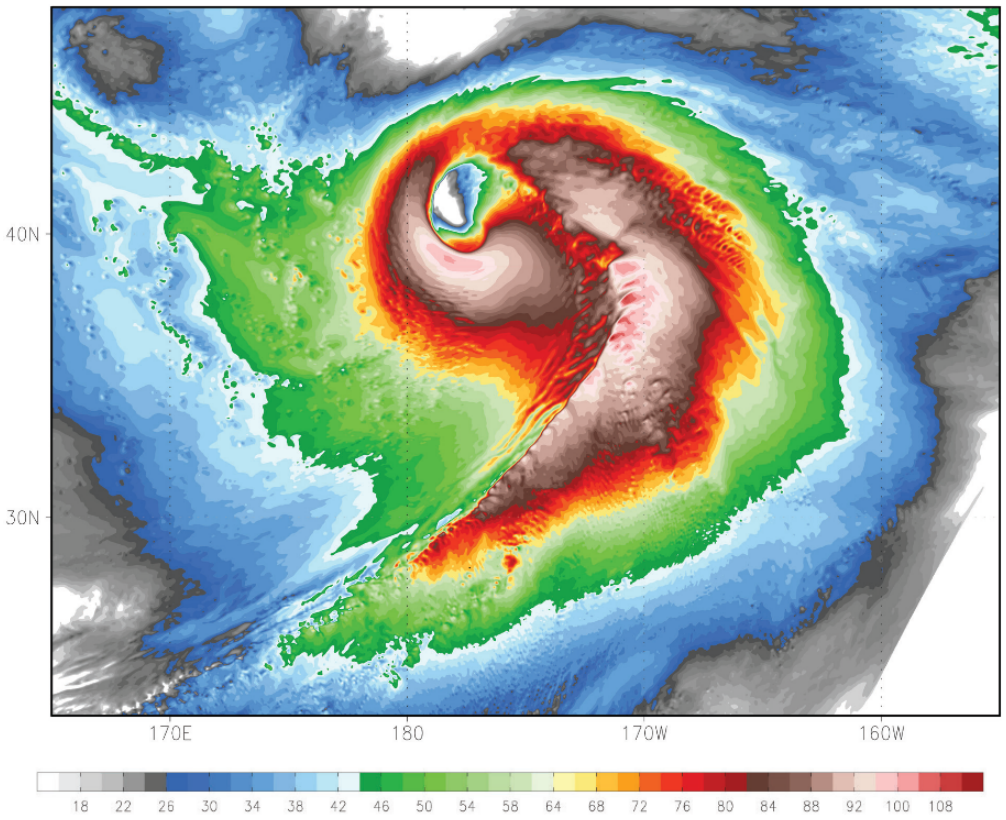

Figure 3.7: Hindcast of a powerful warm seclusion cyclone over the Pacific Ocean in February 2008 using WRF (9km) showing 875hPa wind speed (knots), from *Maue* (2010).

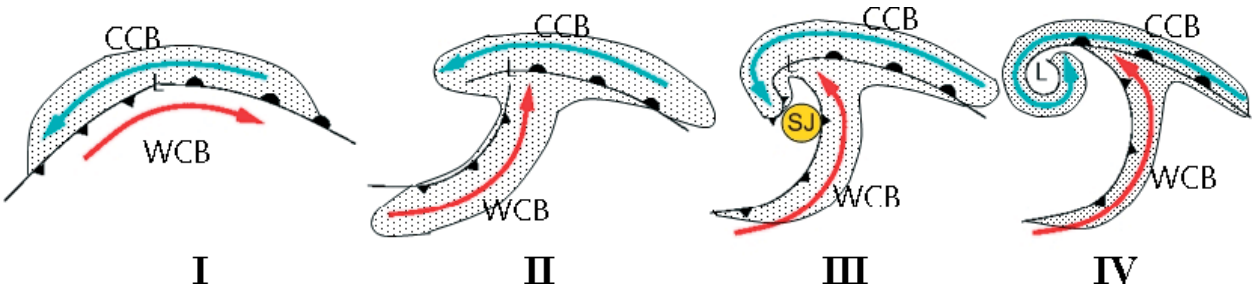

Figure 3.8: Schematic drawing of the development of a sting jet in a warm seclusion cyclone, the warm and cold conveyor belt are indicated by WCB and CCB, respectively. The low pressure centre is denoted by L and the sting jet by SJ, from *Baker* (2009).

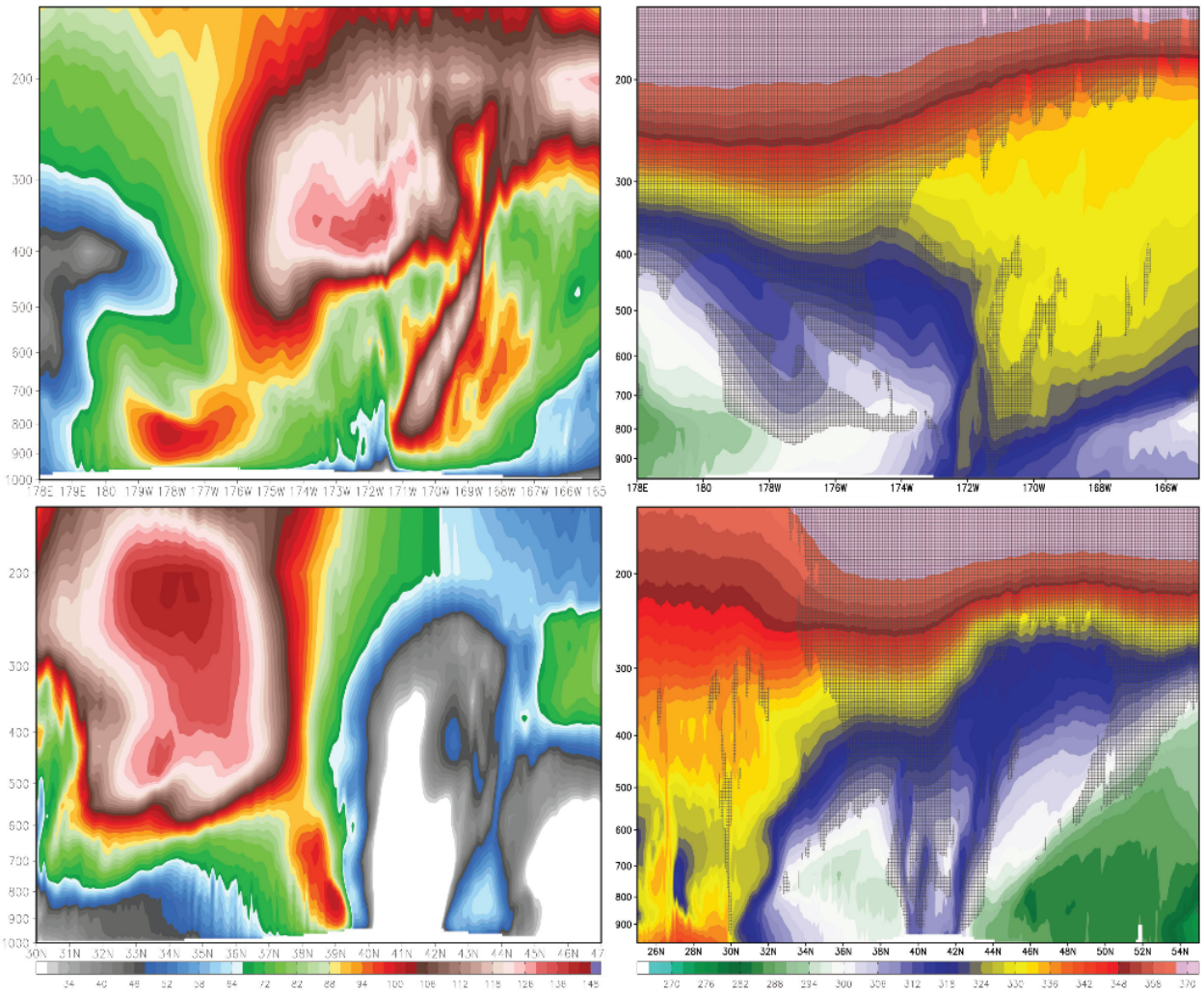

Figure 3.9: Vertical cross sections of the cyclone shown in Figure 3.7; the panels on the left show wind speed (kt) and the ones on the right depict EPT (K). The cross sections are taken just south of the centre, along the back-bent front, from *Maue* (2010).

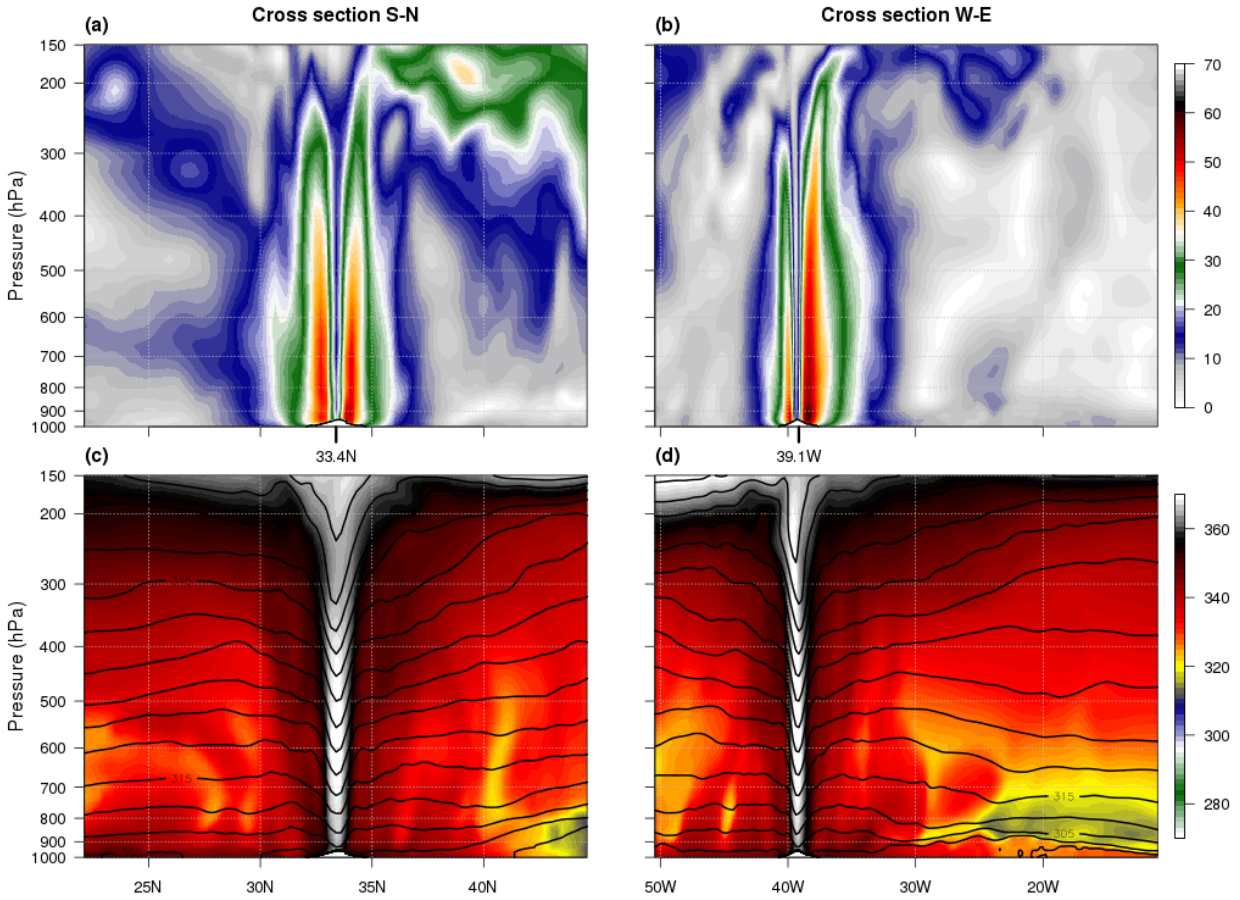

Figure 3.10: Vertical cross sections of Amy taken at the location of minimum MSLP (coordinates are given on the axes of a and b) with wind speed on top (m/s a,b) and EPT (shading, K) and PT (contours, K) at the bottom (c,d) for t = 84h. North-south cross sections are shown on the left side while those from west to east are to the right.

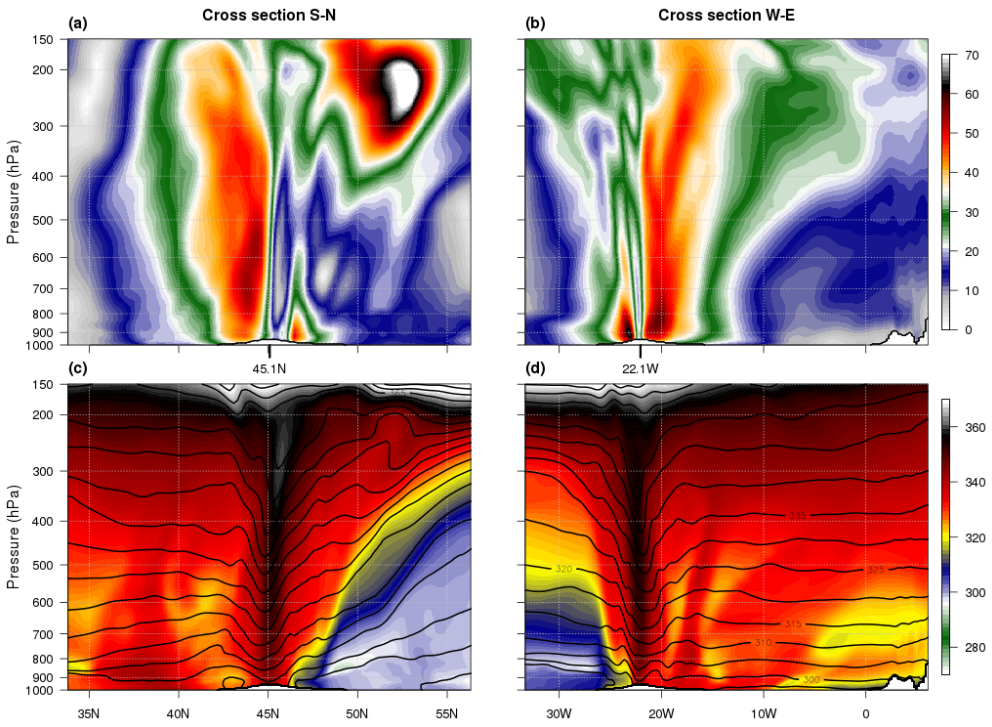

Figure 3.11: Same as Figure 3.10 but for t = 126h.

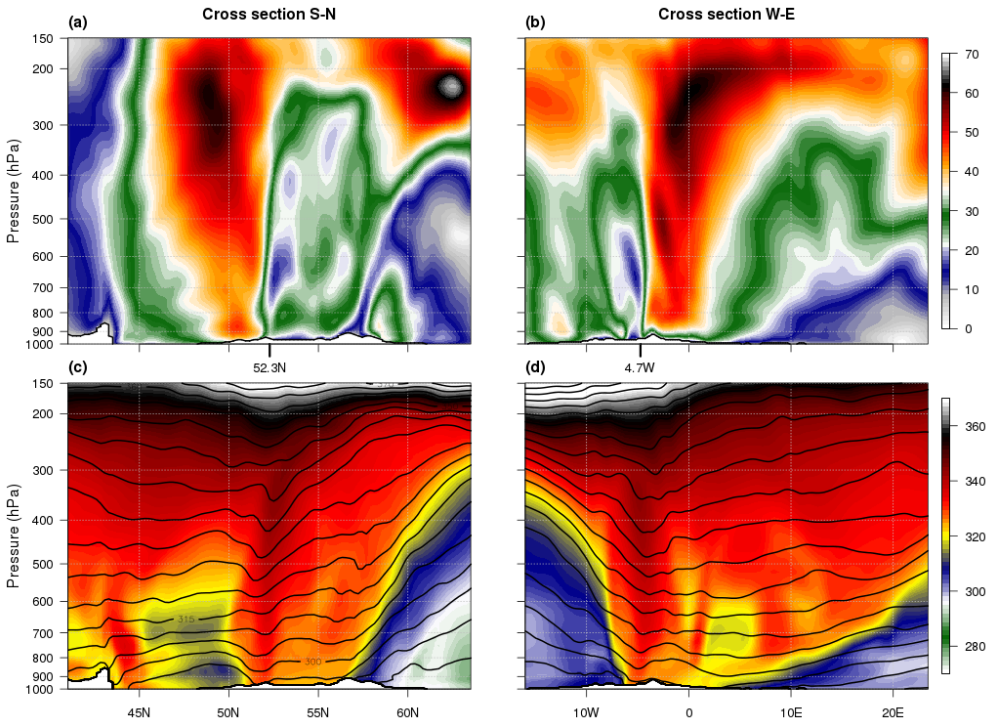

Figure 3.12: Same as Figure 3.10 but for t = 144h.

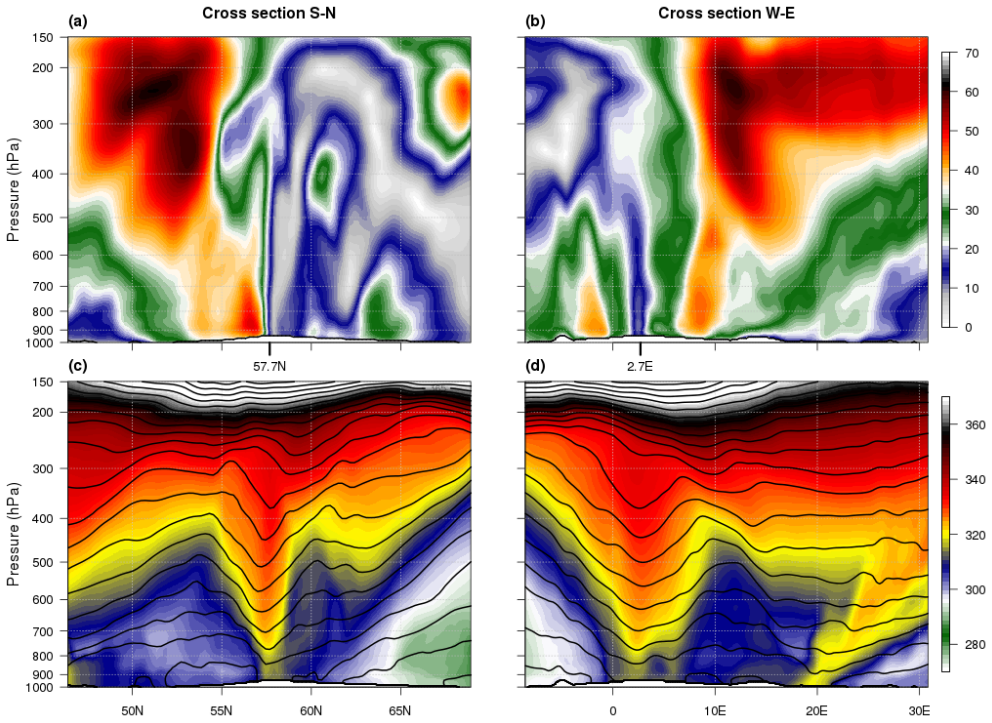

Figure 3.13: Same as Figure 3.10 but for t = 162h.

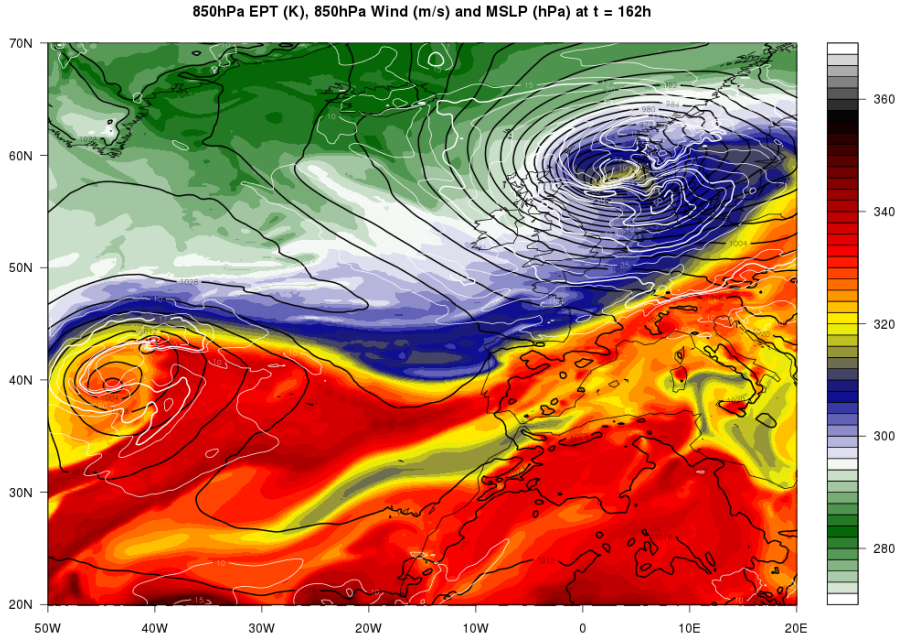

Figure 3.14: Weather pattern surrounding Amy at t = 162h, showing EPT (shading, K), 850hPa wind speed (white, m/s) and MSLP (black, hPa).

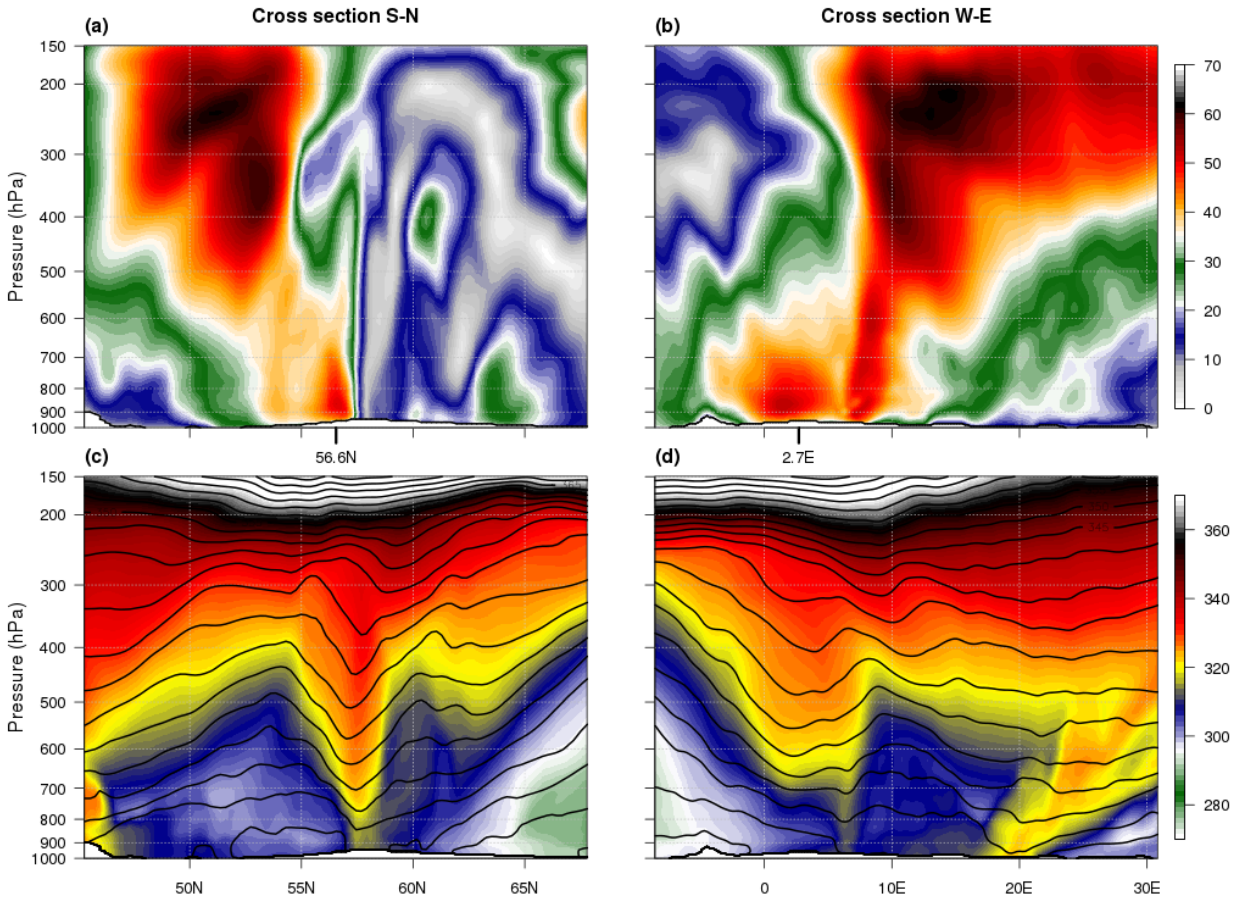

Figure 3.15: Same as Figure 3.13 but for a cross section taken 1.25°south of the MSLP minimum.

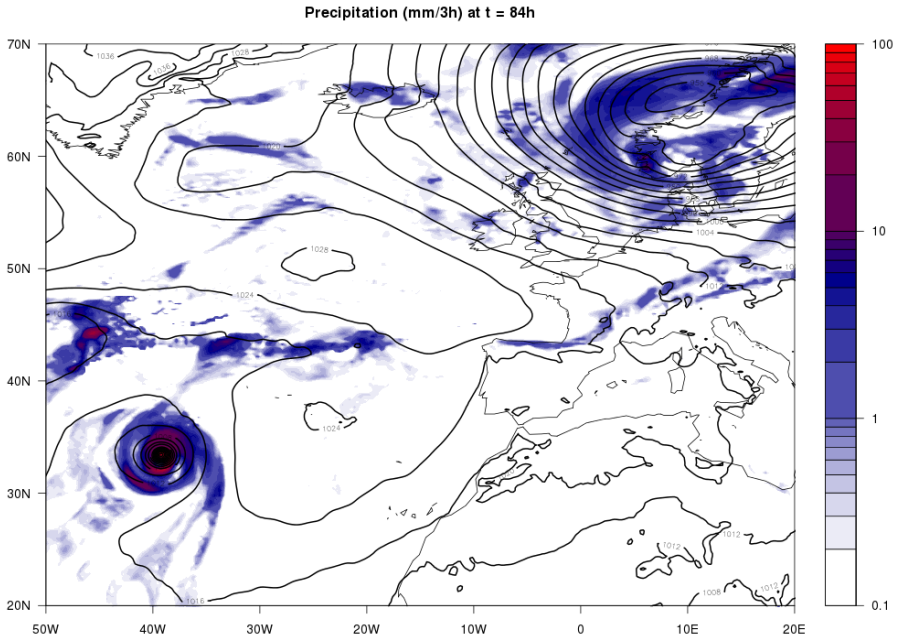

Figure 3.16: 3-hourly precipitation in the vicinity of cyclone Amy until t = 84h.

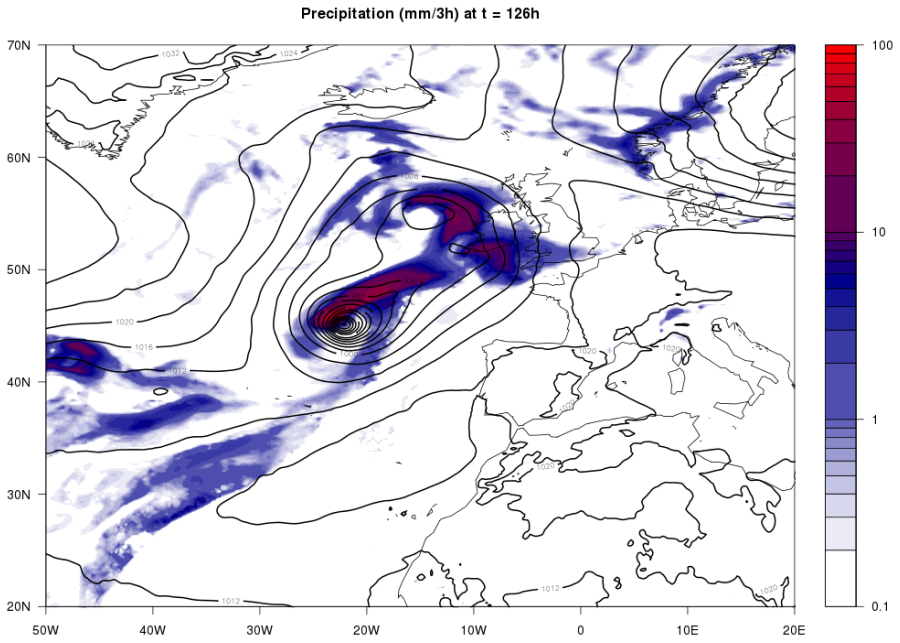

Figure 3.17: Same as Figure 3.16 for t = 126h.

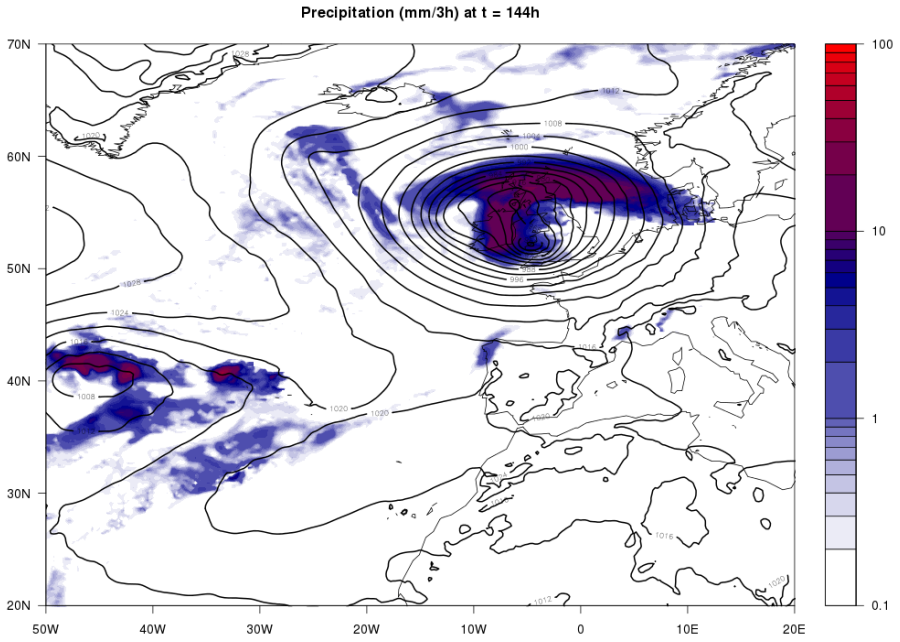

Figure 3.18: Same as Figure 3.16 for t = 144h.

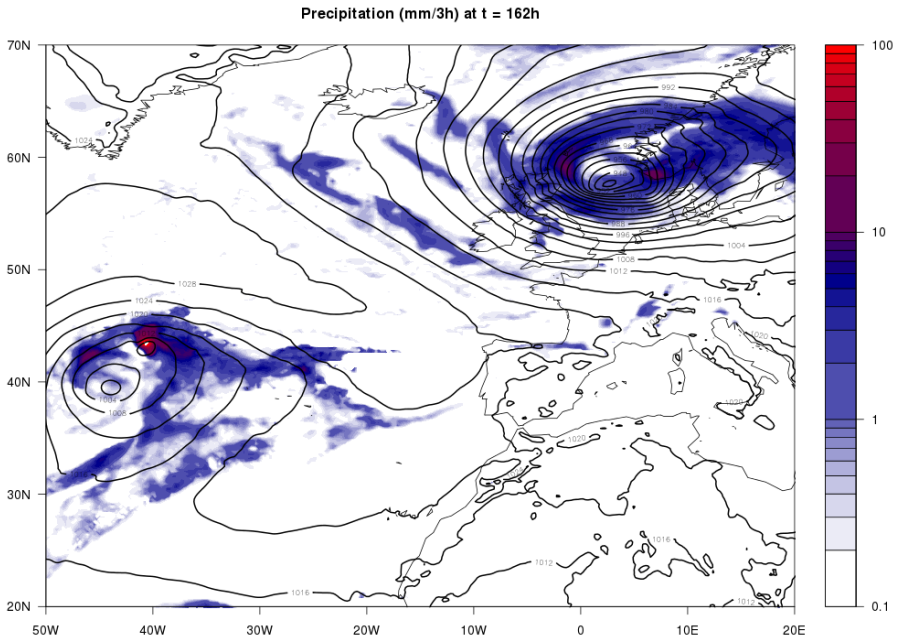

Figure 3.19: Same as Figure 3.16 for t = 162h.

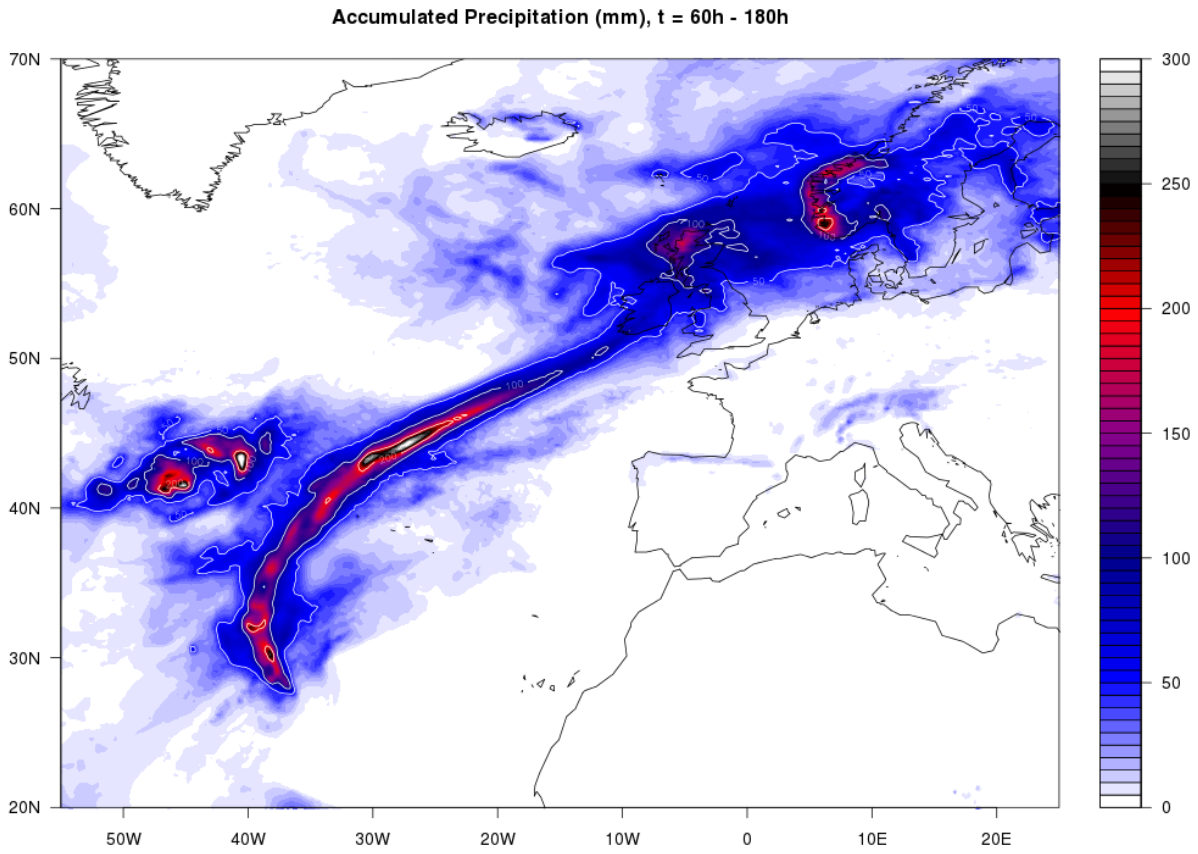

Figure 3.20: Total precipitation during the life cycle of Amy over the affected regions.

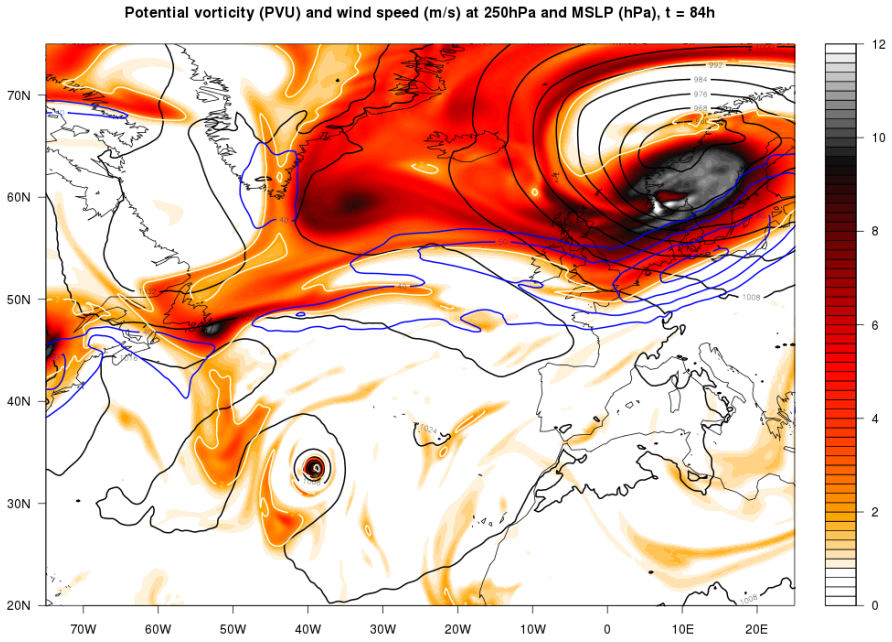

Figure 3.21: PV (shading) and wind speed (blue) at 250hPa of the area surrounding Amy at t = 84h.

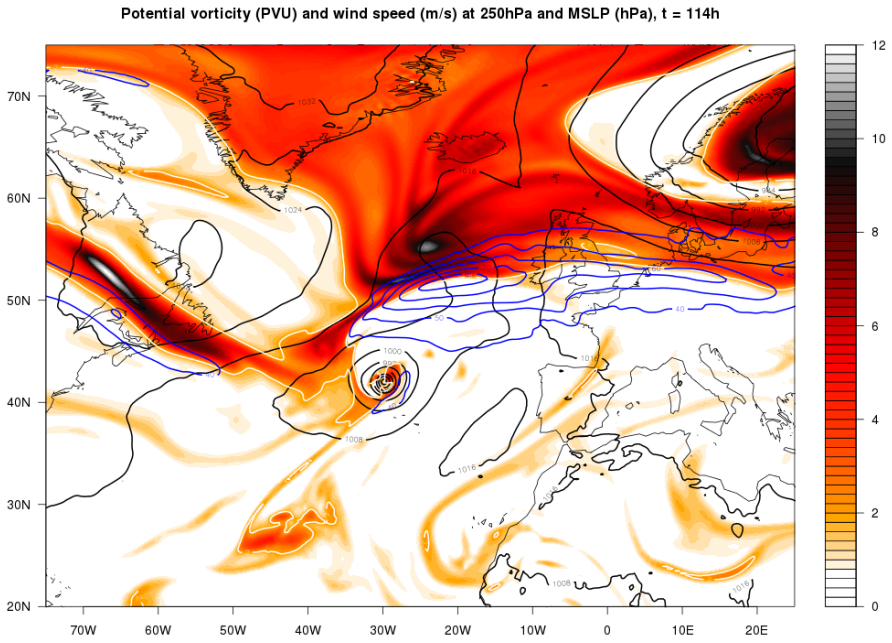

Figure 3.22: Same as Figure 3.21 at t = 114h.

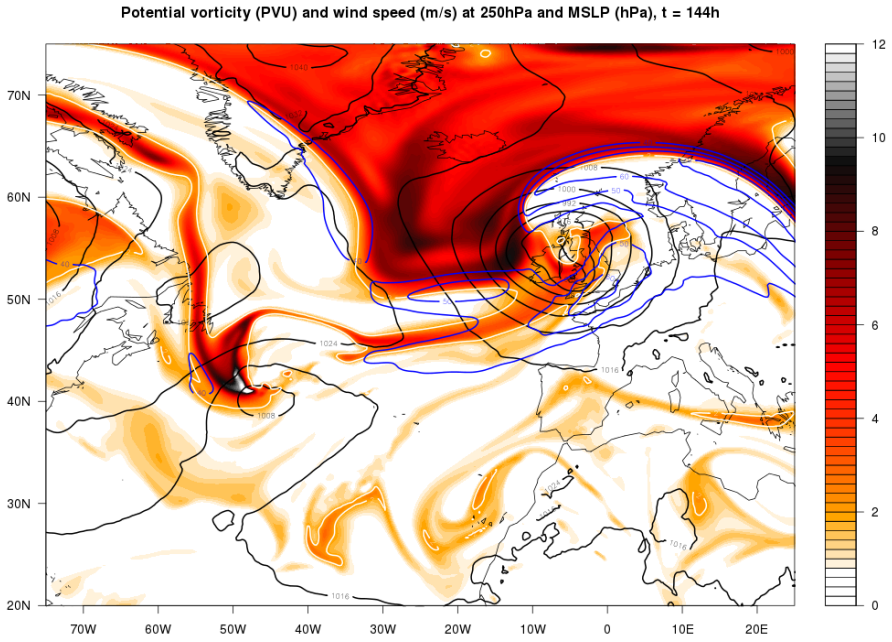

Figure 3.23: Same as Figure 3.21 at t = 144h.

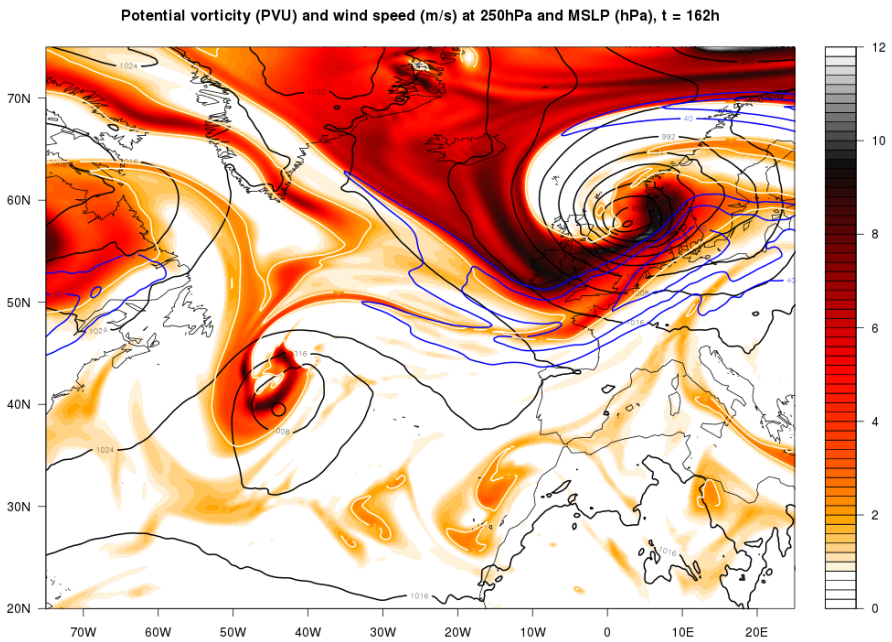

Figure 3.24: Same as Figure 3.21 at t = 162h.

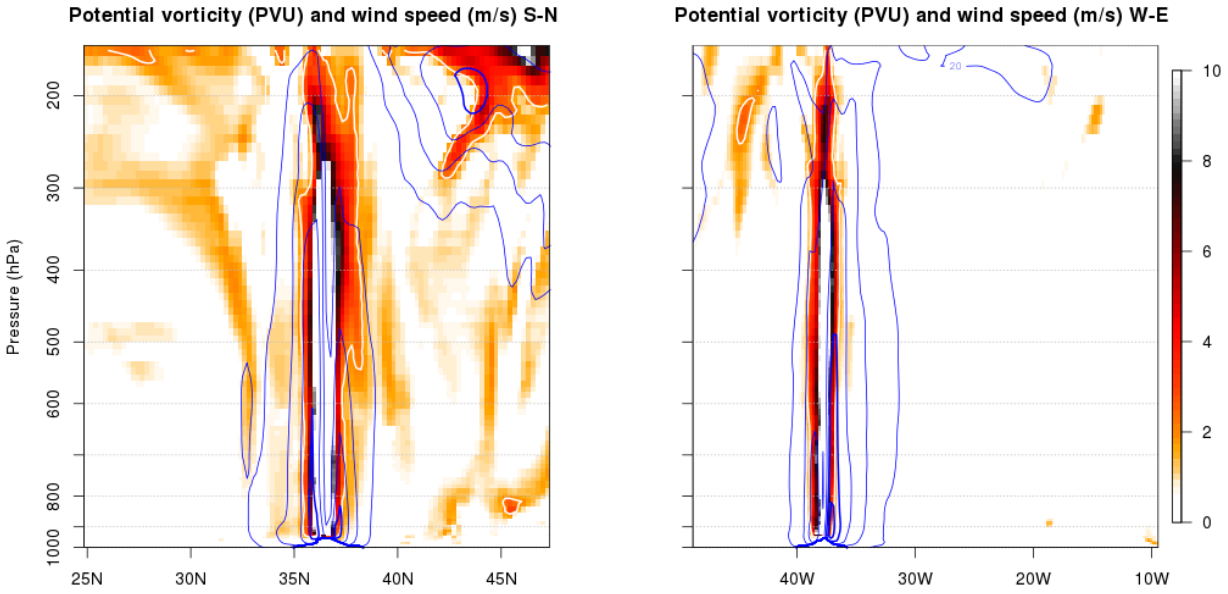

Figure 3.25: Cross sections of Amy at t = 96h in the meridional (left) and zonal (right) direction, showing PV (shading) and wind speed (blue). Contour lines are drawn each 10m/s, thick lines indicate speeds of at least 50m/s.

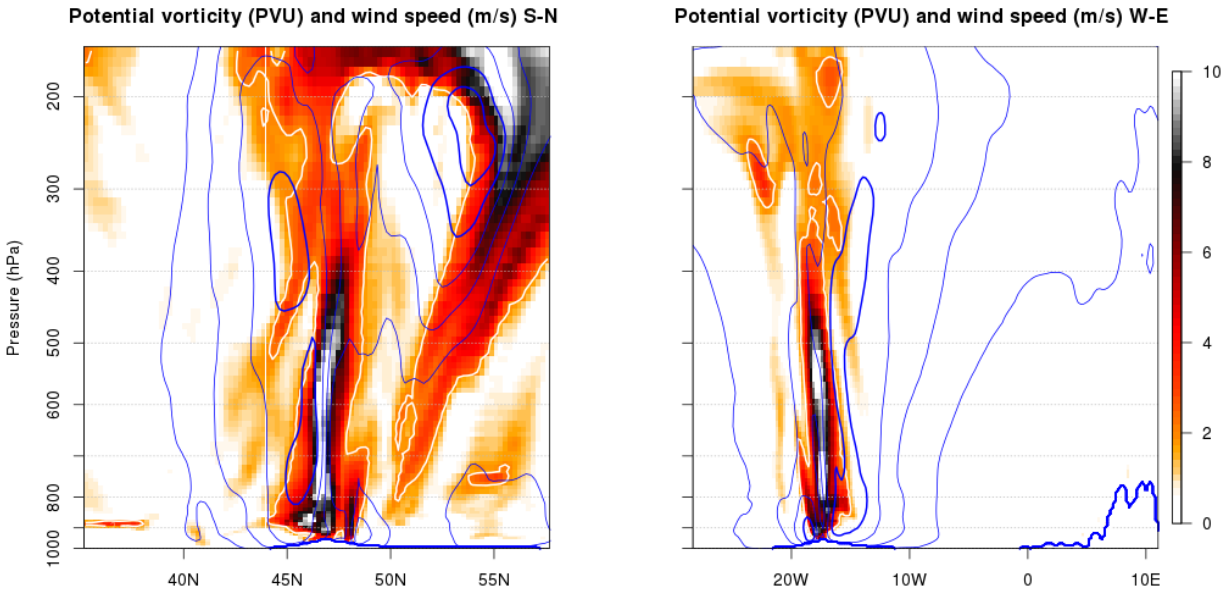

Figure 3.26: Same as Figure 3.25 at t = 132h.

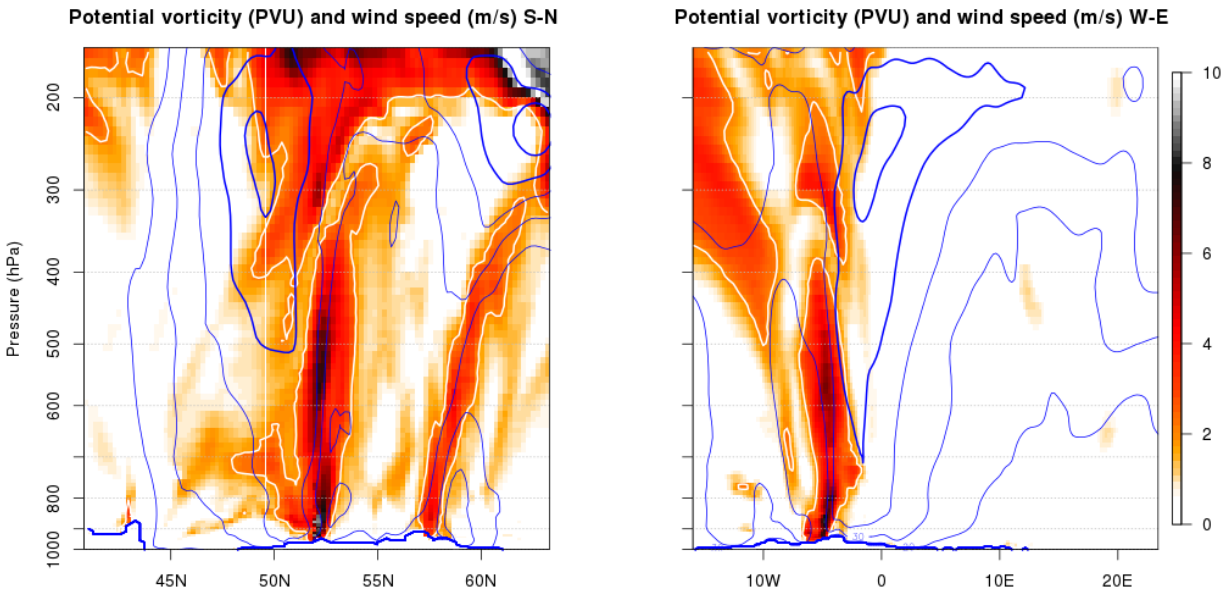

Figure 3.27: Same as Figure 3.25 at t = 144h.

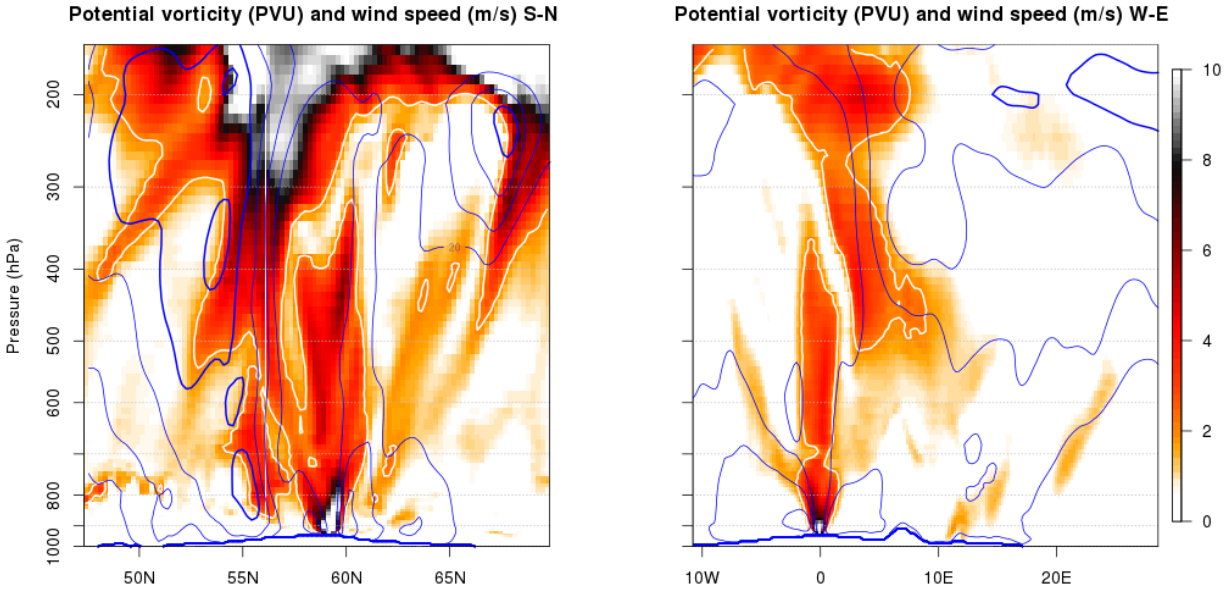

Figure 3.28: Same as Figure 3.25 at t = 156h.

Chapter 4

Datasets and analyses

To assess changes in the intensity and occurrence of severe Autumn storms in Western Europe, three datasets are generated representing the present (2002-2006), near future (2030-2034) and future (2094-2098) climate. Each of the simulations consists of a six member ensemble covering a total of 30 years. As it was pointed out by *Haarsma et al.* (2013), the most striking changes take place during Autumn and are related to cyclones with a tropical origin. Therefore, only the months August through November are considered here with a special focus on the tropical Atlantic.

4.1 Selection and tracking

A good measure for the intensity of a cyclone is the maximum wind speed it generates. Only the most severe storms impacting Western Europe are selected by searching for events during which the 3-hourly wind speed exceeds Beaufort 11 (28.4m/s). This is done for 4 different coastal regions that were specified earlier: the Gulf of Biscay, Norway, the North Sea and the Western UK. Starting near the point where the criterion was met, a set of storms is selected by tracking them back in time. The latter is done using both MSLP and relative vorticity (ζ) in an attempt to optimise the tracking of both tropical and extratropical cyclones. Relative vorticity is determined from the 10m wind speed ($\zeta_{10} = \frac{\partial v_{10}}{\partial x} - \frac{\partial u_{10}}{\partial y}$) which is available at 3 hour intervals just like MSLP. While going backwards in time, the first step is done by simply extrapolating the 2 previous locations with a maximum shift of 20 grid boxes (approximately 5°). Around this initial guess, the position of maximum relative vorticity is determined within a radius of 20 grid boxes. Only when the location is associated with a lower pressure than that of the first guess, it is accepted. This is done to avoid the tracking algorithm of selecting strong local wind gradients at for instance coastal boundaries. Finally, the centre fix is determined by locating the minimum MSLP within a 10 grid box radius of the current guess.

The focus of this study lies on storms that have a tropical origin so only those are considered for further analysis. There is no straightforward definition of the tropical Atlantic Ocean and for hurricane tracking the location of Cape Hatteras is often used as a northern boundary (35°N). Nevertheless, SSTs over the Gulf Stream region are still warm enough for tropical cyclogenesis further north and will only expand in the future (Figure 2.1). As a consensus, the northernmost extension of the August-October average 26°C isotherm is taken as the northern boundary, located at 38°N. Additionally, the Gulf of Mexico is not of interest as is the Mediterranean Sea so the tropical genesis region is defined by: 10°N - 38°N and 85°W - 20°W (gray box in Figure 4.1b,d,f). As long as the maximum 3 hourly 10m wind speed

within a 20 grid box radius of the centre fix exceeds that of a tropical depression (7 Beaufort; 13.9m/s), a cyclone is tracked back in time for a maximum of 10 days. When a cyclone's track enters the defined tropical genesis region at some point in its life cycle, it is considered to have a tropical origin. The sets of storms selected by this method for the different periods and those also having a tropical origin are shown in Figure 4.1. For further analysis, the time at which a local pressure minimum is reached within 24 hours of the initial wind observation is determined. This point is hence referred to as 't_0' and is used to align the final evolution of storms before they impact Western Europe.

4.2 Phase space analysis

4.2.1 Hart diagrams

The evolution of a cyclone throughout its life cycle can be visualised with a phase space analysis. *Hart* (2003) developed such an analysis that was capable of describing both tropical and extratropical systems as well as their transition. The main difference between both types of cyclones lies in the thermal nature of the core; tropical cyclones are characterised by a deep warm core while extratropical ones usually have a deep cold core. A warm seclusion storm is a special case as it exhibits a shallow warm core at a certain stage in its life cycle but still develops in an initially cold core system. Hart's analysis consists of 3 variables: B, V_L^T and V_U^T; the-storm relative thickness asymmetry, lower and upper level thermal wind, respectively. The thickness asymmetry is calculated as the difference between the average 900-600hPa layer thickness within the right and left 500km semicircle relative to the storm motion. This parameter is indicative for the baroclinic forcing that is acting on a developing cyclone. The thermal wind is a direct measure for the thermal nature of the core through the thermal wind balance. It is calculated by the vertical gradient of the horizontal geopotential slope in the 900-600hPa layer for the lower (V_L^T) and the 600-300hPa layer for the upper (V_U^T) level value. The different parameters are thus calculated as:

$$B = \overline{Z_{\text{600hPa}} - Z_{\text{900hPa}}}\Big|_R - \overline{Z_{\text{600hPa}} - Z_{\text{900hPa}}}\Big|_L ; \tag{4.1}$$

$$-V_L^T = \left.\frac{\partial(\Delta Z)}{\partial \ln p}\right|_{\text{900hPa}}^{\text{600hPa}} ; \tag{4.2}$$

$$-V_U^T = \left.\frac{\partial(\Delta Z)}{\partial \ln p}\right|_{\text{600hPa}}^{\text{300hPa}} , \tag{4.3}$$

where $\Delta Z = Z_{max} - Z_{min}$, the difference between the maximum and minimum geopotential height (Z in m) found inside a 500km radius around the storm's centre position.

An example of such an analysis is shown for Hurricane Irene (Figure 4.2), using the MERRA 1/2°by 2/3°(latitude, longitude) reanalysis (http://disc.sci.gsfc.nasa.gov/daac-bin/DataHoldings.pl). Data is available at pressure levels with a 50hPa interval and at a 6 hourly temporal resolution. To calculate V_L^T and V_U^T, 7 pressure levels are used in a linear regression to obtain the vertical gradient. Irene forms as a tropical depression in the Caribbean area and develops into a mature tropical cyclone with a symmetric, deep warm core (day -3 and -2). The Hurricane moves northwards along the US East Coast emerging in an area with lower SST's and higher wind shear. The cyclone attains a tilted structure ($B > 10$) and after a brief hybrid phase (asymmetric warm core) it becomes a deep cold core extratropical low (day -1). It then re-intensifies into a powerful extratropical storm in about 24h, reaching a central pressure below 940hPa. During this process, the cyclone loses its tilt again ($B \to 0$) and develops a shallow warm

core. Hurricane Irene is a typical example of a tropical cyclone that undergoes ETT and re-intensifies rapidly into a warm seclusion storm (*Agusti-Panareda et al.*, 2004).

4.2.2 New method

Hart's phase space analysis nicely shows the evolution and ETT of tropical cyclones through their thermal structure. It is therefore a good method to look at the characteristics of simulated storms studied here. Due to data limitations, some modifications have to be done in order to perform a similar analysis. Most importantly, data is only stored at six vertical levels that mostly do not coincide with those used in the analysis above. Therefore, the two layers used in the calculation are modified to 850-500hPa and 500-300hPa. The vertical regression now reduces to a simple finite differences scheme:

$$-V_L^T = \frac{\Delta Z_{500\text{hPa}} - \Delta Z_{850\text{hPa}}}{\ln 500\text{hPa} - \ln 850\text{hPa}}; \tag{4.4}$$

$$-V_U^T = \frac{\Delta Z_{300\text{hPa}} - \Delta Z_{500\text{hPa}}}{\ln 300\text{hPa} - \ln 500\text{hPa}}. \tag{4.5}$$

Similarly, the equation for B is changed into:

$$B = \overline{Z_{500\text{hPa}} - Z_{850\text{hPa}}}\big|_R - \overline{Z_{500\text{hPa}} - Z_{850\text{hPa}}}\big|_L . \tag{4.6}$$

As surface data is available at a 3 hourly resolution, the analysis can be done at a higher temporal resolution (using 6-hourly 3D fields). An example using this technique is shown for storm Amy in Figure 4.3. It is immediately evident that this storm has a more pronounced warm core structure during its early evolution. Subsequently, there is a long phase of ETT during which the cyclone has a hybrid appearance. Finally, after briefly becoming a cold core system, it re-intensifies quickly and forms a shallow warm core just like Irene did.

The phase space diagram suggests the development of a warm seclusion, which is in agreement with previous results. Although the analysis provides a decent result for this particular storm, there are some important restrictions that have to be considered. The limited vertical resolution does not allow for a decent regression leading to erratic patterns in the thermal wind parameters. Also, the boundaries of the different layers have to be adapted while they were well motivated for the original method. Finally, the main focus here is on the re-intensification instead of the transition itself and especially the possible formation of a warm seclusion. As can be seen in Figures 4.2 and 4.3, the shallow warm core tends to have a signature similar to that of a tropical cyclone. Although quite clear in the case of Amy, it may not be for other storms. Hart diagrams will still be considered, but due to the applied changes they cannot be used on their own to draw conclusions.

To make up for the restrictions in vertical resolution, a new method is presented that focuses on the distinction of a warm seclusion and makes better use of the high horizontal resolution. The two central variables in this analysis are EPT and PV, as they are good indicators of the structure and intensity of a cyclone. The EPT parameter is used as an indicator for the thermal structure of the core. The difference between the (horizontal) mean EPT of the core (1°by 1°) and the minimum value found in the south-east quadrant (5°by 5°) is determined. Only one quadrant is considered to omit gradients that are present when a decaying warm core enters a cooler environment (3.3d). The acquired temperature difference can still be used for a tropical cyclone due to its generally symmetric structure. This

parameter is hence referred to as EPT anomaly/difference or DT and is calculated at 850 and 300hPa. A tropical cyclone should have a high DT value at both levels while a warm seclusion only does at the lower one. The latter can be distinguished from a deep cold core cyclone in which the warm sector is located away from the centre resulting in an overall low DT. The second set of parameters is obtained by averaging the PV over the core (again 1°by 1°) at two different levels. An estimation of the PV is calculated (using Equation 3.3) at 775 and 400hPa using data at 850, 700, 500 and 300hPa, respectively. A schematic overview of the different regions used in both analyses is given in Figure 4.4. Also for the PV parameter, a tropical cyclone is characterised by high values at both levels. Diabatic heating in the lower troposphere should be evident in an increased low level PV for a warm seclusion cyclone (Figure 3.28). A cold core cyclone accordingly has lower PV values at both of the studied levels. With the obtained parameters, two phase spaces are drawn: DT_{300} versus DT_{850} and PV_{400} versus PV_{775}.

4.3 Mean wind field

Associated with the formation of a warm seclusion is the possible development of a sting jet. Its presence has been confirmed in observed storms (e.g. *Browning* (2004)) and is also suggested for Amy. Therefore, it is relevant to assess whether this phenomenon occurs on a more regular basis and whether this changes for future storms. To create a picture of the general wind field, the average horizontal field of all storms is taken by selecting a specific time step for each storm. Different selection criteria are used, consisting of t_0, minimum central pressure, maximum wind speed (10m and 850hPa), maximum DT_{850}, and maximum PV_{775}. Model data are calculated on a Gaussian grid using longitude and latitude coordinates. For a better correspondence, the horizontal field of each storm is first interpolated on a square grid using 25 by 25km intervals. Not only the 10m wind speed but also the horizontal wind at all five other levels is taken into account for the average. This should help making a judgement whether a possible sting jet is indeed caused by the vertical exchange of momentum with upper level winds. In addition to the wind field, the average 850hPa EPT is determined in a similar way. If all or most of the selected storms are in fact warm seclusion cyclones, the associated EPT field should match the one in Figure 3.6b (Stage IV).

4.4 Forcings during re-intensification

Besides a climatology of present and future storms, the aim is also to explain their evolution with a special interest in the intensification prior to possible impacts on Western Europe. As all of the selected cyclones have a tropical origin, they carry a lot of moisture that may be important for their development. Another important component is baroclinic instability, which is responsible for the formation of typical mid latitude cyclones. The different forcings considered here are quantified through three parameters: Z_d, Q_c and IVT, which are specified below.

4.4.1 Baroclinic instability

In analogy to the analysis presented by *Hart* (2003), a good measure for baroclinic forcing is through thermal asymmetry. As cyclone scales are typically larger in the mid latitudes, a radius of 750km is applied here to better capture a large scale trough approaching from the west (as in Figure 3.3). The parameter Z_d is then calculated as the difference between the average 850-500hPa layer thickness in

the right and left semicircle relative to the storm motion;

$$Z_d = \overline{Z_{\text{500hPa}} - Z_{\text{850hPa}}}\big|_R - \overline{Z_{\text{500hPa}} - Z_{\text{850hPa}}}\big|_L . \tag{4.7}$$

4.4.2 Core moisture

The remnants of a tropical cyclone often carry an anomalously large amount of moisture into a relatively cold and dry environment. This moisture may be of great importance for the formation of a warm seclusion as the associated latent heat release provides a positive feedback in the warming core. The amount of moisture Q_c in the core is simply determined by the vertically integrated specific humidity q (in kg/kg) of which the sum is taken over a 300km area surrounding the centre position;

$$Q_c = \sum_{\text{core}} \frac{1}{g} \int q dp \tag{4.8}$$

4.4.3 Atmospheric rivers

Moisture is not only carried by the remnant warm core but also in the warm conveyor belt. As it was pointed out by *Zhu and Newell* (1998), atmospheric moisture fluxes usually organise into narrow bands called atmospheric rivers. *Lavers et al.* (2013) used the integrated vapour transport as a measure for the strength of such an atmospheric river;

$$IVT = \frac{1}{g}\sqrt{\left(\int q \cdot u dp\right)^2 + \left(\int q \cdot v dp\right)^2}, \tag{4.9}$$

where again the vertical integral is taken over the available pressure levels and u, v are the horizontal velocity components at the respective pressure levels. This quantity is used rather than moisture advection ($-\vec{V} \cdot \nabla q$) as the flow in an atmospheric river does not necessarily take place along large gradients.

Here, the associated IVT parameter has to represent the total amount of moisture that is flowing towards a cyclone within its circulation. It is assumed that this happens primarily in an extended warm conveyor belt resembling an atmospheric river. A box around the centre is defined stretching 1500km in all directions apart from the northerly, in which it does only 750km (as the warm conveyor belt is dominantly present to the south). Most of the moisture transport within an atmospheric river takes place in the lower levels of the troposphere (850 and 700hPa), at speeds of typically 30-40 m/s. This means that under optimal circumstances, an air parcel in the defined box can reach the cyclone's centre within the next 12 hours. Far from all of the moisture flow within the box is part of a possible atmospheric river that is related to the considered storm. Therefore, several restrictions have to be implied when calculating the IVT parameter. First of all, only flow with a cyclonic component around the centre is considered (using 850hPa wind). To allow for some deviation (for example at the location of frontal breaking or in a meandering flow), the direction at any location may divert a maximum of 120°clockwise from that pointing towards the cyclone centre (instead of 90). Additionally, moisture flow in the core is omitted as this was already accounted for in the parameter Q_c. Furthermore, the IVT values can be very large here due to high velocities and are not necessarily representative for moisture flowing towards the storm. The same area as the one used to calculate Q_c is hence left out in the calculation. Finally, other tropical cyclones may be nearby, especially in an earlier stage, that exhibit large IVT values. To

minimise their influence, all grid boxes for which the 850hPa EPT exceeds 350K are left out. The IVT parameter (simply called IVT) is then determined by summing all of the remaining IVT values in the box surrounding the cyclone. Hence, IVT refers to the total flow of moisture associated with the large scale circulation of a cyclone instead of the simple quantity defined in Equation 4.9. When calculating Q_c and IVT, a correction is being made for the latitudinal dependency of the meridional distance. An example illustrating the considered quantities and regions for the calculation of Z_d and IVT is given for Amy in Figure 4.5.

4.4.4 Analysis

For each storm, the parameters Z_d, Q_c and IVT are calculated every 6 hours during the final intensification. The considered period is fixed, ending at t_0 and starting 24, 36 or 48 hours before. Baroclinic forcing and core moisture are determined for all but the last point of the period as they are intended to indicate the intensification during a consecutive 6 hourly period. A similar reasoning holds for the atmospheric river but for 12 hours, thus omitting the last two points (t_0 and $t_0 - 6$h). Then, the time average of each parameter is taken and compared to the maximum pressure drop over the entire period.

A second method is also introduced which makes use of a variable period to focus better on the intensification phase. Within a fixed period still ending at t_0 but starting 24, 48 or 72 hours earlier, the period during which the central MSLP deepens is determined. Only this shorter period is then used for the calculation of Z_d, Q_c and IVT with similar considerations regarding which points are omitted. As the number of points used in the calculation is now different for each storm, they are summed instead of averaged and again compared to the associated pressure drop.

In summary, six sets of parameters are calculated for each storm and compared to the pressure drop during the final intensification by calculating the respective correlations. In the results, a fourth parameter (P_4) is introduced to assess the mutual importance of both the atmospheric river and baroclinic instability. It is acquired by adding the normalised parameters IVT and Z_d, using the average and standard deviation for the studied set of storms;

$$P_4 = \frac{IVT - \overline{IVT}}{\sigma(IVT)} + \frac{Z_d - \overline{Z_d}}{\sigma(Z_d)}. \tag{4.10}$$

In the results below, this fourth parameter is simply referred to as $IVT + Z_d$. Apart from correlations between parameters covering the entire intensification period, the evolution itself is also studied. For this, time series of Z_d, Q_c and IVT (without summing or averaging) along with central MSLP are presented.

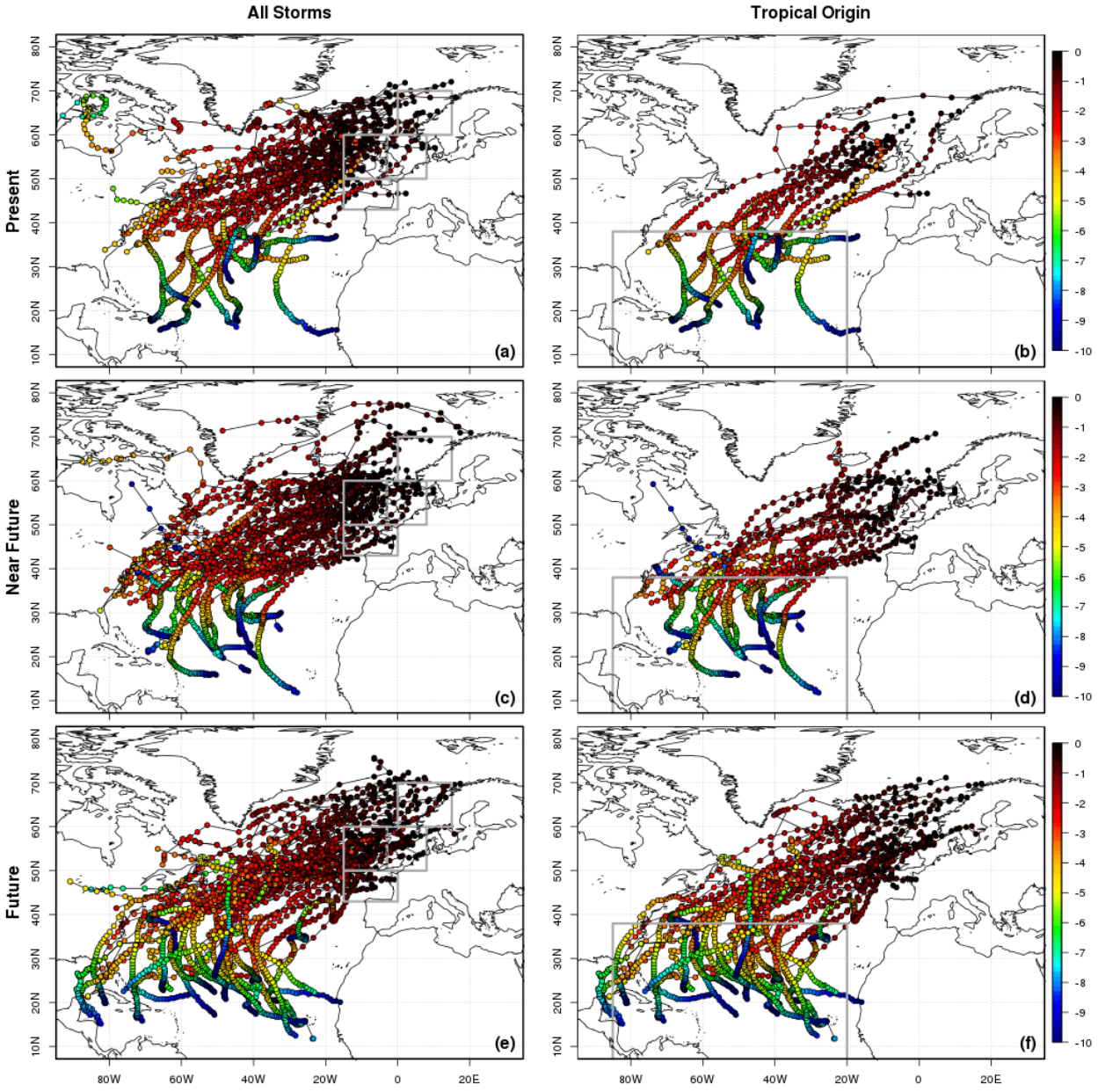

Figure 4.1: Storm tracks for all (left) Autumn storms impacting Western Europe with at least Beaufort 11 wind and only those that also have a tropical origin (right, indicated by the gray box) for the present (a,b), near future (c,d) and future (e,f) climate. Colours indicate the time before the wind speed criterion in one of the 4 areas (drawn in gray for a,c,e) was met in days.

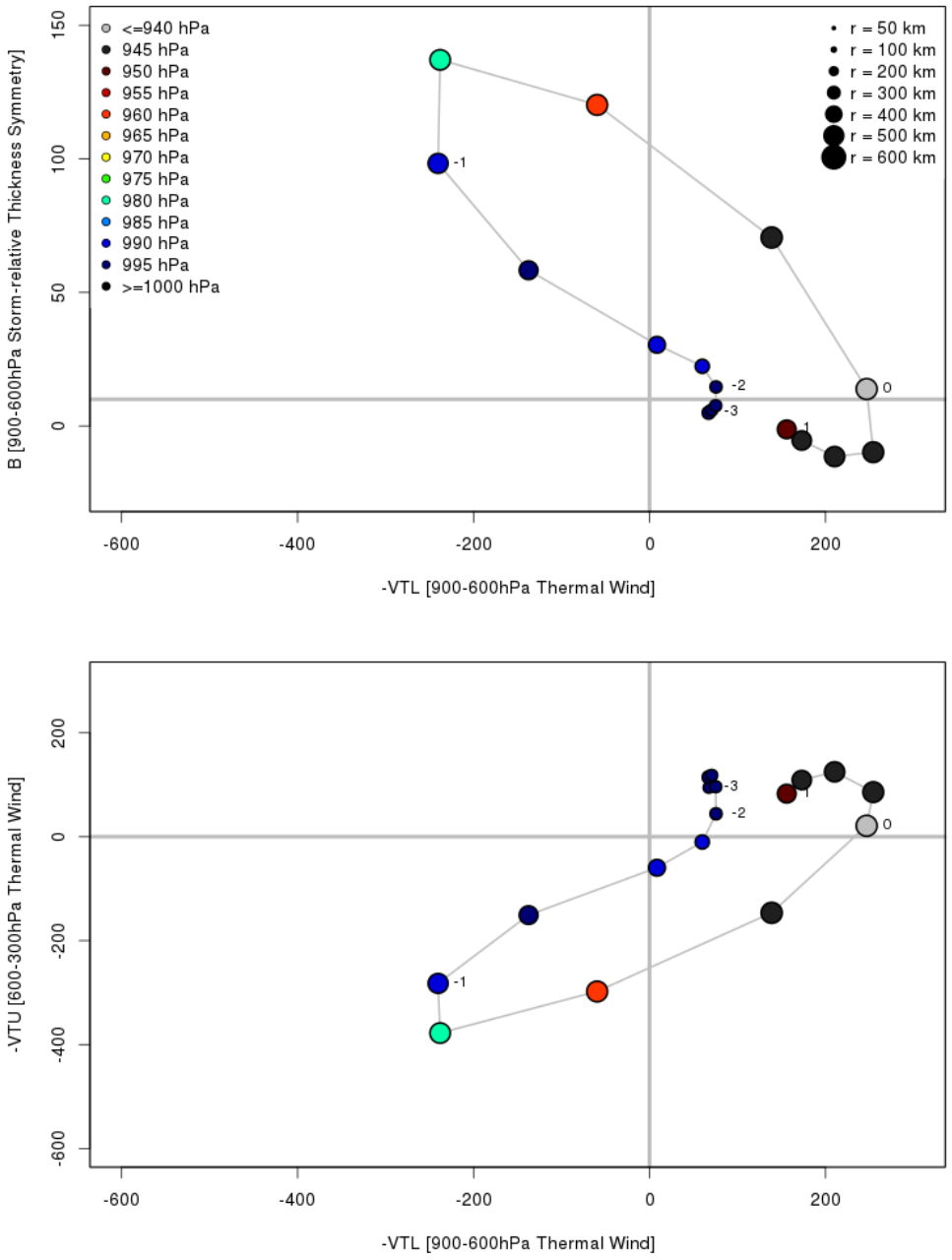

Figure 4.2: Hart diagram of Hurricane Irene using the MERRA reanalysis dataset. Colours indicate the central pressure and marker sizes denote the mean radius of gale force (17 m/s) wind. Numbers indicate the time relative to the point of lowest central pressure in days and gray lines separate different types of core structures as determined by *Hart* (2003). A 24 hour running mean is applied to smoothen the result.

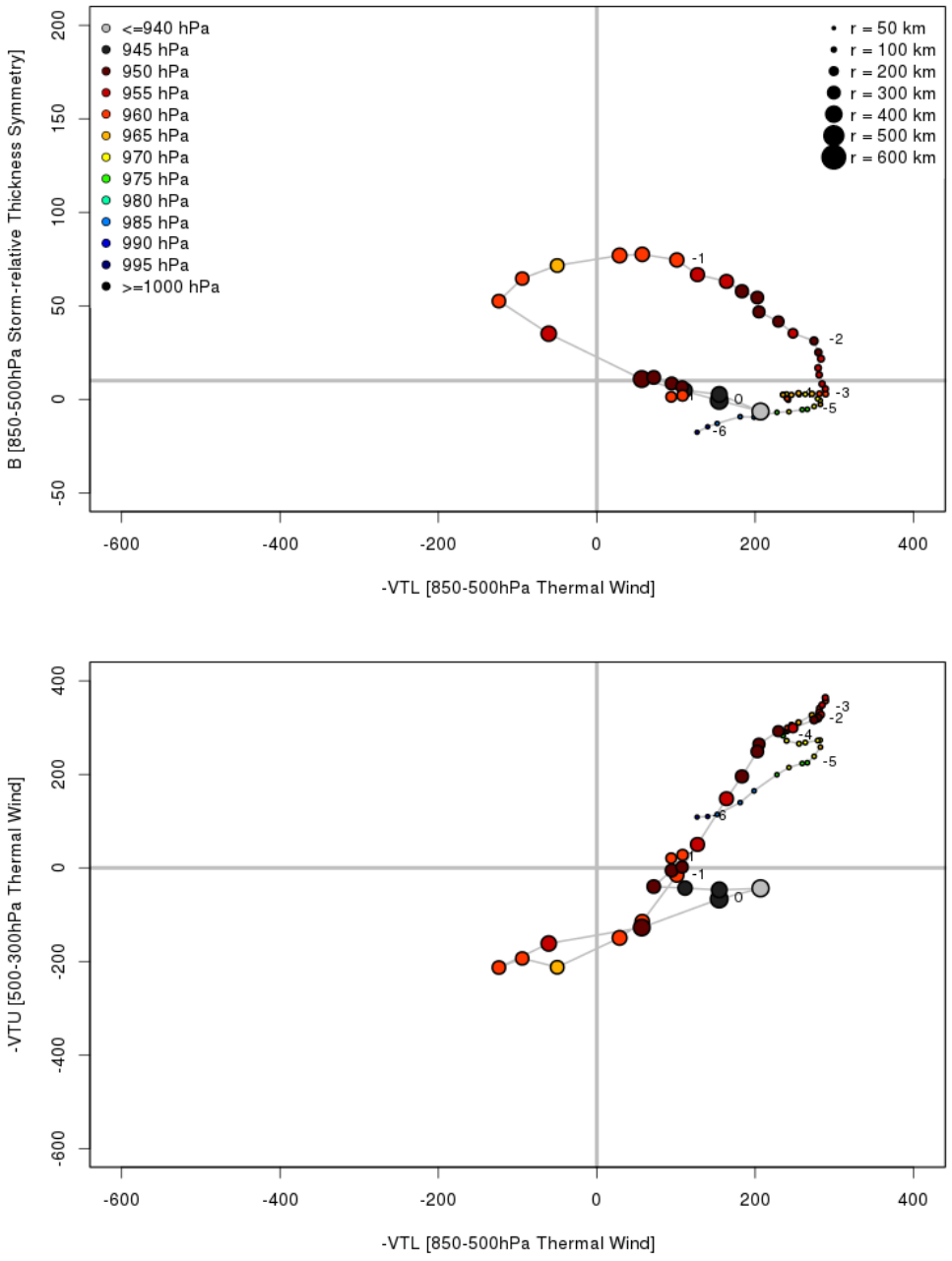

Figure 4.3: Hart diagram for Amy using model data, marker colours and scales are similar to those of 4.2 but axis scales are different. A 12 hour running mean is applied to the (3-hourly) result.

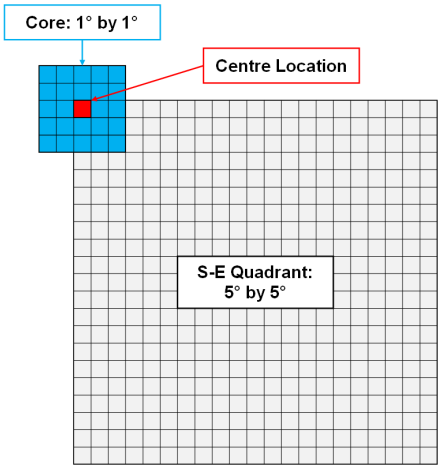

Figure 4.4: Schematic of the different regions used for the phase space analysis, each small square represents one (0.25°by 0.25°) grid box.

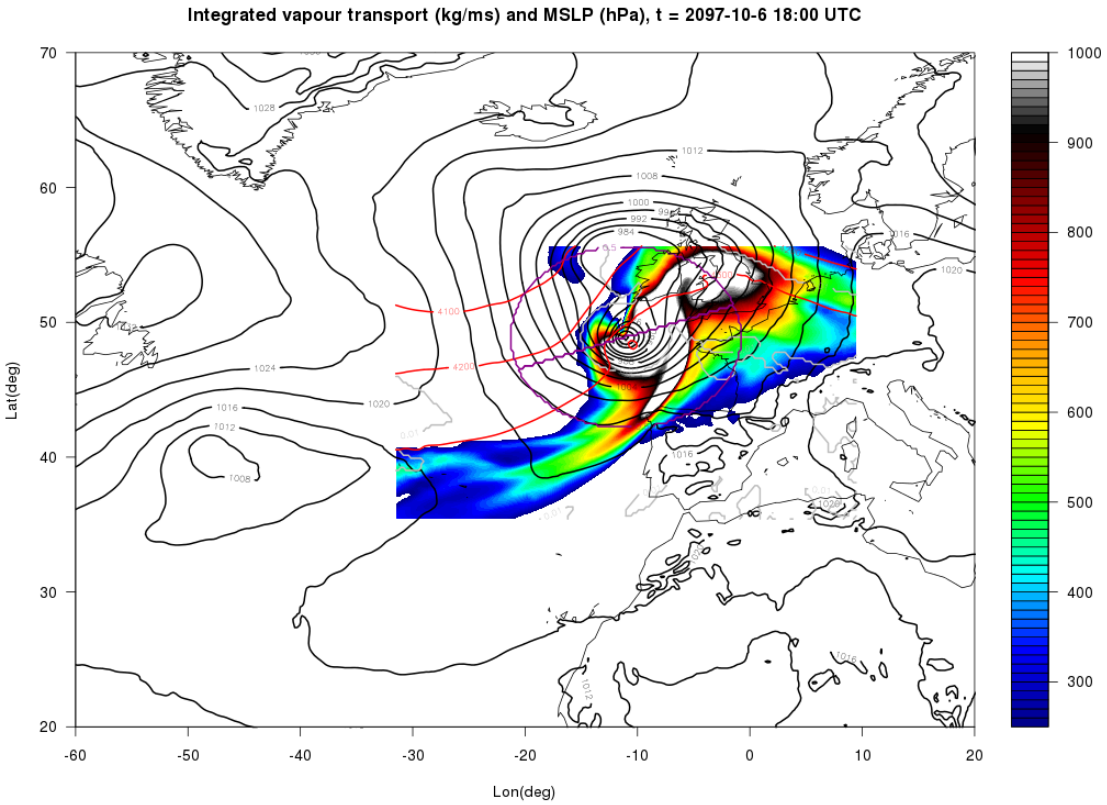

Figure 4.5: Example of the variables (except q) used in the calculation of the forcing parameters for Amy at t = 138h. Except for MSLP, quantities are only shown in the box that is used for the calculation of IVT. The purple lines show the location of both semicircles used to determine Z_d, red contours depict the 850-500hPa layer thickness (m). Shading indicates the IVT while gray contours show the regions that are omitted such as the core and a region north-east of the centre (flow away from the storm).

Chapter 5

Results

5.1 Tracks and intensity

5.1.1 General changes

A first look at the complete set of storms and those with a tropical origin was already given in Figure 4.1. When taking all of the tracked storms into consideration, it is clear that their number increases towards the future. Furthermore, a large increase is observed in the number of storms that impact Western Europe while having a tropical origin: from 15 in the present to 23 in the near future and 37 in the future climate. As the main focus is on the latter set of storms, their tracks and intensity are studied in more detail (Figure 5.1). As expected, most storms in the present climate form as tropical cyclones in the deep tropics (south of $\sim$20°N), curve northward and eventually eastward towards Europe. Both wind speed and central MSLP show a clear intensification during the last 2 days before t_0. In the near future, the general pattern for storms originating in the deep tropics does not change substantially. However, there is a considerable increase in the number of storms forming in the north-west of the Atlantic Ocean. There is also a slight increase in the average intensity in agreement with the overall increase of SSTs. For the future climate, the overall pattern changes quite dramatically; a lot more tropical cyclones make the transition into severe Autumn storms. A general warming and expansion of the tropical cyclone genesis region leads to more storms reaching Europe. In contrast to the results for the near future, the average intensity at t_0 has increased significantly. In addition, the spread in central MSLP several days earlier has become larger, indicating that some very severe tropical cyclones are among the selection. These observations are in agreement with the changes in SST; especially in the future the 26°C isotherm moves north-eastward along with a general warming resulting in $>$30°C temperatures across a large portion of the tropical Atlantic.

A general change of the storm tracks towards the future is their furthest extension towards Europe. While most storms reach their maximum intensity west of the British Isles in the current climate, many storms move further east into the North Sea and Scandinavian regions. It appears that the northward and eastward expansion of the tropical genesis region leads to a similar expansion of the impacted region. The increase in high wind speed events can also be seen in wind frequency maps (Figures 5.2 and 5.3), where Beaufort 10 (24.5 m/s) is used instead of 11 to clarify the patterns. A plume of increased frequencies runs from the tropics along 60°W towards Europe, extending further east in the future. The increase in the tropics is accompanied by a decrease to its west, in accordance to a gen-

erally eastward shift of the tropical cyclone genesis region. These results suggest a reduced chance of tropical cyclone landfalls along the US East Coast during the studied season.

5.1.2 Post-tropical and extratropical storms

An important discrepancy with the expectations is the general absence of an earlier intensity maximum before the final intensification. The large variance suggests the presence of another central pressure minimum for only a part of the studied storms. An inspection of individual storms reveals that a considerable amount has never been a tropical cyclone at all. For the phase space analysis presented in 4.2.2, the core PV was calculated at 775 and 400hPa. As this is a good measure for the strength of a tropical cyclone, it can be used to distinguish them from other systems. Any storm of which the core PV exceeds 3.5 PVU (potential vorticity units) at both levels is considered to be an actual tropical cyclone. Hence, storms that were a tropical cyclone at some point in their life cycle are called post-tropical while the other are referred to as extratropical. the storms that are called extratropical here can be cold core cyclones but also weak tropical systems such as subtropical storms and tropical depressions.

Splitting each set of storms into these two subsets results in a much clearer picture for the intensity evolution (Figure 5.4). Now, post-tropical cyclones on average exhibit a previous intensity maximum for all periods, which is most pronounced in the future climate. Extratropical cyclones generally form in the northern part of the tropical Atlantic while post-tropical systems originate further south. The increase of storms in the near future originating in the north-west Atlantic is mainly related to extratropical systems while the pattern for post-tropical cyclones remains virtually unchanged. As suggested before, the increase in the future climate is mainly caused by tropical cyclones originating from the deep tropics due to the expansion and further warming of their genesis region. A summary with some simple statistics for both subsets and intensity measures is given in Table 5.1. As a final remark, the intensity of post-tropical cyclones gradually increases towards the future. In contrast, that of extratropical systems decreases slightly at first to strongly increase as well in the future. Thus mainly the number of storms impacting Western Europe in the near future increases while conditions also become more favourable for their final intensification in the future.

	Number	**PT**	**ET**	$\mathbf{p_{min}}$ (hPa)	$\mathbf{v_{10,max}}$ (m/s)	$\mathbf{DT_{850,max}}$ (K)
Present	15	10	5	955.2 ± 16.5	31.76 ± 2.63	17.28 ± 4.21
Near Future	23	10	13	954.6 ± 13.2	32.61 ± 3.56	17.35 ± 5.81
Future	37	22	15	947.3 ± 11.7	33.46 ± 3.91	18.18 ± 5.57
All	75	44	33			
RI	50	22	28			

Table 5.1: Intensity measures and subsets (PT: post-tropical, ET: extratropical) of studied storms for the different periods, all storms and those featuring rapid intensification (RI, $-\frac{\partial}{\partial t}p_{min} > 2$hPa/3h).

5.2 Phase space diagrams

5.2.1 Hart diagrams

The phase space analysis presented by *Hart* (2003) is applied to all of the simulated cyclones that were selected for the present (Figure 5.5), near future (Figure 5.6) and future (Figure 5.7) climate. The average of all post-tropical and extratropical storms is taken after applying a 12 hour running mean to the individual results. Similar to Hurricane Irene (Figure 4.2), post-tropical storms exhibit a symmetric deep warm core in the early stages of their life cycle. During ETT, the cyclones on average develop a hybrid structure with an asymmetric warm core while their intensity declines. Afterwards, storms become deep cold core systems that re-intensify and develop a shallow warm core while becoming more symmetric again. The expansion of the wind field can be seen during ETT and continues through the final intensification. Extratropical systems show a very different early development; they start as weak cold core disturbances that evolve into deep cold core cyclones. Eventually, these storms also acquire a shallow warm core and become almost indiscernible from post-tropical ones in the final stage of their life cycle.

In agreement to previous observations, the final intensity of cyclones increases in the future. Furthermore, the evolution towards a shallow warm core becomes more pronounced, especially for post-tropical cyclones (PTCs). The tropical precursors of the latter also show a more distinct deep warm core in agreement with a stronger system. Despite starting as a warmer system, the cold core phase of post-tropical cyclones does not seem to change significantly. Consequently, future storms undergo a longer extratropical transition; from an average of 1.5 days in the present to 2.5 days in the future. These hybrid cyclones can be particularly dangerous as they exhibit the hazards of both tropical and extratropical storms. Another peculiar observation is the absence of a weakening for deep cold core systems. As the poles are predicted to warm faster than the equator, the meridional temperature gradient should weaken implying less baroclinic development. As far as this set is representative, the deep cold core observed for extratropical cyclones (ETCs) is just as strong in the future as it is in present simulations (Figures 5.5d and 5.7d).

5.2.2 New method

Examples

Before looking at the mean results as was done for the Hart diagrams, some individual storms are discussed shortly to get an impression of the new method's performance. First of all, the phase space diagram of Amy is considered because the evolution of this storm is well known by now (Figure 5.8). For clarity, the intensity and track are also given, with the addition of 850hPa wind in comparison to Figure 3.1. The latter shows a distinct peak at the time when a sting jet is thought to be present. The core temperature anomaly depicts a deep warm core and a strong PV column for the tropical cyclone (two to five days before t_0). During ETT, the warm core weakens and especially the upper level PV core degrades at first. During the re-intensification, the formation of a shallow warm core and an increase of PV can be observed. Although Amy eventually becomes a cold core cyclone, it does not weaken that much during ETT and still contains the remnants of a warm core afterwards (Figure 3.4).

Another storm (called 1NO) shows a clearer evolution (Figure 5.9); the central MSLP rises by almost

30hPa during ETT. This storm originates from the Western Atlantic and becomes a strong tropical cyclone. Both its warm core and PV column are stronger than those of Amy, in agreement with the intensity measures. Again, the PV column degrades at the upper level first while the opposite happens for the warm core. The latter almost completely disappears but then the low level temperature anomaly increases strongly again. The evolution of the PV column is not that clear, probably because the considered level is a little too high to show the effect of latent heat release well (Figure 3.28). Still the PV parameters are useful in determining the strength of a tropical cyclone and to show the ETT.

Some tropical cyclones do not seem to undergo a clear ETT, an example of such a storm is 1BI (Figure 5.10). This system follows a path somewhat similar to that of Amy but with an earlier eastward turn. It enters an area that is conducive for baroclinic development while it is still a developing tropical cyclone. Consequently, there is no observed weakening before the storm intensifies and forms a warm seclusion. Some weakening of the lower warm core can be seen but the PV column continues to strengthen up to t_0. This storm is probably a hybrid system upon its arrival in Europe with a lot of similarities to Hurricane Sandy (2012). When looking at the according Hart diagram (Figure 5.11), the storm indeed becomes asymmetric but never develops a deep cold core.

Finally, an example of an extratropical cyclone is given (Figure 5.12). There is quite some scatter in the phase space parameters but any results prior to about three days before t_0 are not considered in further analyses as the intensity drops below the critical threshold (13.9m/s). The cyclone forms over the warm Gulf Stream region just east of the US East coast and moves north-eastward over the Atlantic Ocean. This is a typical genesis region for winter storms, where warm water of the Gulf meets the cold Labrador Current. A large temperature (and moisture) gradient is present in the atmosphere and Rossby waves move eastward into the area inducing baroclinic instability. As it passes east of Labrador, the cyclone develops a warm seclusion and undergoes an explosive intensification. No warm core or PV column is observed until this final intensification during the last day before t_0. Notice that also the upper level parameters rise, which is related to the tropopause folding down over the developing cyclone, increasing potential temperature as well as PV (*Uccellini et al.* (1985); see also Figures 3.13 and 3.28 for Amy).

Averaged results

The mean evolution of modelled storms looks quite consistent for the different periods (Figure 5.13). PTCs are deep warm core systems featured by high PV in both the upper and lower troposphere. During ETT, both the warm core and PV column degrade where again upper level PV decreases first (probably due to high wind shear). The final re-intensification is marked by an initial quick increase in low level EPT anomaly followed by a similar increase at the upper level. PV parameters rise almost simultaneously at both levels when DT_{300} increases. Tropopause folding and latent heat release thus become important after the initial formation of the warm seclusion. ETCs do not show much development until about two days before t_0, when they undergo an evolution similar to that of PTCs. This confirms that the majority of storms in all of the studied period form a warm seclusion during their final intensification.

As was shown by the Hart diagrams, tropical cyclones leading to storms that impact Western Europe become more intense in the future. Indeed, both of the parameters indicating the warm core and PV column increase significantly in the near future and future simulations. Due to the limited set of storms, the average results are quite noisy but consistent with previous observations showing that future storms

tend to be warmer and more intense during their final stage. An interesting trend can also be observed for ETCs; some of them appear to be forming a warm core as well 2 to 4 days before t_0 in the near future and future. This means that some of them are actually developing tropical cyclones but leave the genesis region before reaching a mature state.

Extratropical development

Some obscurity remains on the observed changes for ETCs; mainly concerning their nature and the large increase in number for the near future climate. The Hart diagram results (Figured 5.5-5.7) showed that the cold core development remains unchanged or even slightly strengthens. This is in contrast with the projected decrease in baroclinic instability, related to the uneven heating of polar and tropical regions (*Gitelman et al.*, 1997). To elucidate this matter, the mean 850hPa EPT and PT is calculated for the considered periods (Figure 5.14a,c). In both fields, the tropical and polar regions can be distinguished, separated by a zone of strong gradients between 30°N and 60°N where mid-latitude cyclones typically form. The future warming is stronger at high latitudes but in the Atlantic this is not the only change taking place. The meridional overturning circulation is expected to weaken, causing a relative cooling in the north-eastern Atlantic Ocean. This counteracts the average weakening of the meridional temperature gradient and even leads to a local increase. Furthermore, the EPT gradient is also of importance for extratropical cyclones with a shallow warm core as latent heat release can speed up their intensification (*van Delden*, 1989). Despite the smaller warming, tropical air can take up a lot more moisture resulting in an increase in the EPT gradient. Tropical cyclones carrying warm and moist air to the mid-latitudes lead to a further increase of the EPT in the central northern Atlantic (related to the wind speed shift seen in Figure 5.3).

To get a better view on where the gradients are changing and how, the zonal mean 850hPa EPT and potential temperature (PT) are calculated as well as the zonal mean meridional gradients between 80°W and 40°W (Figure 5.14b,d). The zonal mean clearly shows an enhanced warming of the tropics in terms of EPT while the opposite happens for the PT. The average gradient is strongest around 50°N where the warm Gulf Stream meets the cold Labrador Current (the cold tongue in Figure 5.1b). As the Atlantic warm pool expands northward in the near future, the cold current remains in place and the gradient in both EPT and PT increases (50°N-60°N in Figure 5.14b,d). An associated decrease in the meridional PT gradient can be observed around 40°N, consistent with a northward shift of the baroclinic zone. The latter can also be seen in similar fields for 300 and 200hPa which are not shown here. In the future, the Labrador current starts retreating to the north (Figure 5.1f) while the warm pool expands further and the baroclinic zone continues to shift northwards. This is reflected by a further decrease of the PT gradient south of 50°N but no change to the north.

The region where both currents meet is favourable for the development of warm seclusion cyclones. Surface low pressure areas form downstream of a trough moving eastward over the US mainland. The southerly flow to its east carries a lot of warm and moist air from the Gulf Stream region while moving north-eastward. It then crosses Newfoundland and meets the much colder air coming from the north, providing strong air temperature gradients in combination with baroclinic instability. This is exactly the region where Hurricane Irene underwent explosive intensification in 1999. To check whether this kind of storms will occur more frequently in the future, another subset is made by selecting only those storms that cross the considered region (35°N-50°N, 70°W-50°W) and impact Western Europe (Figure 5.15).

The result is quite striking, showing almost a doubling in the number of storms that develop over the Gulf Stream region (see also Table 5.2). For the near future, there is a large increase in the number of storms with little change in strength while for the future mainly their intensity increases.

In general, more storms will intensify over the Gulf Stream region due to the increased temperature gradients. In addition, the warming Atlantic Ocean will support the development of tropical cyclones further to the north and later in the season. Both effects are probably at work simultaneously in the near future, while in the future the developing storms mainly carry more moisture allowing them to intensify further. Particularly the increased SSTs are important in the future, as many storms pass through the region rather than forming in it (which is the case for the near future).

	Number	$\mathbf{p_{min}}$ (hPa)	$\mathbf{v_{10,max}}$ (m/s)
Present	16	954.3 ± 11.5	32.24 ± 2.76
Near Future	28	956.1 ± 10.3	32.35 ± 2.96
Future	25	947.2 ± 13.4	33.73 ± 3.96

Table 5.2: Number and intensity of storms crossing the Gulf Stream region and impacting Western Europe in the present, near future and future.

5.3 Mean wind field

The evolution of the studied storms showed that, despite having distinct life cycles, their final development is very similar. Most storms form a warm seclusion after which post-tropical and extratropical cyclones become almost indiscernible. Therefore all storms are considered again for the mean fields at the point where they impact Western Europe.

5.3.1 Maximum intensity

Different time selection criteria were mentioned for which the mean fields are calculated. Generally, the time of maximum 850hPa wind speed should be the best to depict a sting jet as it is not much affected by orography. The result is shown for all present and future storms (Figure 5.16a,b), as the one for near future storms resembles that of the present strongly. A warm seclusion is evident for both periods as an isolated area of potentially warmer air. The warm sector can be seen to the east as well as the dry intrusion wrapping around the core from the north-west. Storms are on average located at the left exit region of a jet streak which is favourable for cyclogenesis, in resemblance to Amy (Figure 3.24). For present storms, a region of high wind speeds is located south of the centre, which is where the maximum is to be expected due to the isallobaric wind component caused by the eastward motion. An extension of this region is seen to the east along with strong 850hPa wind, lying close to the end of the back bent front and underneath the jet streak. Looking at the horizontal wind speed at different vertical levels (Figure 5.16c), the area coincides with high wind speeds at all levels suggesting the vertical exchange of momentum.

Future storms (Figure 5.16b,d) feature considerably higher EPT and wind speeds but have a similar structure. The pattern of a warm seclusion, location of the wind speed maximum and position relative

to a jet streak all resemble the present storms. In accordance to previous results, a more intense picture appears for future storms through a lower central pressure and higher wind speeds. The 10m wind speed maximum is again co-located with strong flow at upper levels suggesting an extension of the jet downwards towards the cyclone centre. The position and strength of the jet streak are very similar to those for present storms yet the wind speed is considerably higher. This can be partly due to a stronger pressure gradient but the vertical structure in Figure 5.16d also looks better organised. Larger EPT values in the core enhance vertical motion that probably results in a circulation that is capable of bringing down wind from the jet more efficiently.

5.3.2 Evolution

The development of a warm seclusion is a quick process, taking only about 12 to 24 hours for most storms. In addition to the mean storm structure at one point in time, the evolution starting 12 hours before and ending 6 hours after is studied here. Additionally, the results using different time selection criteria are presented as an indication for the different processes that are at work. Only future storms are considered here for simplicity since they are the best developed and other periods show similar results.

Being a good measure for storm intensity, minimum central MSLP is looked at first as a time selection criterion (5.17). Up to 12 hours before this point, the warm seclusion is evident in the 850hPa EPT after which it is surrounded ever further by the dry intrusion. The latter eventually cuts off the core from the warm conveyor belt, thereby separating it from its source of warm and moist air. The warm core can still partially sustain itself, slowly weakening afterwards while the favourable jet streak region wanes. A wind maximum at both 10m and 850hPa develops along the back bent front, just north of the progressing dry intrusion. It reaches a maximum 3 to 6 hours before the minimum central pressure when it becomes aligned with the jet streak. When doing the same but using the time of maximum DT_{850}, the formation of the warm seclusion is shown well (Figure 5.18). Starting as a wave in the EPT front, the head of the warm conveyor belt evolves into a warm core in just 12 hours. The cold front can be seen progressing eastward parallel to the warm front instead of moving cyclonically around the centre, consistent with the conceptual model of *Shapiro and Keyser* (1990). Again a wind maximum consistent with a sting jet forms, but less pronounced and only after the warm core has reached its maximum intensity. The pattern using PV_{775} looks very similar to this result with a slight shift of about 3 hours (not shown). Consistent with the formation of a warm core through latent heat release, the PV maximum occurs just before the temperature maximum. Finally, to complement Figure 5.16 the evolution using the maximum 10m wind speed is also presented (Figure 5.19). The results closely resemble those using 850hPa winds but look slightly less intense. Land interaction is probably interfering for some storms as they impact coastal and often mountainous regions. The highest wind speeds at 850hPa occur about 3 hours earlier which is in agreement with the idea of a sting jet developing downwards.

The general evolution of a warm seclusion can thus be sketched as follows. A baroclinically unstable wave forms along a strong surface temperature front. In the circulation of the developing wave, warm and moist air is transported northward and curls into the centre. The tip of the warm conveyor belt is then encircled by cold and dry air secluding a warm core in which latent heat release becomes important. This warms the core further while the system intensifies, reaching a maximum in low level PV. Shortly after, the warm core reaches its maximum strength while the cold air further wraps around it

in which a sting jet develops. The wind speed then reaches a maximum before the central pressure bottoms out, the warm core becomes separated from the warm conveyor belt and the storm weakens.

5.3.3 Vertical motion

Although EC-Earth is a hydrostatic model, meaning that vertical motion is not calculated explicitly, a final indication for the presence of a sting jet would be an associated region of downward motion. Therefore, the mean 500hPa vertical motion is compared to the structure of the wind field at different heights (Figure 5.20). The average is taken over all future storms, 3 hours before the maximum 10m wind speed is reached. The pattern immediately shows the warm and cold conveyor belts twisting into each other. The former ends in a cloud head expanding westward over the centre of the cyclone and outward across the colder air. The latter wraps around the warm core and ends in a region of strong downward motion which coincides with the location of the sting jet. Most of the upward motion is seen north of the centre across the active warm front, partly enhanced by dropping pressure ahead of the storm. The small area of downward motion in the core is possibly the tropopause fold reaching below 500hPa. The average pattern is not very convincing as there is a lot of variance for individual storms and the vertical motion is often strongly influenced by orography. Two specific storms (1NO and 7UK) are considered showing a region where high wind speed at different levels overlap with downward motion (Figures 5.21 and 5.22). Storm 1NO in Figure 5.21 is located between Scotland and southern Scandinavia of which the effect on vertical velocity is clearly visible. The sting jet is located at the end of the back bent front for both storms, indicated by the diverging isobars towards the north-east.

5.4 Re-intensification

In this section, the different forcings that are at work during the final intensification before storms hit Western Europe are investigated. They are studied through the parameters IVT, Z_d and Q_c representing atmospheric river strength, baroclinic instability and core moisture, respectively. As not the final stage but the preceding evolution is considered here, the subsets of post-tropical and extratropical storms are again distinguished.

5.4.1 History of forcings

The intensification period typically lasts 24 to 48 hours so the forcing parameters are only calculated during the last 72 hours up to t_0. Post tropical cyclones (Figure 5.23) initially exhibit a strong atmospheric river and high core moisture content. Both these parameters decline as the storms undergo ETT and move into a region that is colder and dryer. Meanwhile, the baroclinic instability increases after which the storm starts intensifying again. During the intensification, the IVT increases while the baroclinic instability wares off. The intensification speeds up, suggesting that the atmospheric river provides a positive feedback in this process. Although the average increase in IVT is not that much, the timing for each storm is slightly different and the individual effect is much larger as suggested by the variance during the last day. A slight increase in core moisture would be expected but the evolution is dominated by a decline as the storm moves to higher latitudes. Towards the future, the IVT considerably increases, both before and after re-intensification. Future post-tropical storms even have atmospheric rivers of comparable strength to the one during their tropical phase. A summary of the average forcing parameters during the last 48 hours before t_0 is given in Table 5.3, featuring a minor

increase in baroclinic forcing for future storms but a 50% and 43% increase in IVT and Q_c, respectively. It should be noted that, although the pressure drop is slightly smaller in the future, the minimum pressure is considerably lower which indicates that cyclones have a lower initial central pressure and/or weaken less during their ETT (see also Figure 5.4a,c).

Extratropical cyclones show a different evolution but are governed by the same processes during their intensification (Figure 5.24). At first, the IVT is much lower, especially for present storms as the system is yet to develop. Again during the early intensification, the atmospheric river develops while baroclinic instability is high after which the deepening accelerates. Both IVT and core moisture are much lower than they are for post-tropical storms with the latter showing a similar decline. As was suggested by the phase space analysis results (Figure 5.13), near future and future extratropical cyclones are partly immature tropical cyclones during their early life cycle. This is supported by the significantly higher moisture content in both the core and the warm conveyor belt. Moreover, future extratropical cyclones also exhibit a large spread in central pressure similar to post-tropical cyclones (Figure 5.23e). In fact, the evolutions of baroclinic forcing and central MSLP also look rather similar. Despite some differences between PTCs and ETCs, it can thus be concluded that future storms carry more moisture into the mid latitudes and become more tropical in nature.

	Subset	$\mathbf{IVT}$ (10^6 kg/ms)	$\mathbf{Z_d}$ (m)	$\mathbf{Q_c}$ (10^4 kg/m^2)	$\mathbf{P_{drop}}$ (hPa)
Present	All	1.47	100	0.92	36.6
	PT	1.46	96.3	1.03	30.4
	ET	1.49	108	0.71	49.1
Near Future	All	1.62	96.2	0.99	33.9
	PT	1.62	81.0	1.24	26.9
	ET	1.61	108	0.79	39.2
Future	All	2.14	96.1	1.27	37.0
	PT	2.19	89.0	1.47	28.3
	ET	2.06	107	0.99	49.9

Table 5.3: Average forcing parameters for all, post-tropical and extratropical storms in the present, near future and future climate during the last 48 hours before t_0 and the associated drop in central pressure.

5.4.2 Correlations

The length of the final intensification is not equal for all storms, causing a lot of uncertainty and probably partly obscuring the results. Instead of taking a fixed period leading to t_0, the period during which the central pressure deepens can be isolated and used for the analysis. Within the last 48 hours before t_0, the time at which a relative minimum in central pressure is obtained is taken as the starting point. The end of the intensification period is marked by the highest central pressure found within the same interval occurring at least 6 hours later. When cyclogenesis is favoured for a longer amount of time, a storm will probably deepen further. Consequently, not the average but total forcing parameters are considered now and compared to the according pressure drop. The average results are quite similar to those shown in Table 5.3 but the ratios between post-tropical and extratropical cyclones are changed. Due to a longer intensification, the latter now generally show larger parameter values but the overall trends remain the same (Table 5.4).

Parameter values for individual storms can now be compared to the associated pressure drop during intensification. This is done for all 3 forcing parameters as well as the normalised sum of IVT and Z_d (Figure 5.25), where a distinction is made between the different periods and subsets. Overall, atmospheric river strength and baroclinic forcing are well correlated with the pressure drop while core moisture is not. The correlation between $IVT + Z_d$ and the intensification is higher than the one for both of the individual forcings, indicating that their combined presence is important. Looking at separate subsets it can be concluded that the intensification is connected more strongly with the atmospheric river strength and core moisture for extratropical cyclones. The latter is probably due to the formation of a warm core during the warm seclusion development, carrying more moisture for stronger storms.

The correlation coefficients shown in Figure 5.25 can be calculated for each period and different subsets (Table 5.5). Results for all storms are also shown but the parameter values are now normalised for each period to eliminate any trends. Although clear differences were seen for the average forcings, only minor changes occur for the correlations indicating that the results are quite robust. An additional set of storms is made up by those that undergo rapid intensification (denoted by 'RI'), characterised by an average deepening rate of at least 2hPa/3h. Mainly the IVT and to a lesser extent the core moisture appear to be important for these rapidly intensifying systems. This is done to exclude storms that show little or no intensification during the last days before they hit Western Europe. Overall, core moisture is badly correlated with the pressure drop while all parameters are for storms occurring in the near future. The former was already observed in the scatter plot and indicates that the amount of moisture a cyclone carries within its inner circulation is not important for the intensification. The atmospheric river, on the other hand, is crucial for the deepening by providing warm and moist air to the transformed core. The absence of strong correlations for near future cyclones is more surprising, as overall good results are seen for the present and future simulations. When looking only at rapidly deepening storms, correlations slightly improve overall but are considerably higher for the near future. It appears that several of those cyclones undergo little to no re-intensification. Separating rapidly intensifying storms from others shows a different pattern in which the pressure drop seems hardly related to the forcings that are present for the latter (Figure 5.26).

	Subset	$\mathbf{IVT}$ (10^6 kg/ms)	$\mathbf{Z_d}$ (m)	$\mathbf{Q_c}$ (10^4 kg/m^2)	$\mathbf{P_{drop}}$ (hPa)
Present	All	9.05	649	6.29	36.2
	PT	8.03	564	6.23	29.8
	ET	11.1	820	6.39	49.1
Near Future	All	9.19	619	6.68	33.5
	PT	7.38	477	7.08	26.1
	ET	10.6	728	6.37	39.2
Future	All	12.7	618	8.87	37.0
	PT	12.4	529	9.68	28.2
	ET	13.1	748	7.68	49.9

Table 5.4: Average forcing parameters and central pressure drop for all, post-tropical and extratropical storms in the present, near future and future climate during the intensification period within the last 48 hours before t_0.

	Subset	$\mathbf{IVT}$ (10^6 kg/ms)	$\mathbf{Z_d}$ (m)	$\mathbf{Q_c}$ (10^4 kg/m^2)	$IVT + Z_d$
Present	All	**0.82**	**0.73**	**0.50**	**0.88**
	PT	**0.86**	**0.82**	**0.55**	**0.92**
	ET	0.70	0.04	0.67	0.66
Near Future	All	**0.19**	**0.41**	-0.21	0.33
	PT	-0.36	0.16	-0.43	-0.11
	ET	0.44	0.46	0.27	**0.53**
Future	All	**0.50**	**0.65**	0.13	**0.68**
	PT	**0.52**	**0.48**	0.33	**0.60**
	ET	**0.67**	**0.64**	**0.55**	**0.74**
All	All	**0.47**	**0.59**	0.10	**0.61**
	PT	**0.39**	**0.49**	0.20	**0.51**
	ET	**0.58**	**0.48**	**0.45**	**0.64**
All RI	All	**0.56**	**0.57**	**0.27**	**0.65**
	PT	**0.60**	**0.47**	0.36	**0.64**
	ET	**0.62**	**0.56**	**0.48**	**0.70**

Table 5.5: Correlations between the different summed forcings and the associated pressure drop during the intensification period (max 48h). Font styles indicate significance levels (<90%, 90%, **95%** and **99%**) using Student's t-test of correlation (Student, 1908).

5.4.3 Hybrid storms

During ETT, PTCs have a hybrid structure as they exhibit properties of both tropical and extratropical cyclones. While most storms complete this ETT and re-intensify as initially as cold core systems, some of them never do so. A good example is near future storm 5UK which shows only small changes in central pressure during the 4 days leading to t_0 (Figure 5.27). During this period, the cyclone retains a deep warm core and a strong PV column before finally evolving into a shallow warm core in the last 24 hours. The storm still reaches Western Europe as a potent system but never looses its warm core and does not weaken substantially prior to a possible re-intensification. This is confirmed by the according Hart diagram (Figure 5.28) which shows that the storm never acquires a deep cold core. Generally, cyclones are considered to be hybrid when they have an asymmetric warm core (*Hart*, 2003), reflected by both high B and V_L^T values. Storms that have little or no re-intensification are excluded by the rapid intensification selection discussed above. Looking at scatter plots for post tropical (Figure 5.29) and extratropical (Figure 5.30) storms separately reveals some significant differences. While the pattern hardly changes for the latter, the correlation with IVT increases strongly for PTCs when only those rapidly intensifying are considered.

A principal components analysis is performed for the different periods and subsets to disentangle the seemingly different relations present in the scatter plots (Table 5.6). For present storms, a dominant relation is present with a positive correlation between all three forcing parameters and the central pressure drop. This first empirical orthogonal function (EOF) represents 71% of the variance while the second one only explains 15. Especially in the near future, the second EOF becomes more pronounced and shows a strong reverse relationship with core moisture. These are hybrid storms whose core remains warm in nature resulting in high Q_c values and little to no pressure drop. Other cyclones loose their warm core during the transitioning stage after which they intensify again, resulting in a negative correl-

	EOF	Var. (%)	$\mathbf{P_{drop}}$ (hPa)	$\mathbf{IVT}$ (10^6kg/ms)	$\mathbf{Z_d}$ (m)	$\mathbf{Q_c}$ (10^4kg/m^2)
Present	1	71	0.54	0.53	0.48	0.44
	2	15	0.30	-0.16	0.55	-0.76
Near Future	1	53	0.22	0.60	0.59	0.50
	2	31	-0.82	0.08	-0.23	0.52
Future	1	55	0.55	0.56	0.52	0.32
	2	28	-0.33	0.30	-0.45	0.77
All	**1**	**56**	**0.50**	**0.57**	**0.51**	**0.40**
	2	**26**	**-0.48**	**0.28**	**-0.42**	**0.72**
All PT	1	54	0.47	0.59	0.48	0.44
	2	26	-0.50	0.27	-0.47	0.68
All ET	1	67	0.49	0.51	0.46	0.53
	2	15	0.32	0.51	-0.79	0.11

Table 5.6: First 2 empirical orthogonal functions, their explained variance and coefficients for different periods and subsets of storms.

ation between core moisture and pressure drop during the hybrid phase. This EOF representing hybrid systems is present in all periods and shows that the deepening is mainly due to baroclinic instability. This is consistent with the early peak in Z_d seen in the forcing history (Figures 5.23 and 5.24). Hybrid storms are clearly present among PTCs in the future results as well but are probably masked by the large amount of conventionally transitioning tropical cyclones. The increased length of the ETT possibly adds to the contribution of the second EOF. No such hybrid properties are seen for extratropical cyclones since they do not have a remnant warm core, reflected by a very different second EOF.

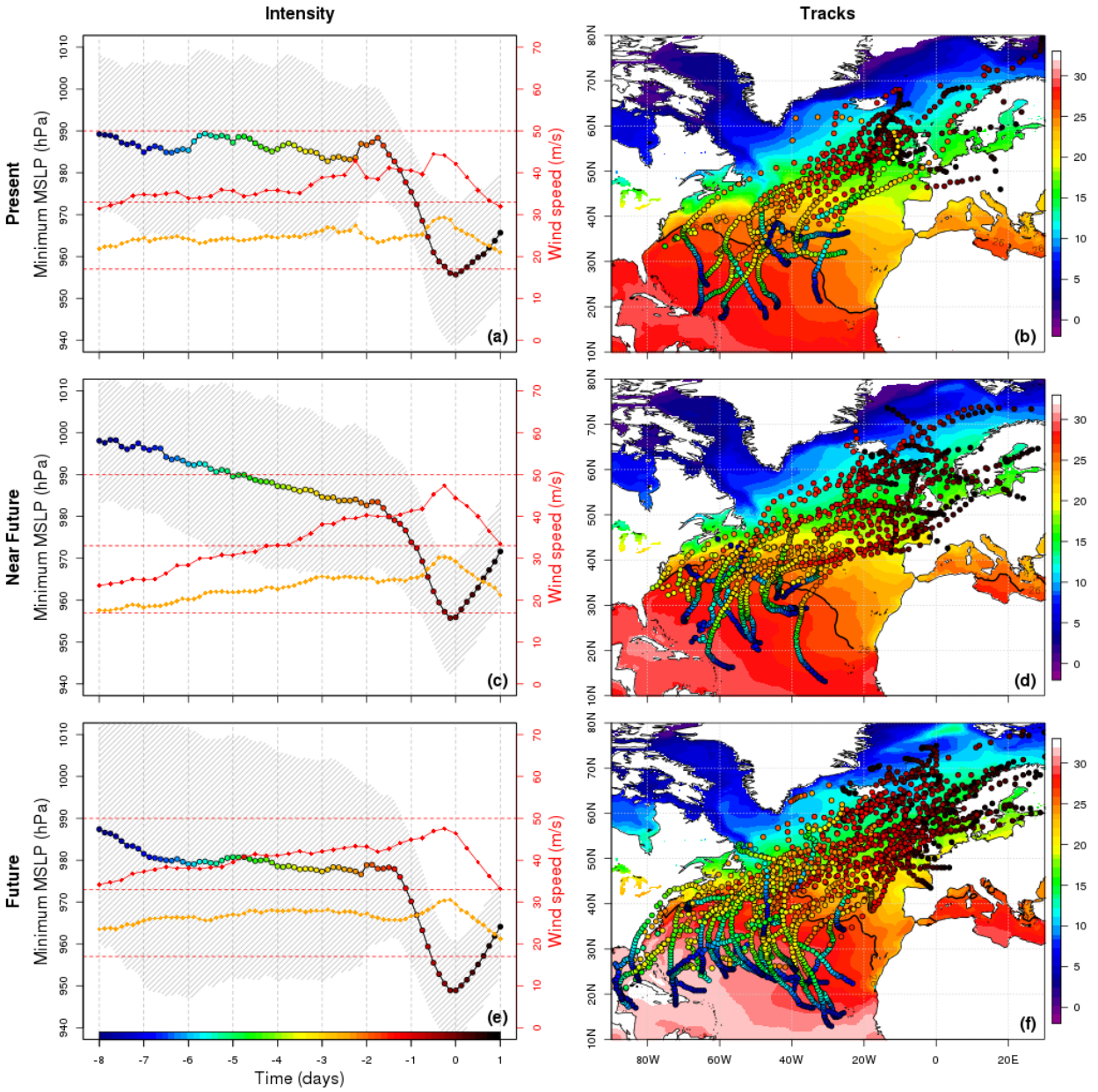

Figure 5.1: Intensity measures (left; minimum MSLP in black, maximum 10m wind speed in orange and 850hPa wind speed in red) and tracks (right) of severe Autumn storms impacting Western Europe with a tropical origin. Hatching shows the variance of the central MSLP of the selected set of storms. Colours filling the black circles indicate the time relative to t_0 in days. The background pattern in the right panels depicts the mean SST of the according period in °C.

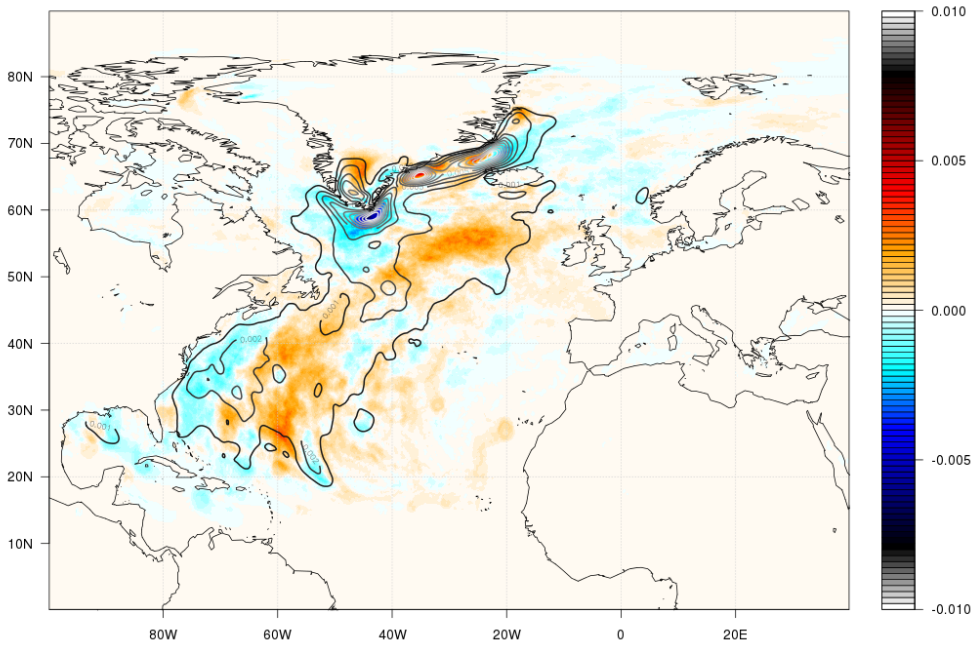

Figure 5.2: Frequency (contours, normalised) of the 3 hourly 10m wind speed exceeding Beaufort 10 (24.5 m/s) during the months August through November for the present climate simulation. Shadings show changes between the near future and present climate.

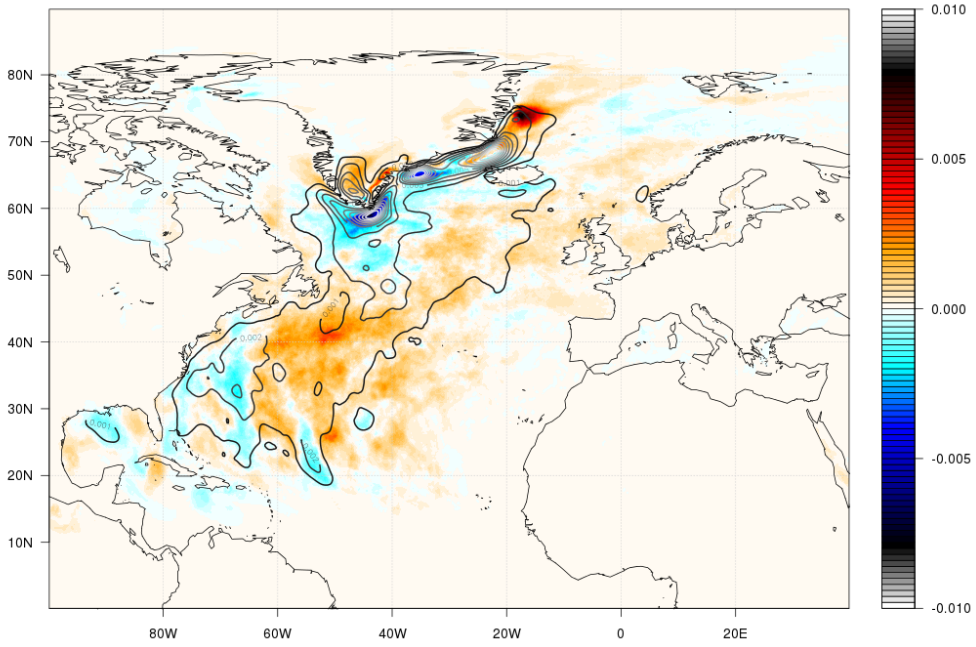

Figure 5.3: Same as Figure 5.2 for the present and future climate.

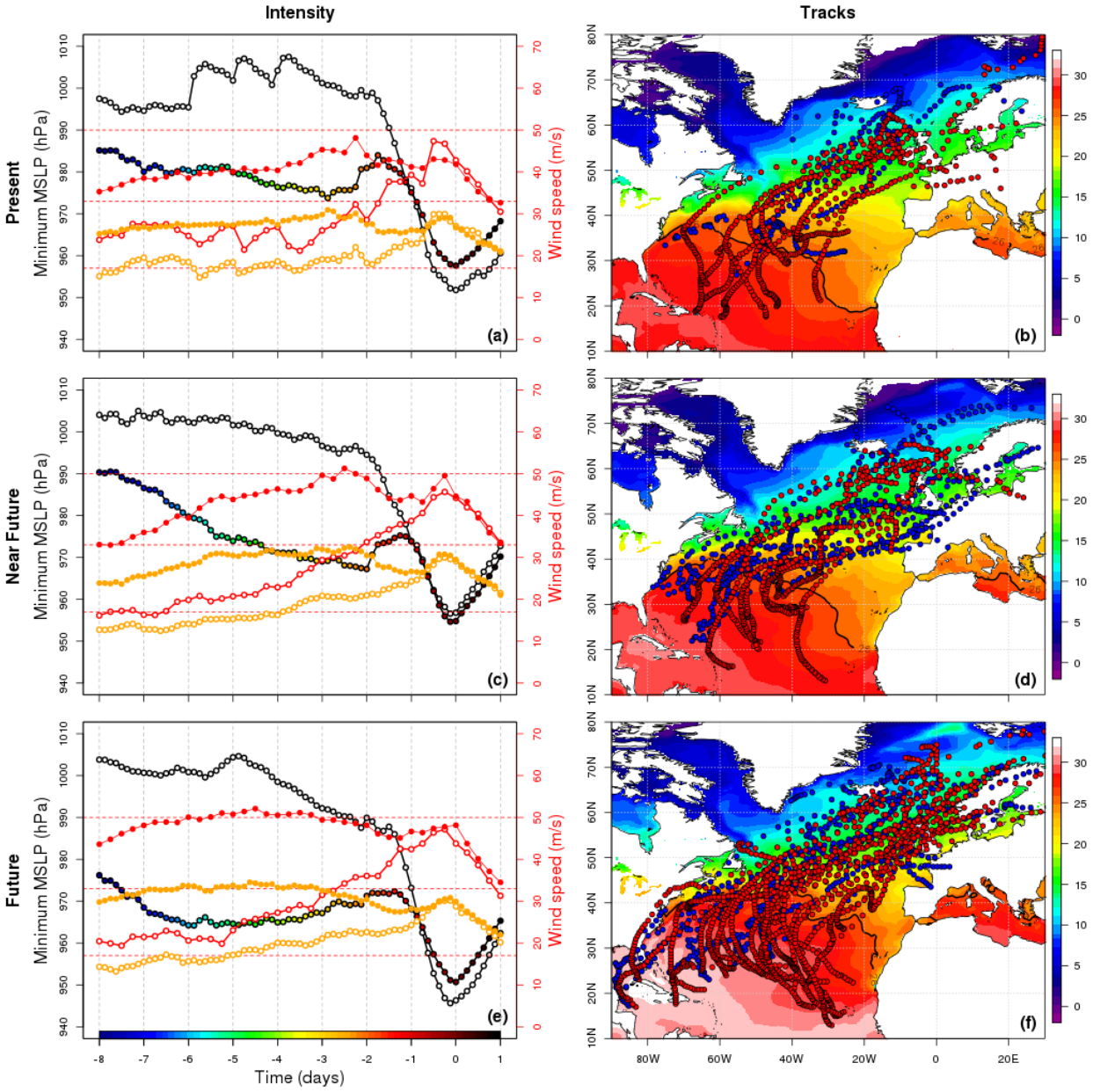

Figure 5.4: Similar to Figure 5.1 but discerning post-tropical (left: filled, right: red markers) from extratropical storms (left: open, right: blue markers).

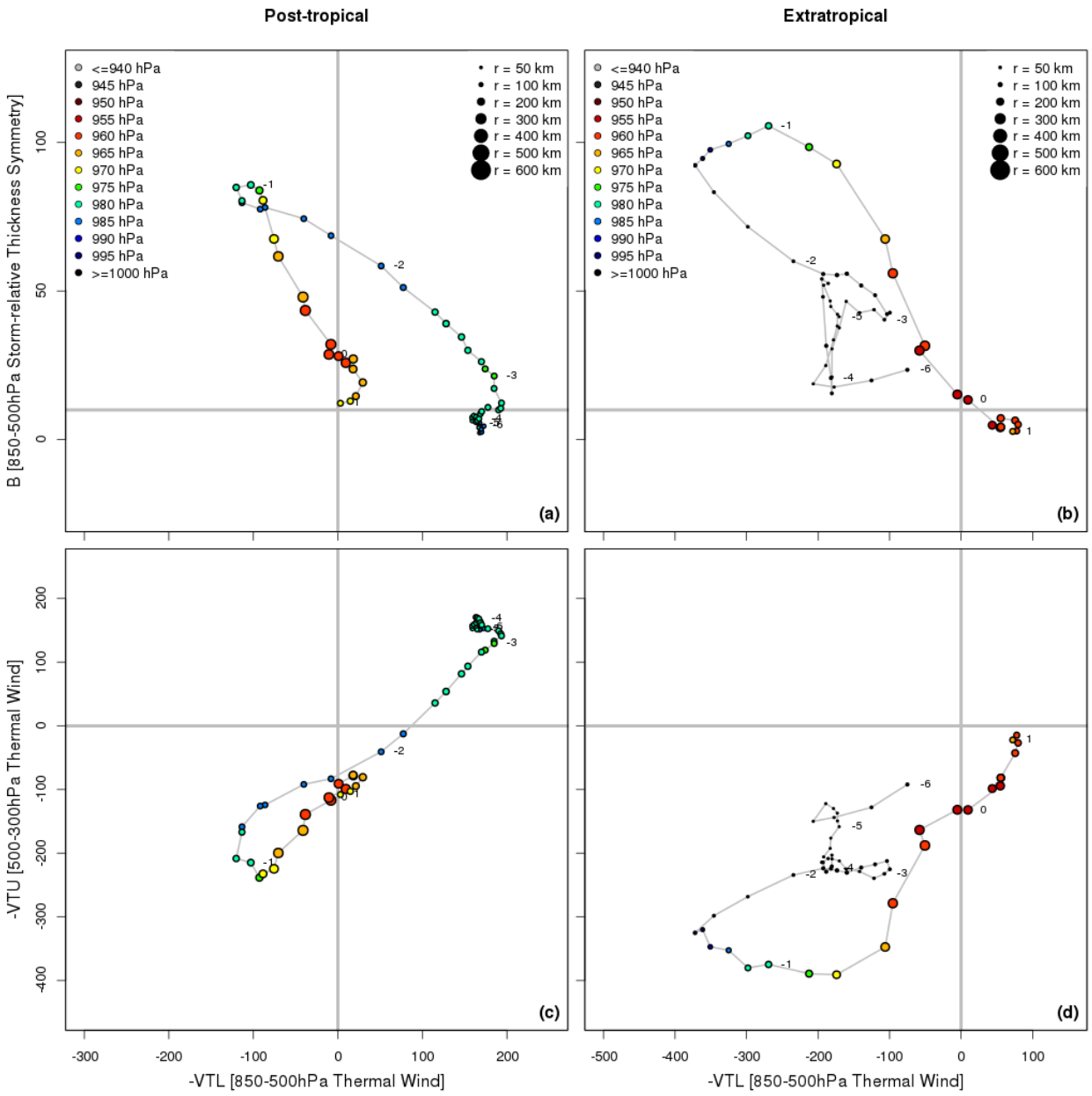

Figure 5.5: Average Hart diagrams for post-tropical (left) and extratropical (right) cyclones in the present climate. Legends and set-up are similar to those used in Figures 4.2 and 4.3.

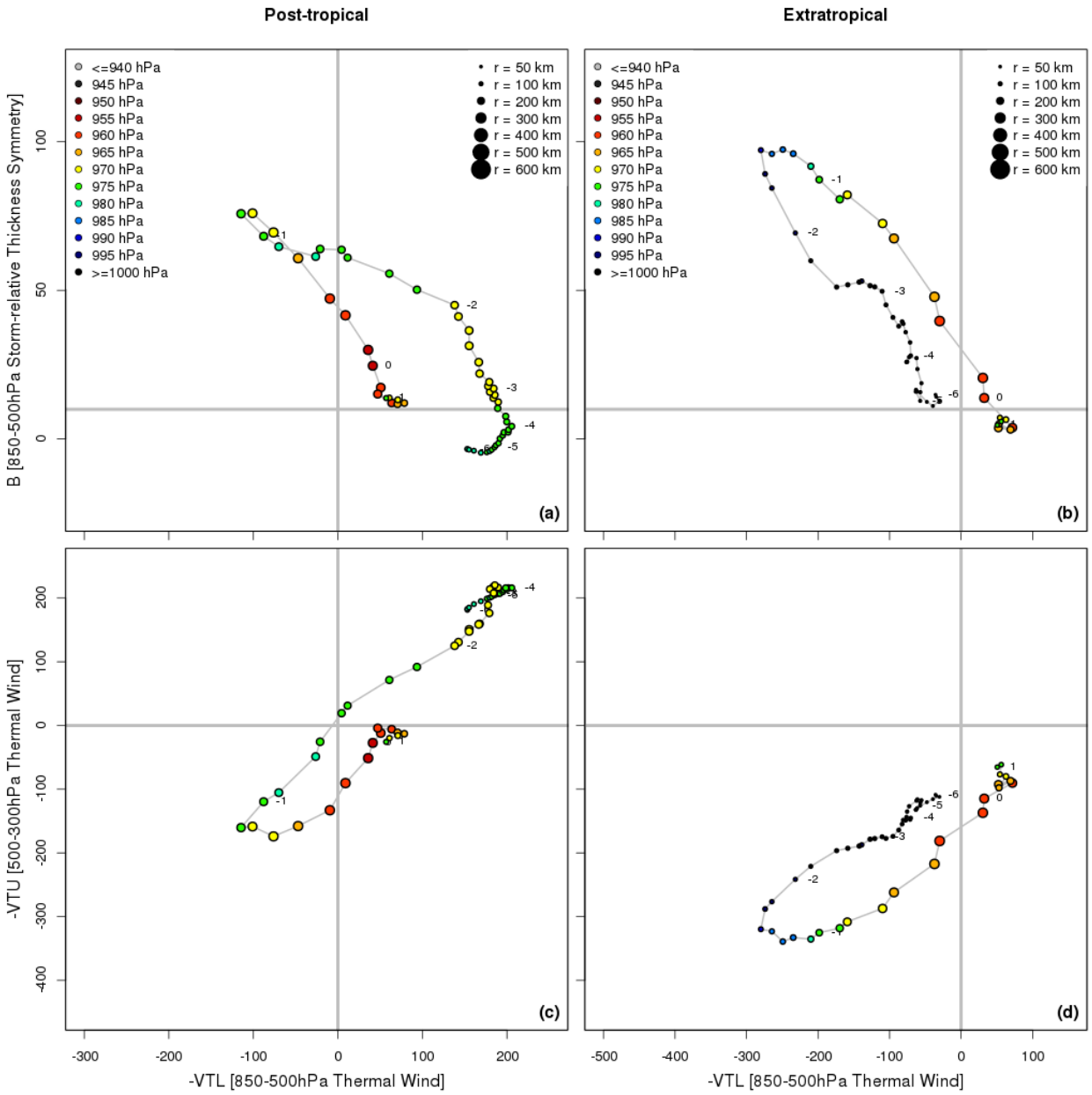

Figure 5.6: Same as Figure 5.5 but for storms in the near future.

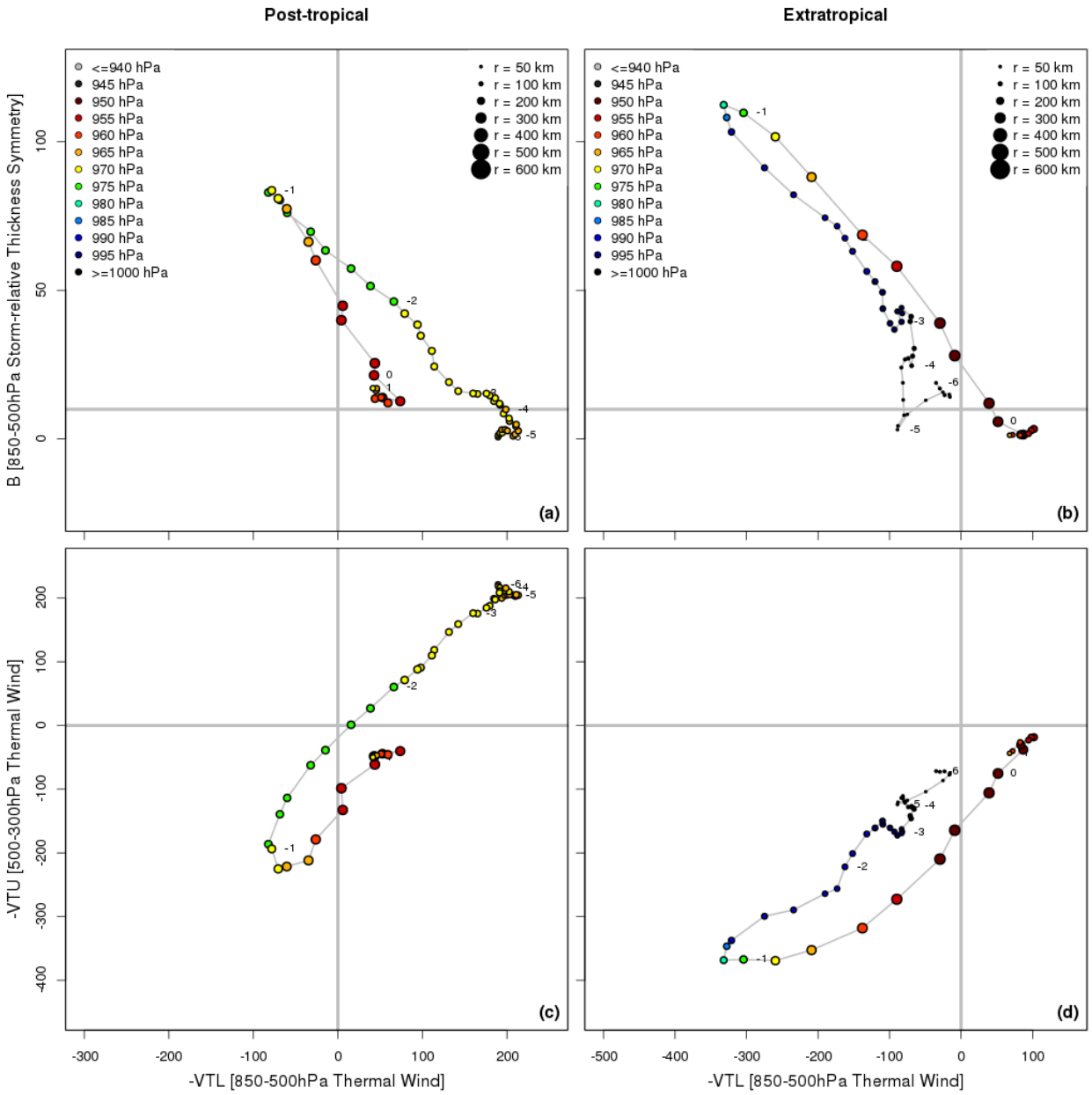

Figure 5.7: Same as Figure 5.5 but for storms in the future.

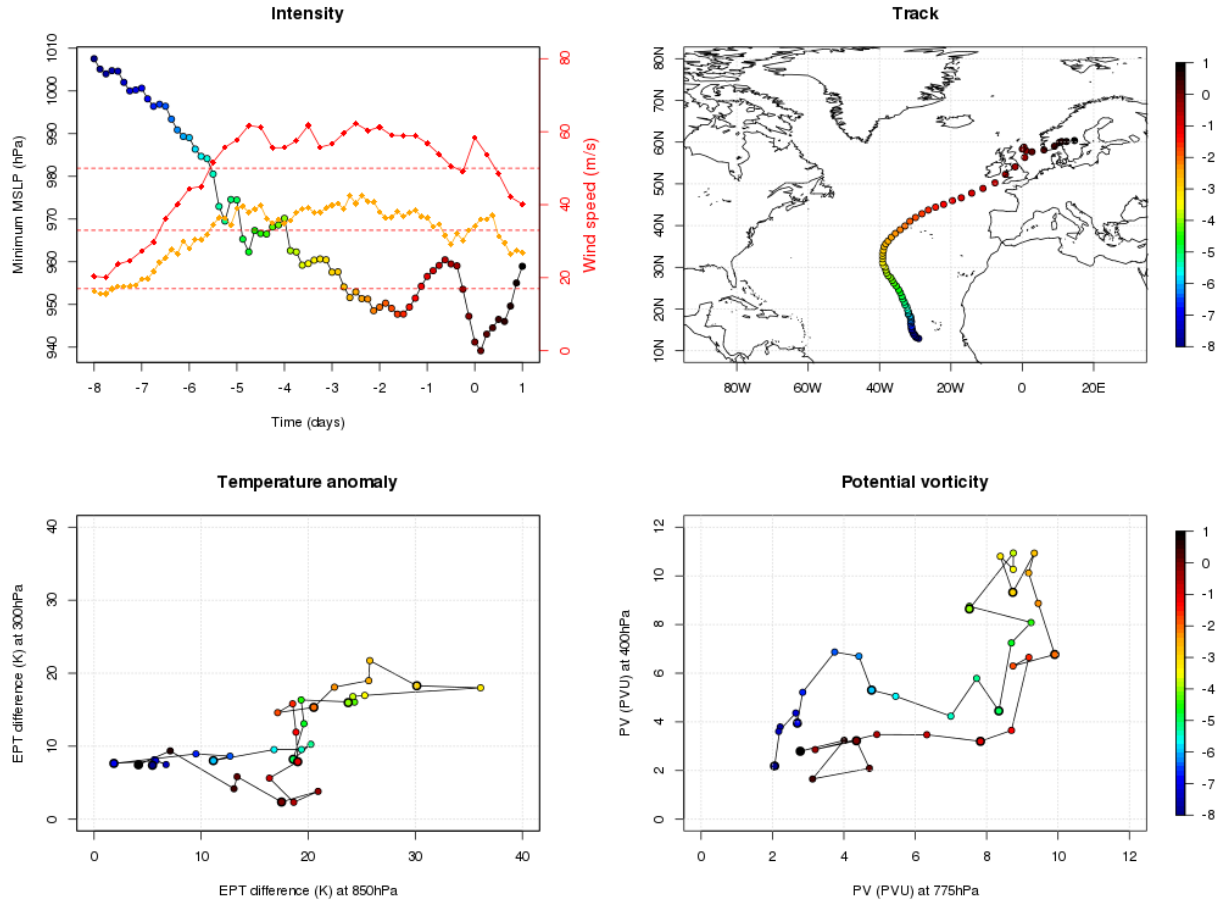

Figure 5.8: Intensity (Minimum MSLP in black, 10m wind speed in orange and 850hPa wind speed in red), track and both parts of the phase space analysis for Amy. Colour fills indicate the time relative to t_0 in days and in the phase space diagrams thick markers denote 24 hour periods.

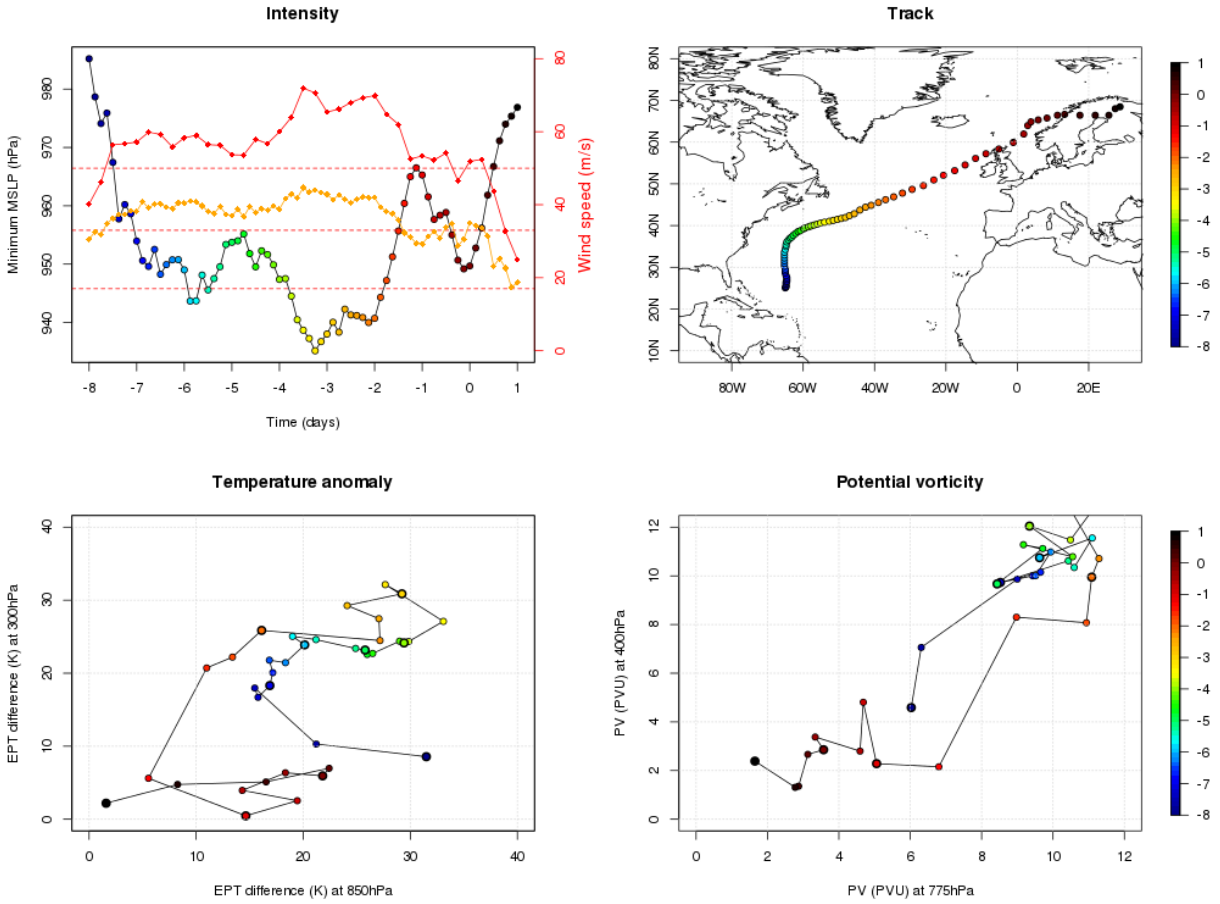

Figure 5.9: Same as Figure 5.8 but for storm 1NO, a typical post-tropical cyclone.

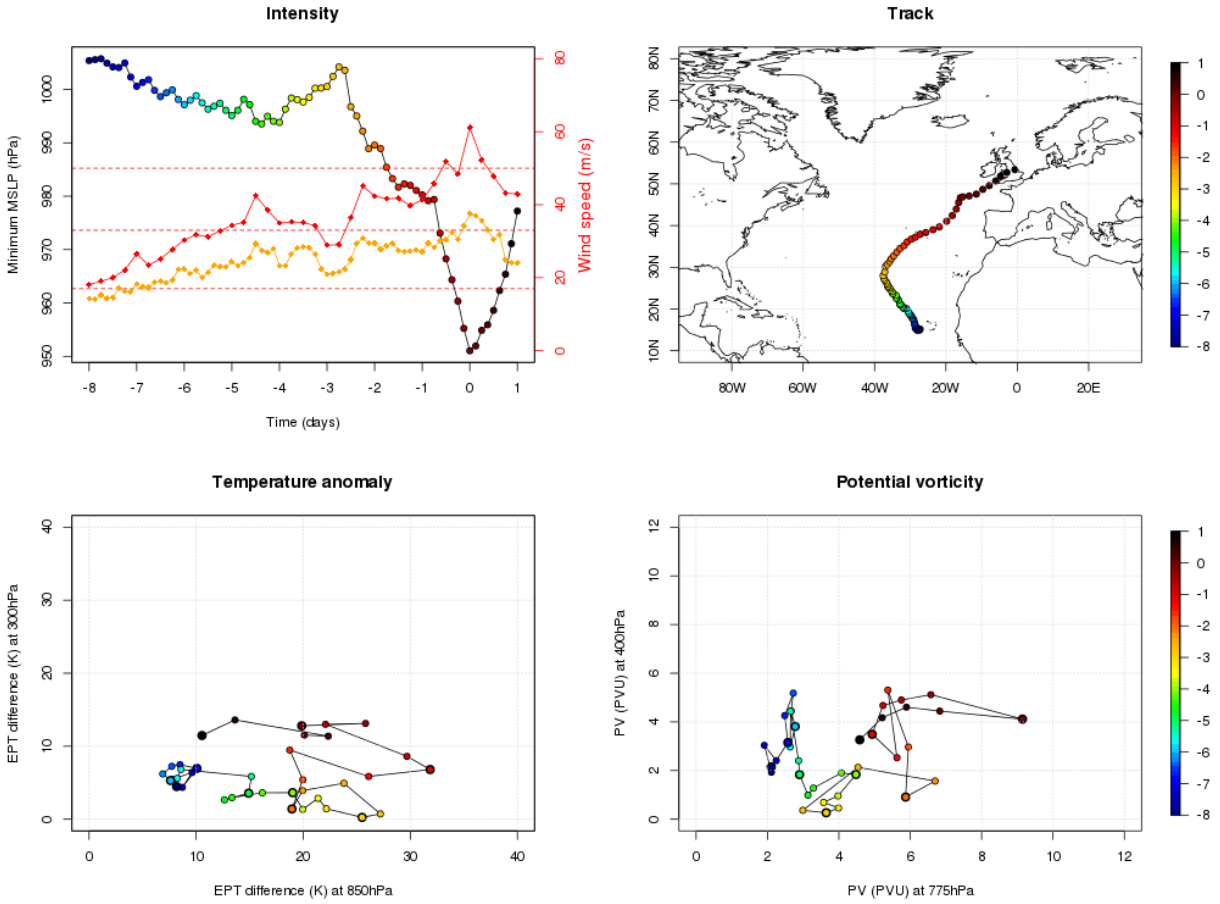

Figure 5.10: Same as Figure 5.8 but for storm 1BI, a tropical or hybrid cyclone.

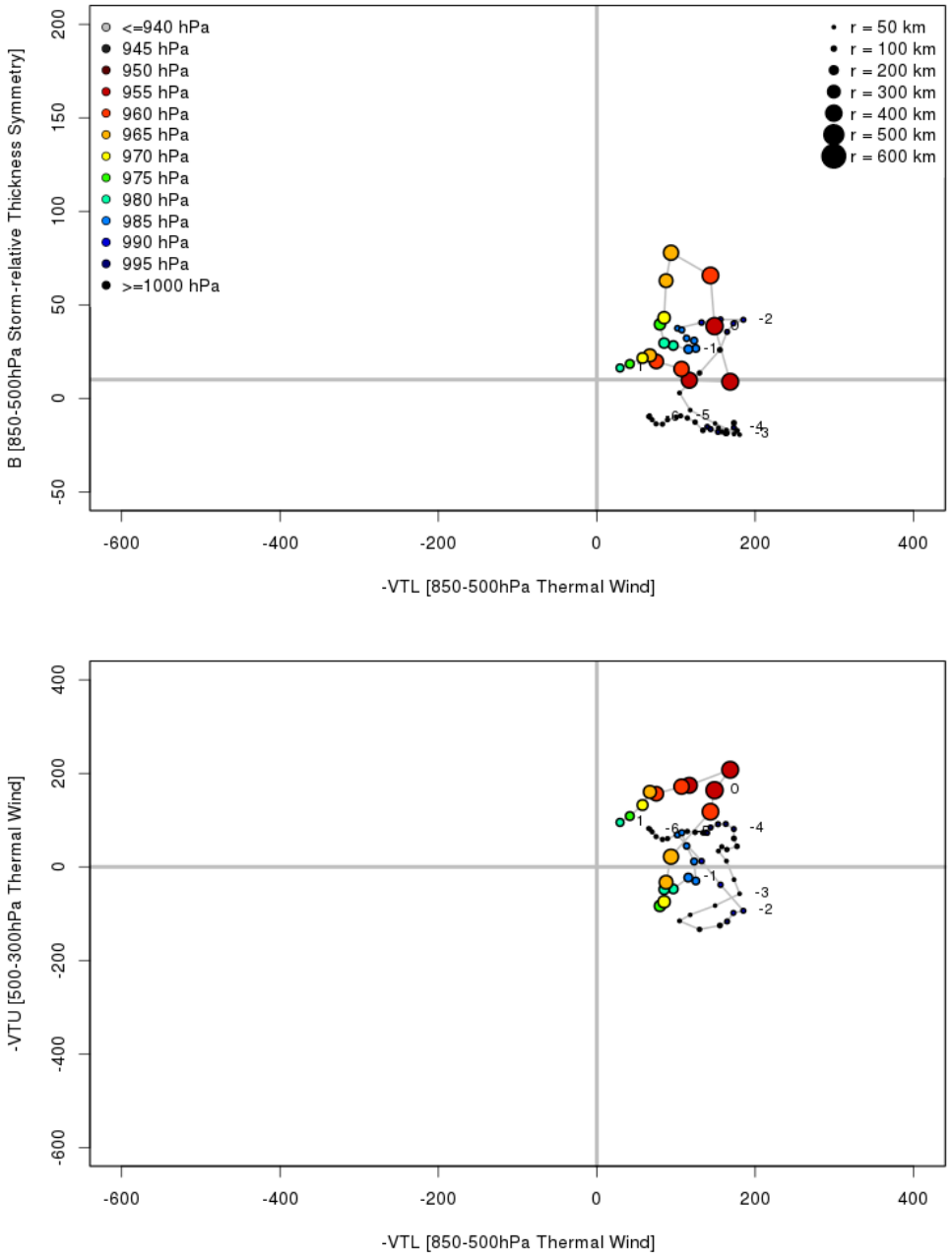

Figure 5.11: Hart diagram for storm 1BI, legends and axes are similar to those of Figure 4.3.

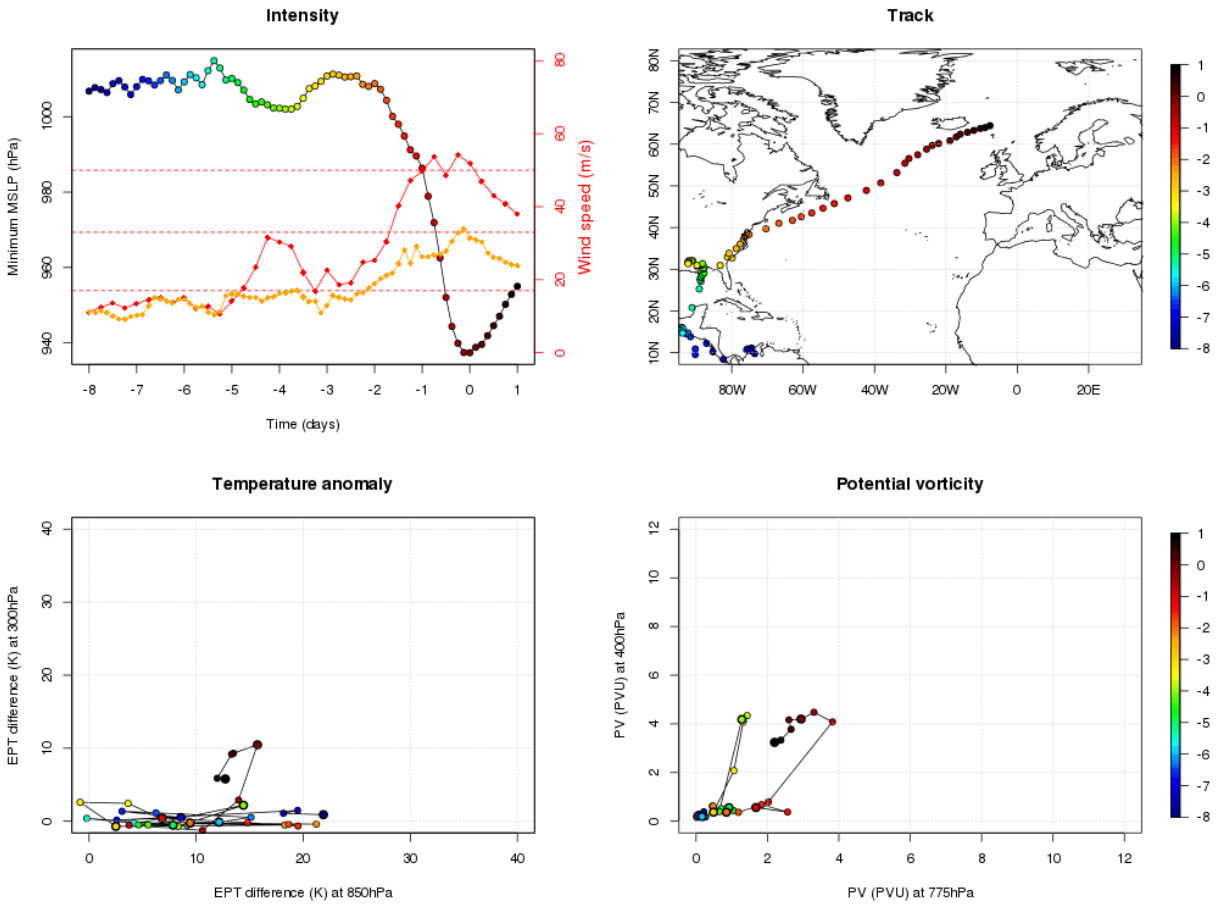

Figure 5.12: Same as Figure 5.8 but for storm 10UK, a typical extratropical cyclone.

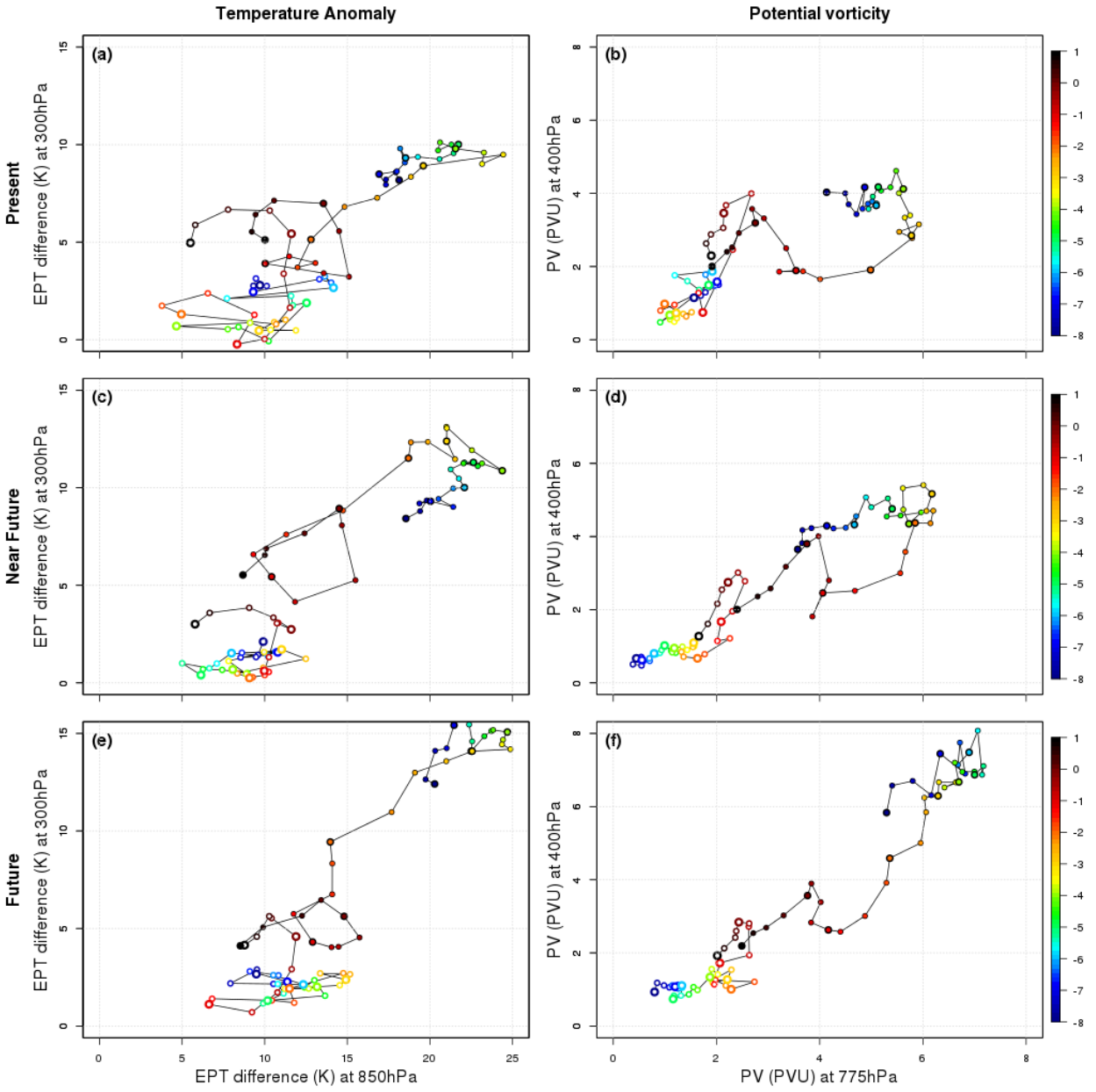

Figure 5.13: Phase space diagrams of EPT (left) and PV (right) for the present (a,b), near future (c,d) and future (e,f) climate. ETCs are represented by open markers, PTCs by filled ones and colours indicate the time relative to t_0 in days.

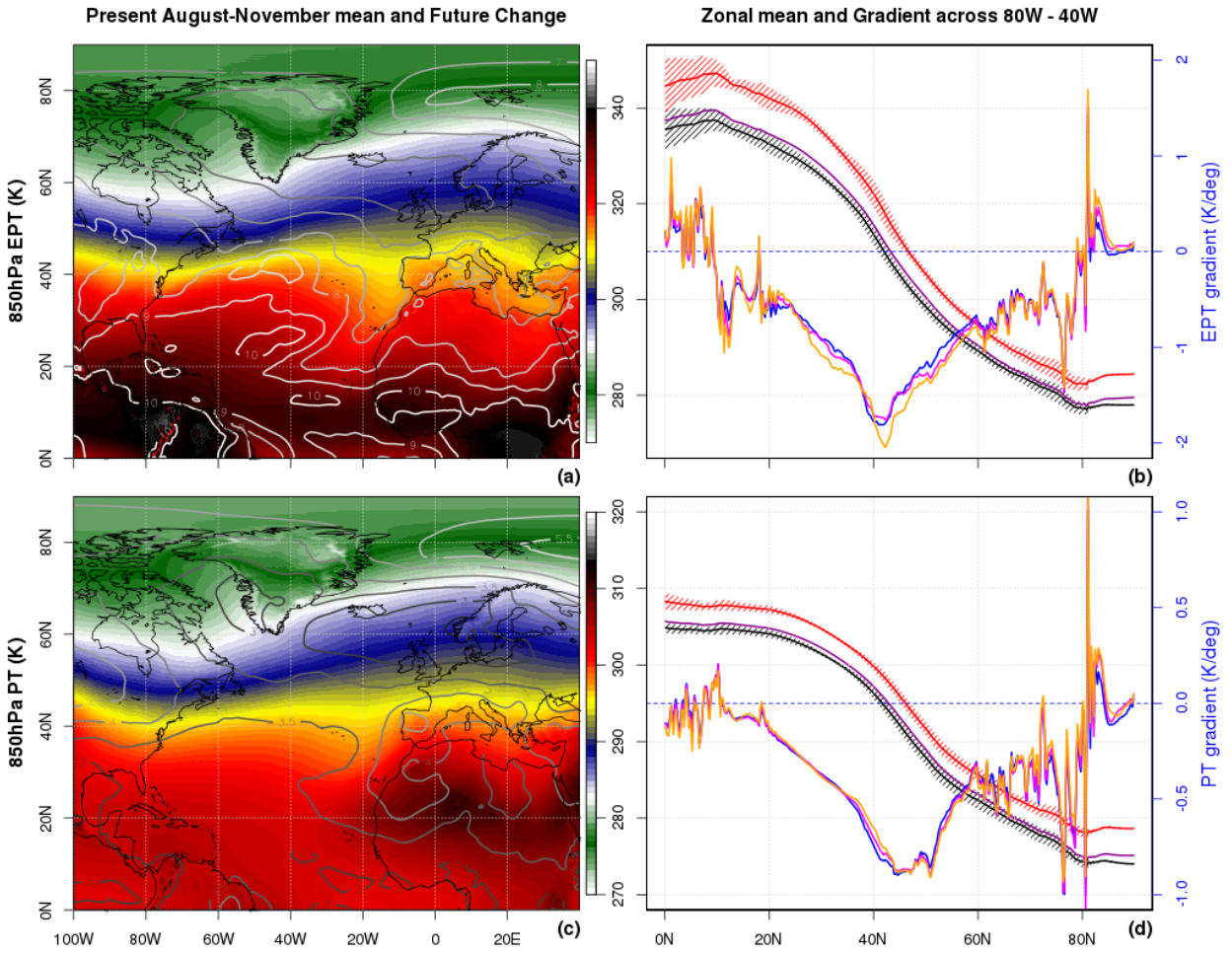

Figure 5.14: Present August-November mean (shading) and future change (contours) of 850hPa EPT (a) and PT (c). In the right panels is the 80°W-40°W zonal mean 850hPa EPT (b) and PT (d) for the present (black), near future (purple) and future (red) along with the gradients in blue, pink and orange, respectively. The variance of the zonal mean is given only for the present and future result to avoid too much overlap.

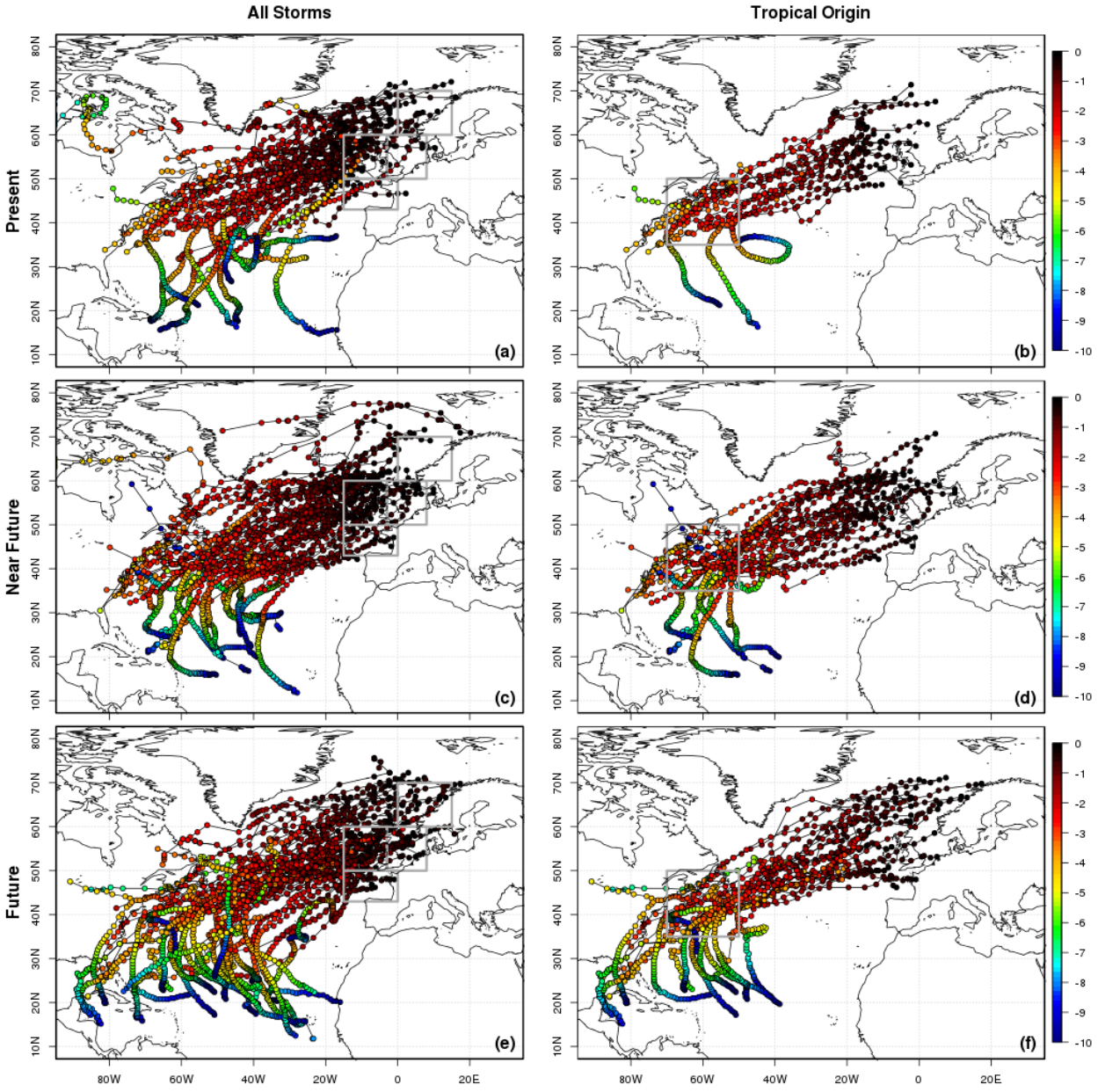

Figure 5.15: Tracks of all severe Autumn storms impacting Western Europe (left) and those also crossing the north-eastern Gulf Stream region (35°N-50°N, 70°W-50°W, right) for the present (a,b), near future (c,d) and future (e,f). Colours indicate the time relative to the point where the wind criterion (28.4 m/s) was met, in days.

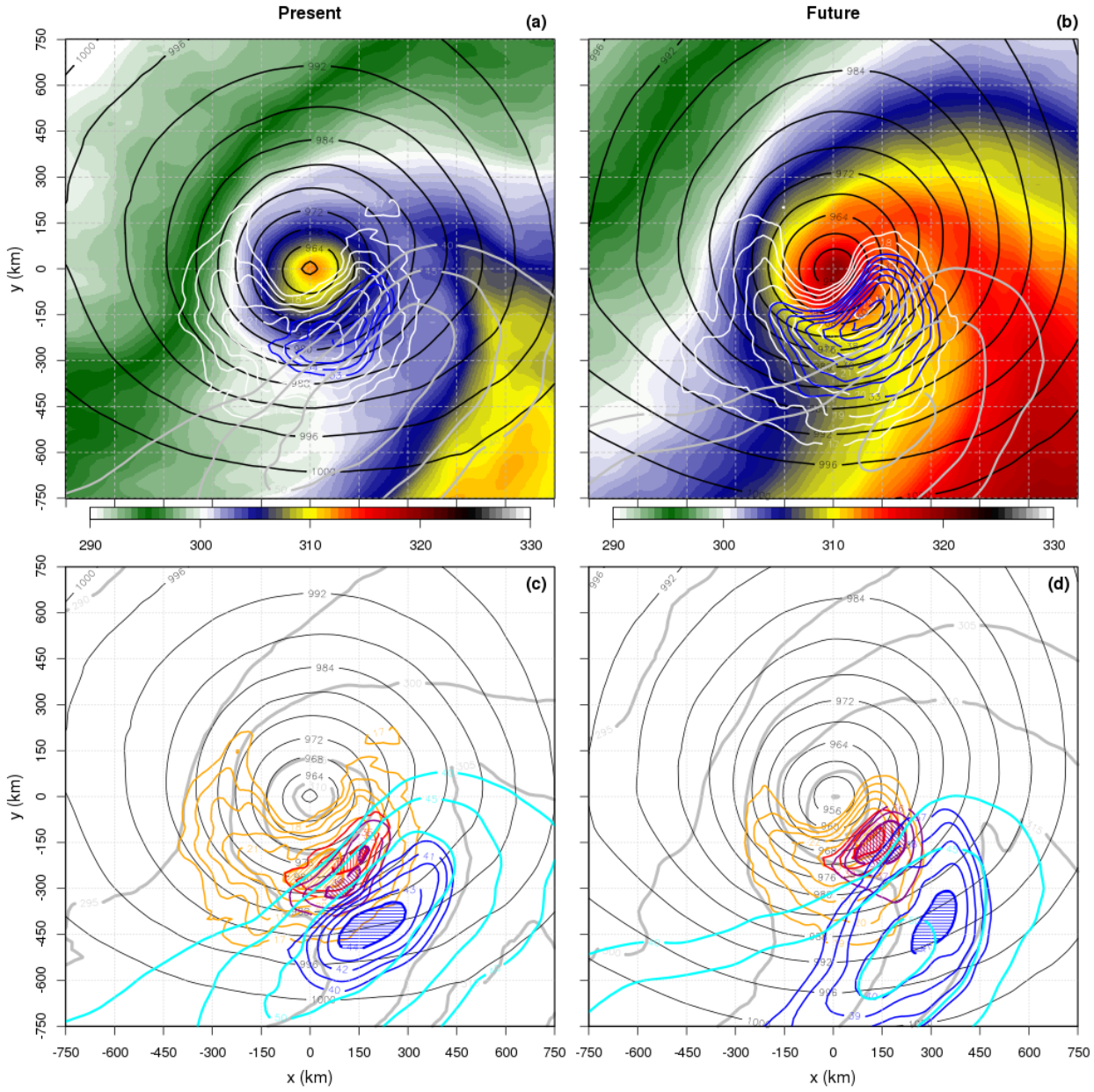

Figure 5.16: Mean 850hPa EPT (K, shading), MSLP (hPa, black) and wind speed (m/s, white: 10m, blue: 850hPa and gray: 300hPa) for all present (a) and future (b) storms at the time of maximum 850hPa wind. Lower panels depict the mean horizontal wind speed at 10m (orange), 850hPa (red), 700hPa (purple), 500hPa (blue) and 300hPa (cyan) along with contours of 850hPa EPT (gray) and MSLP (black) for present (c) and future (d) storms.

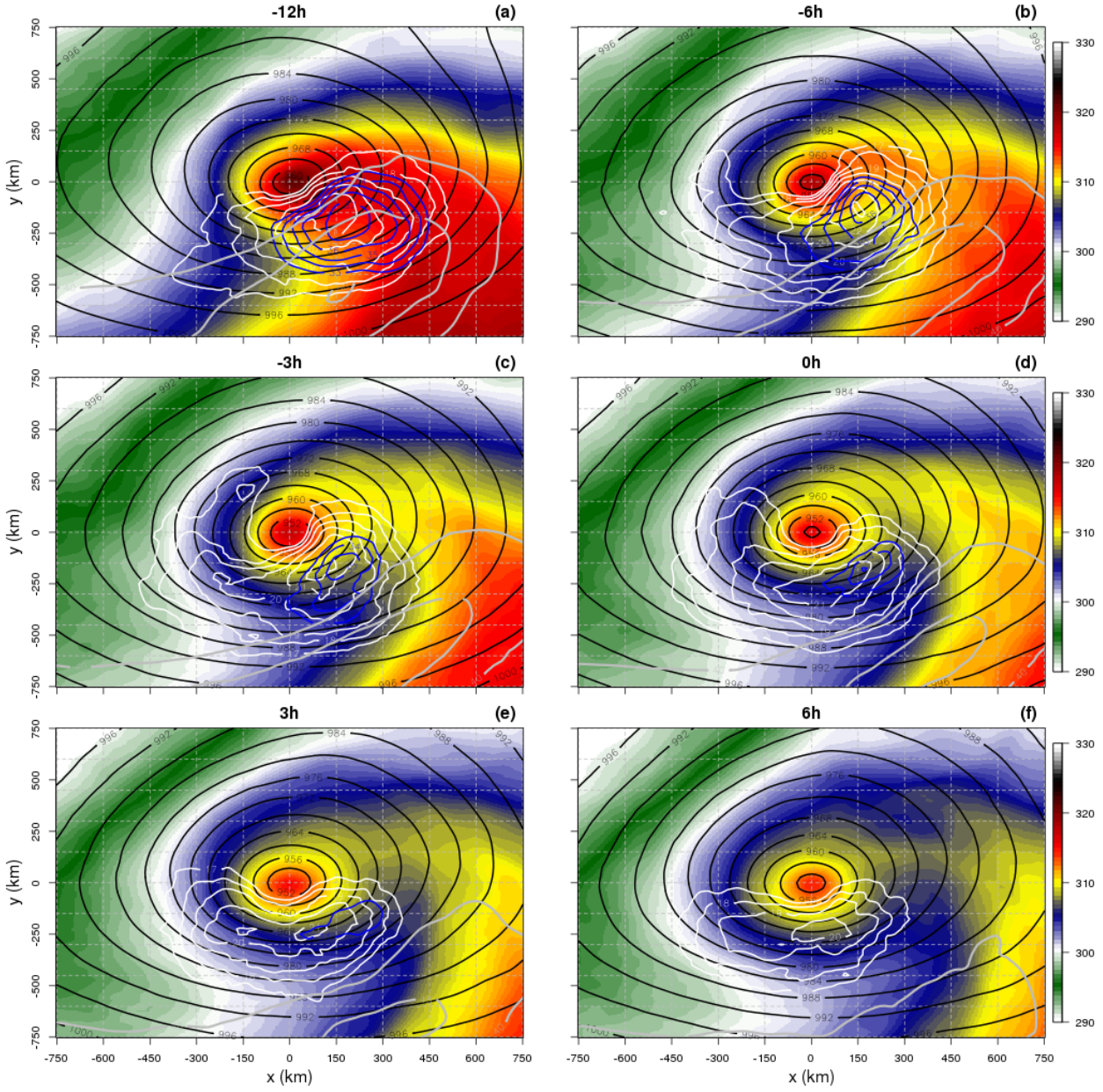

Figure 5.17: Mean 850hPa EPT (K, shading), MSLP (hPa, black) and wind speed (m/s, white: 10m, blue: 850hPa and gray: 300hPa) for all future storms using the minimum central MSLP criterion. Time relative to the selected moment is indicated above each panel in hours.

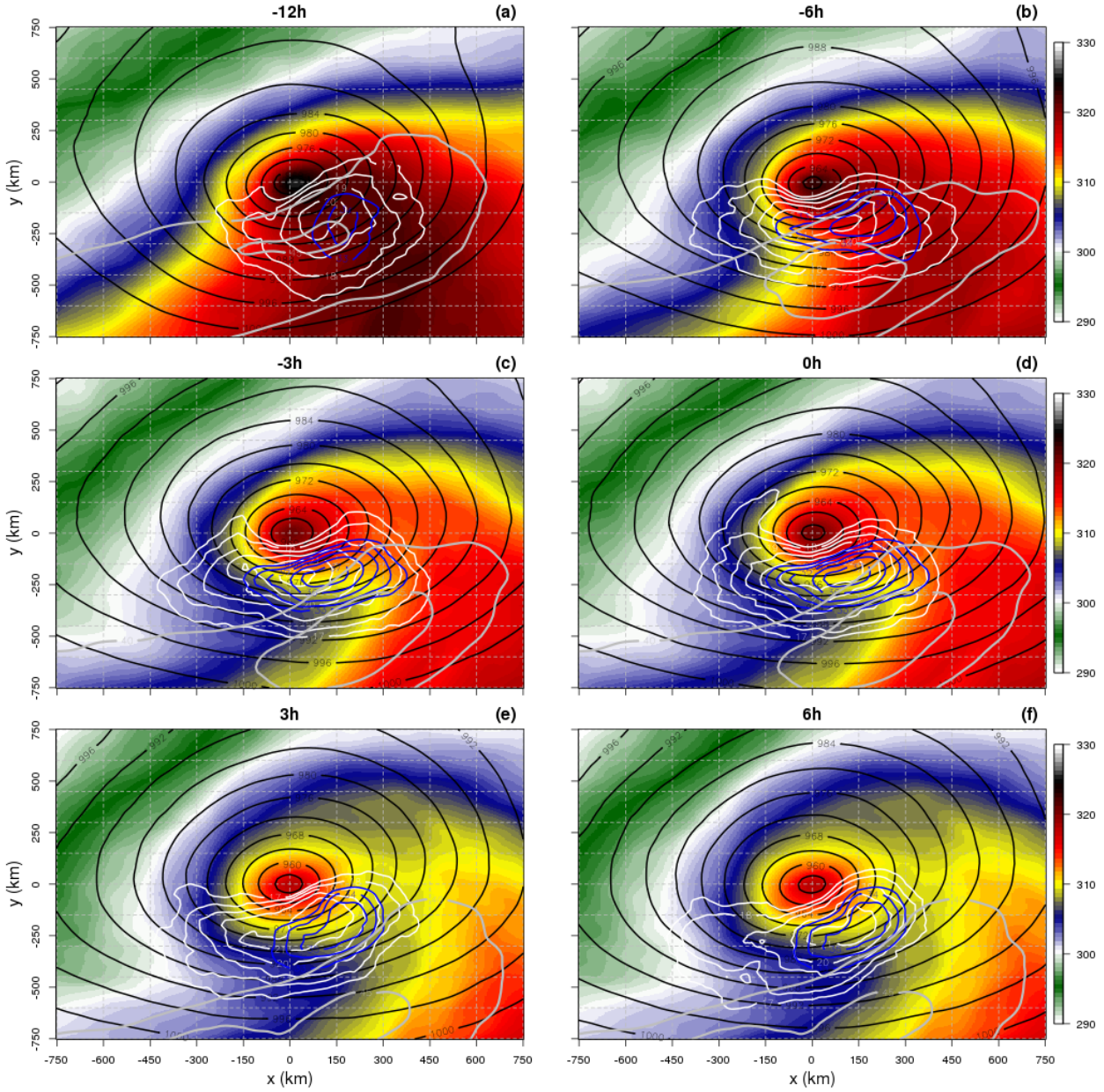

Figure 5.18: Same as for Figure 5.18 but for maximum DT_{850}.

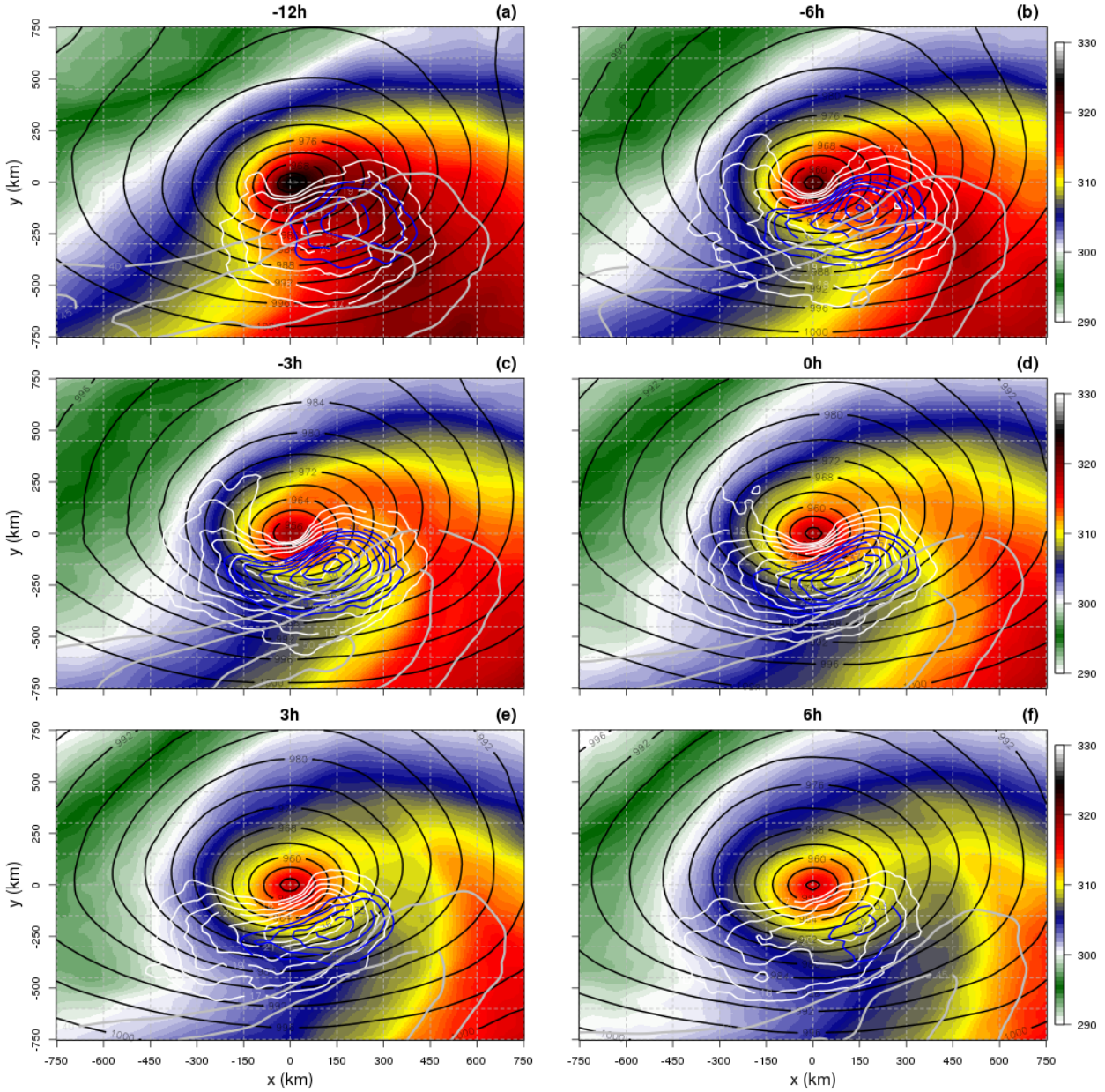

Figure 5.19: Same as for Figure 5.18 but for maximum 10m wind.

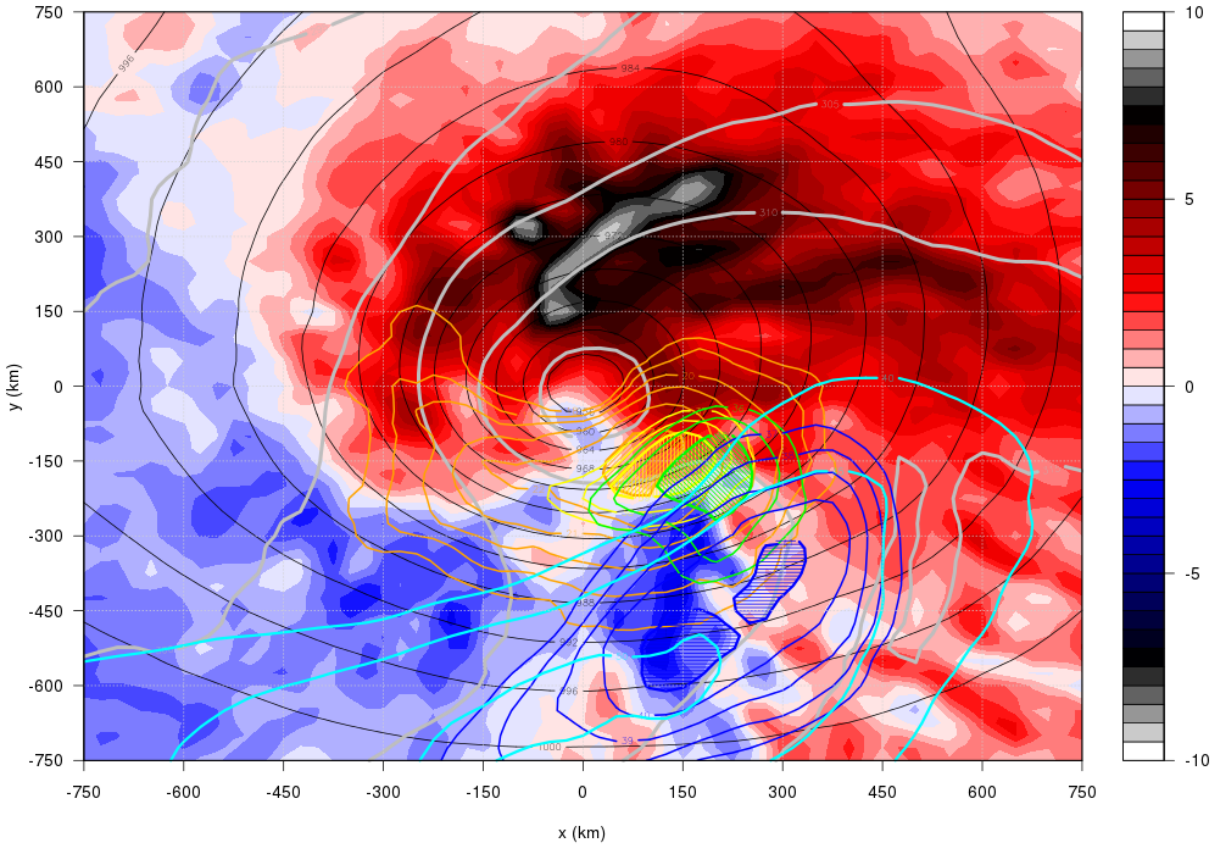

Figure 5.20: Mean 500hPa vertical motion (shading, m/s), MSLP (black, hPa), 850hPa ET (gray, K) and horizontal wind speed (m/s, orange: 10m, yellow: 850hPa, green: 700hPa, blue: 500hPa and cyan: 300hPa) for all future storms 3 hours before the highest 10m wind speed occurs.

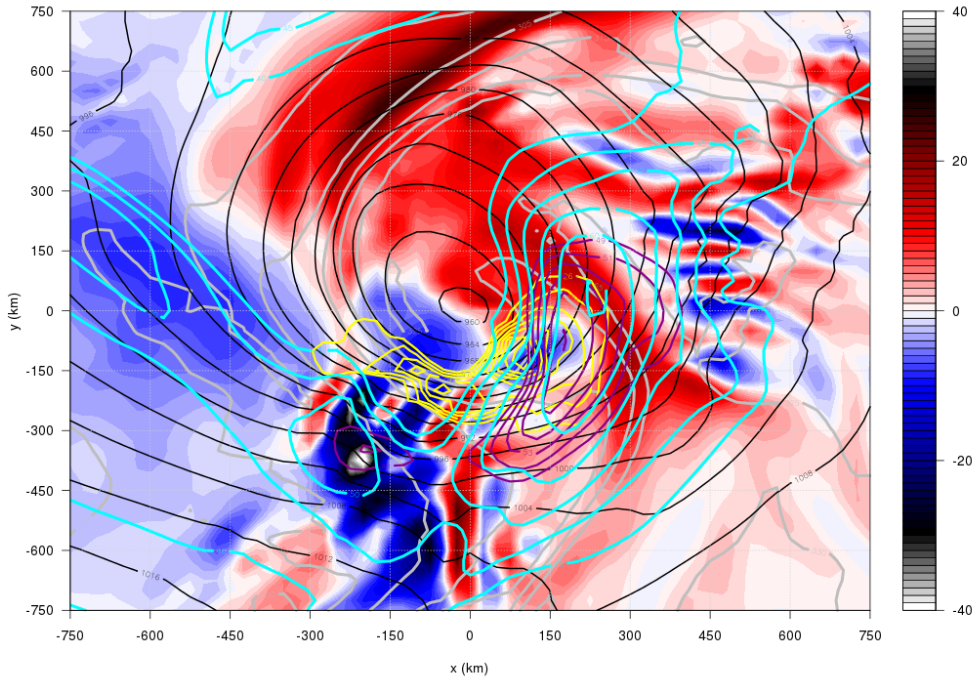

Figure 5.21: 500hPa vertical motion (shading, cm/s), MSLP (black, hPa) and horizontal wind speed (yellow: 10m, 500hPa: purple and 300hPa: cyan) for future storm 1NO 12 hours before t_0.

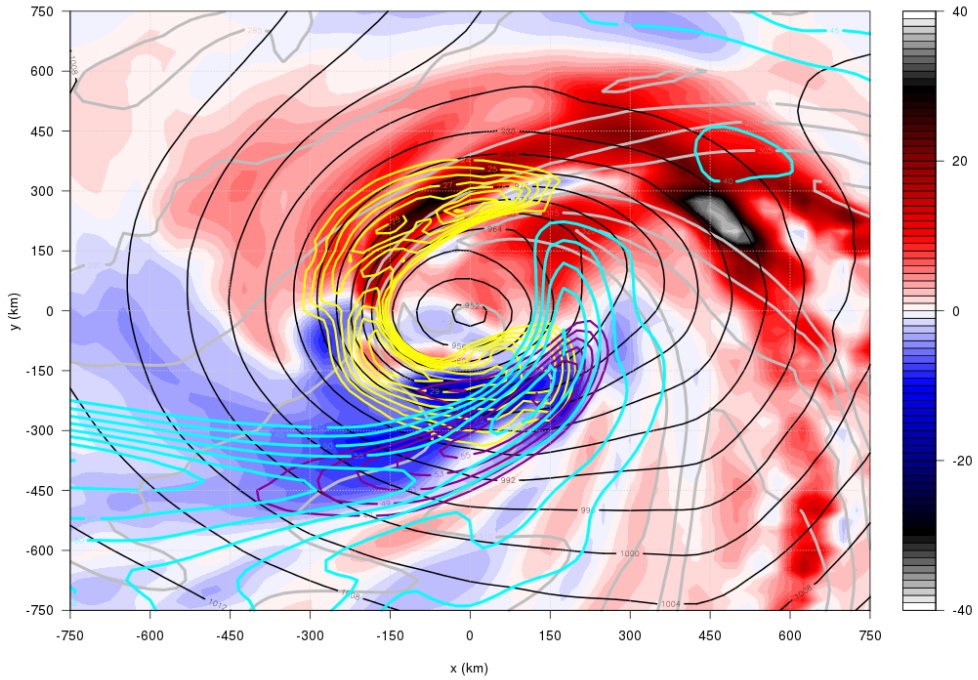

Figure 5.22: Same as Figure 5.21 for future strom 7UK at 18hours before t_0.

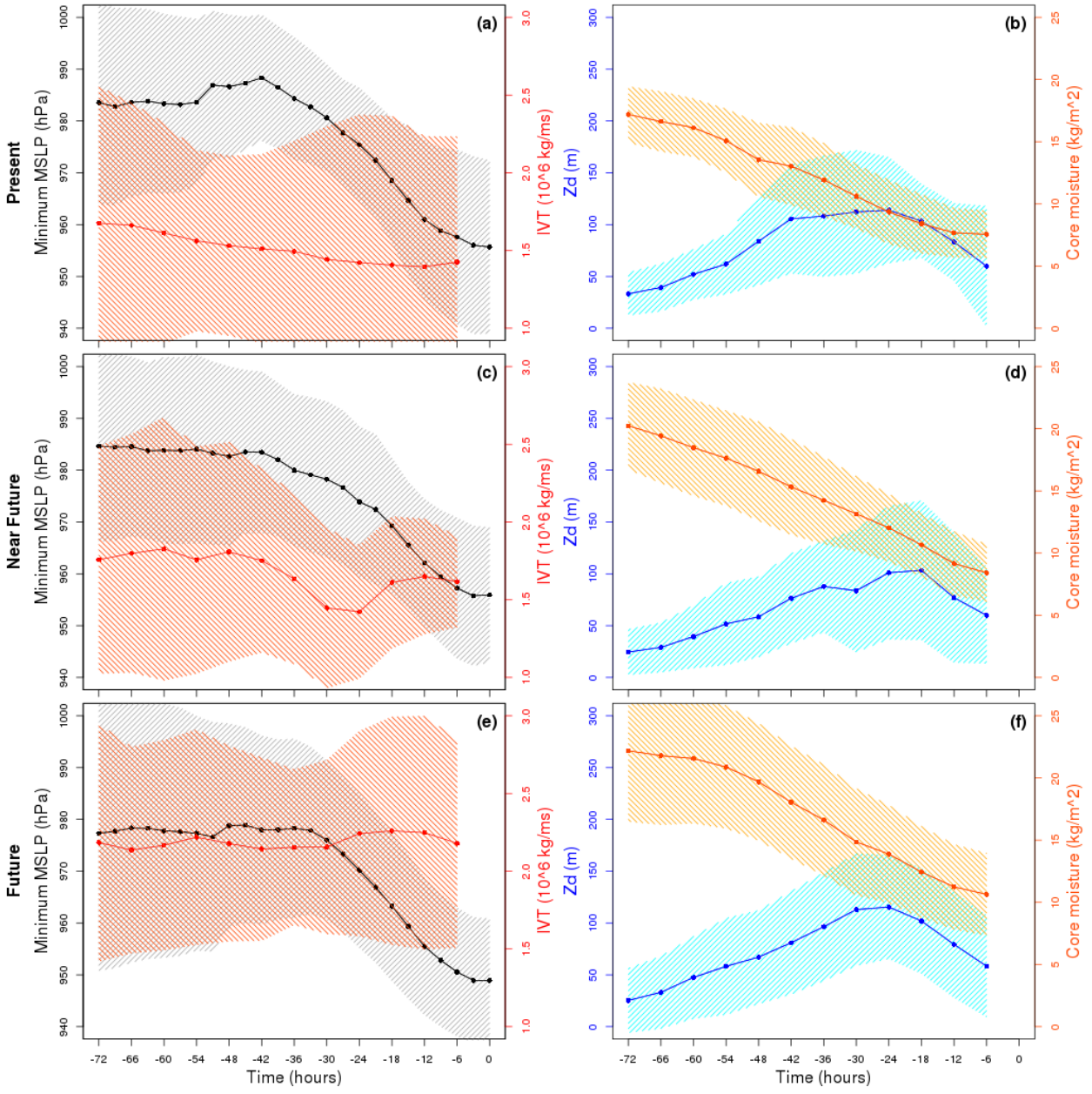

Figure 5.23: IVT (red), central MSLP (black), Z_d (blue) and Q_c (orange) during the last 72 hours before t_0 for all post-tropical cyclones in the present (a,b), near future (c,d) and future (e,f) climate. Hatching indicates the variance for each variable within the respective subset of storms.

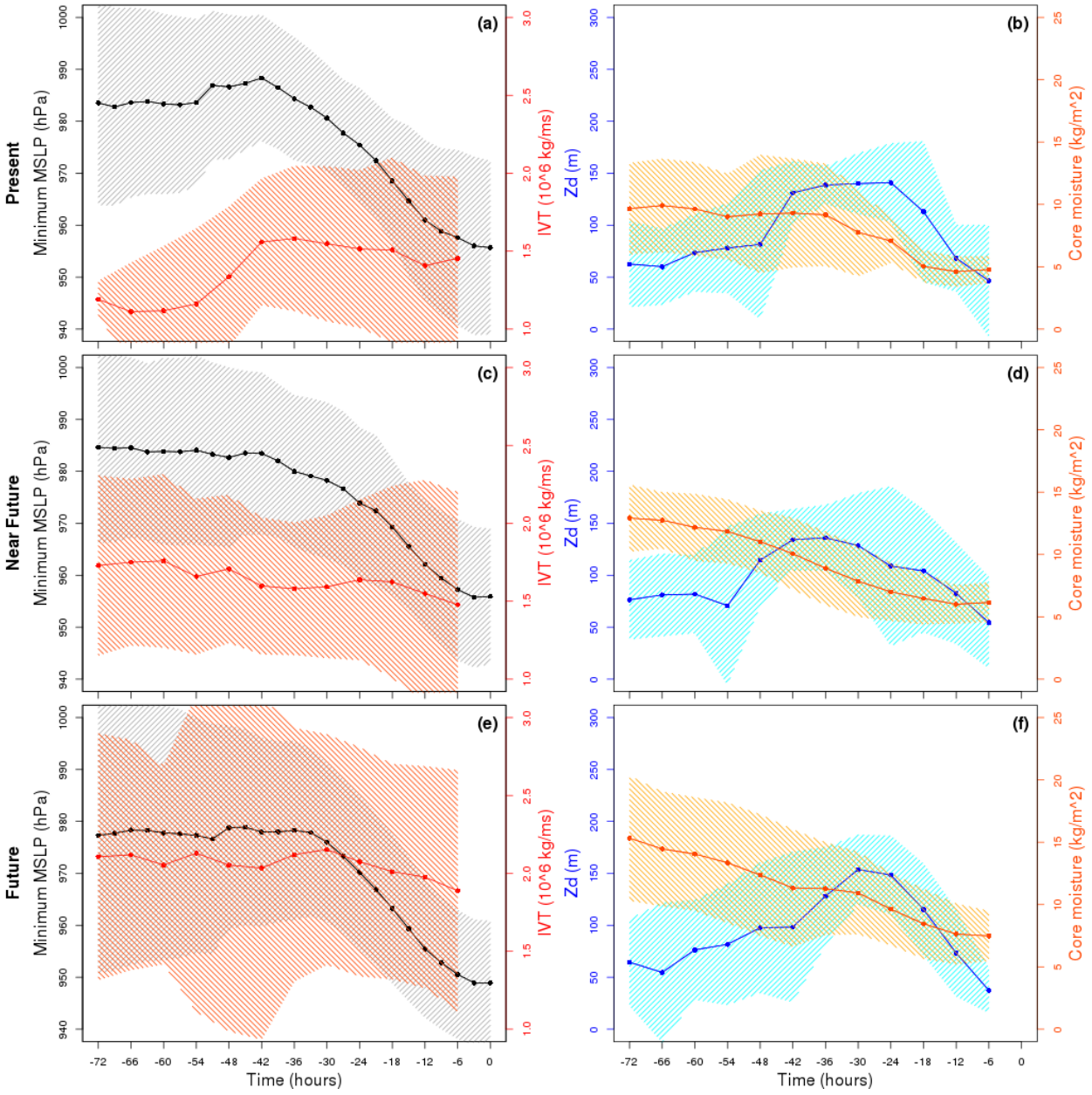

Figure 5.24: Similar to 5.23 but for extratropical cyclones.

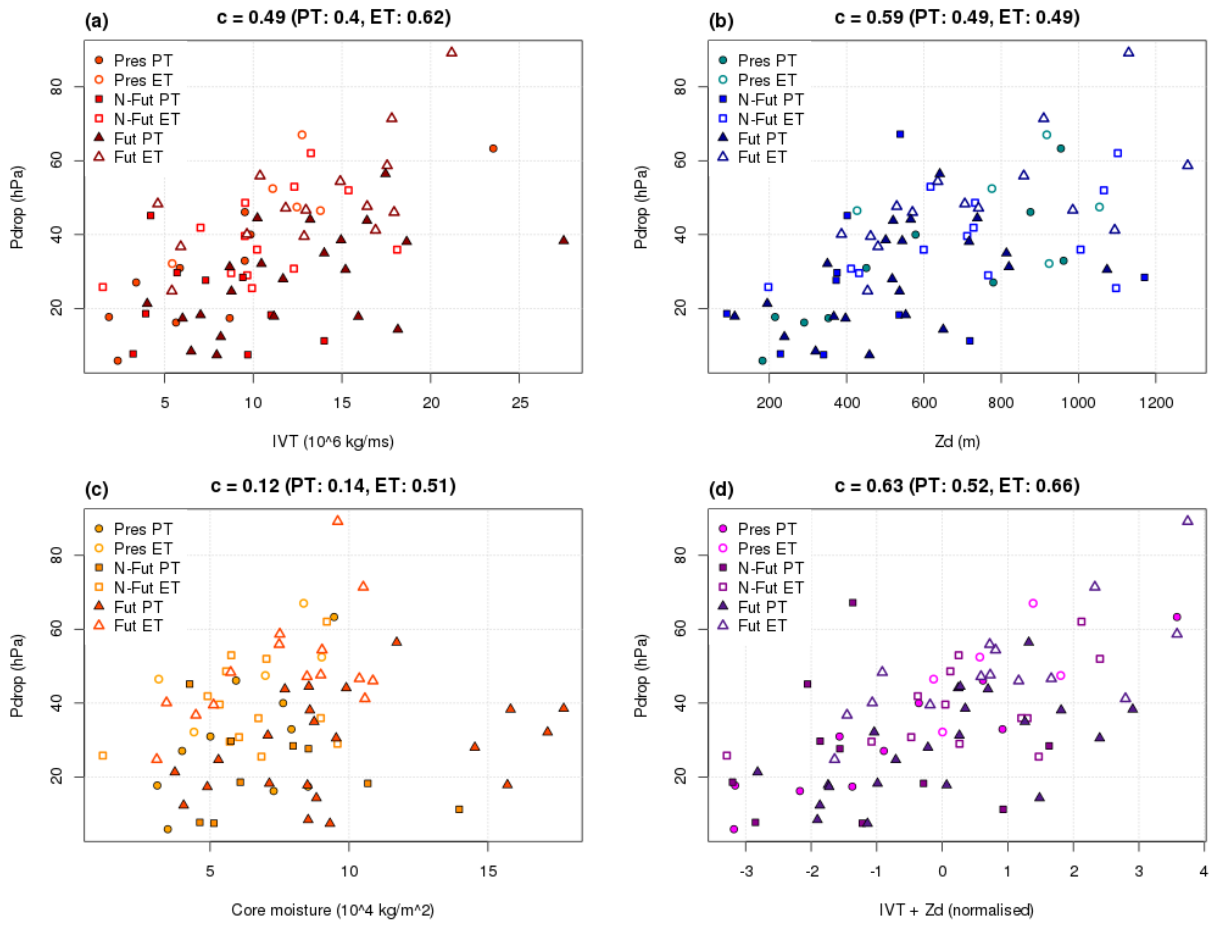

Figure 5.25: Scatter plots of IVT (a), Z_d (b), Q_c (c) and $IVT + Z_d$ (d) with the central pressure drop during the final intensification for all studied storms. Markers distinguish storms of different periods and subsets, the correlation coefficient for all, PT and ET cyclones is given above each panel.

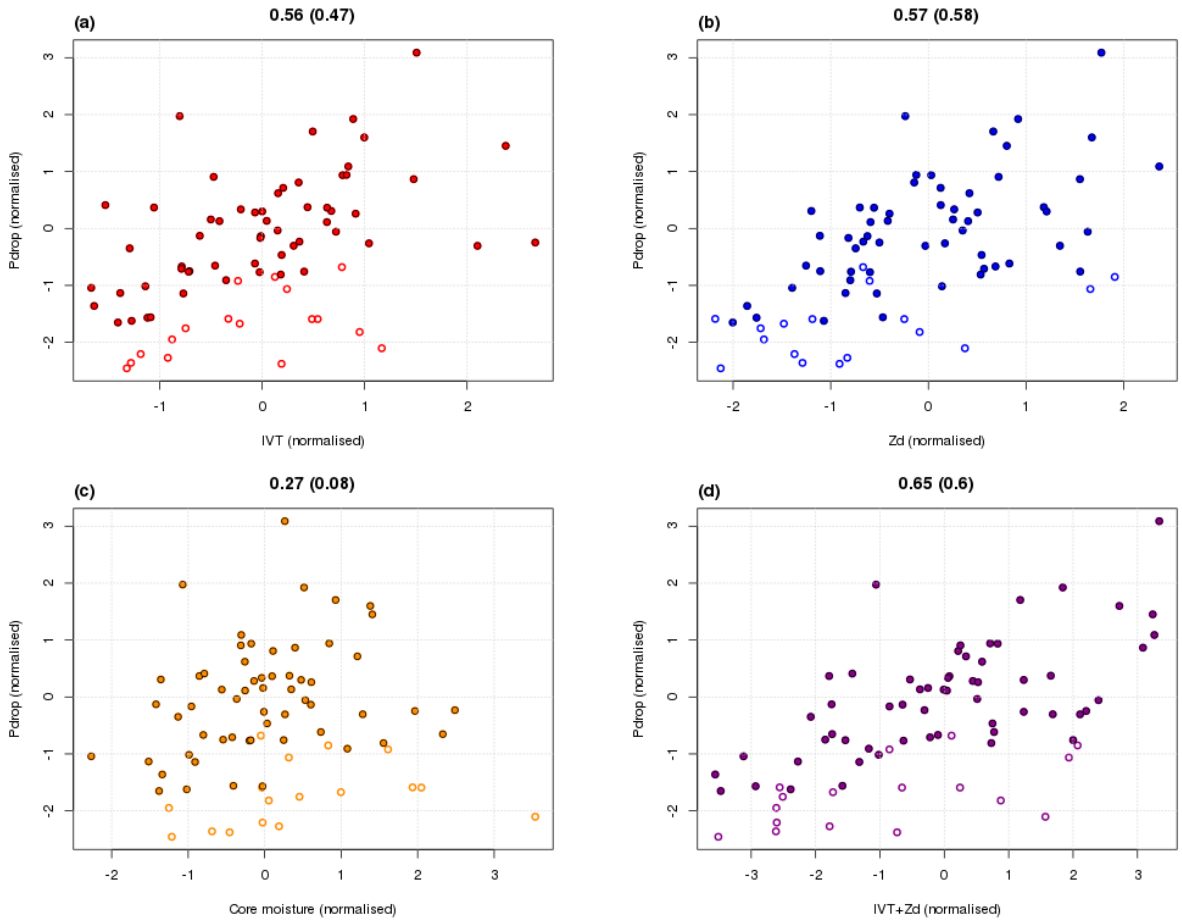

Figure 5.26: Scatter plots of IVT (a), Z_d (b), Q_c (c) and $IVT + Z_d$ (d) with the central pressure drop during the final intensification for all studied storms. Filled markers denote cyclones that meet the rapid intensification criterion (2hPa/3h) while open markers indicate those that do not. Correlations are given above each panel for all rapidly intensifying storms along with those for all storms between brackets.

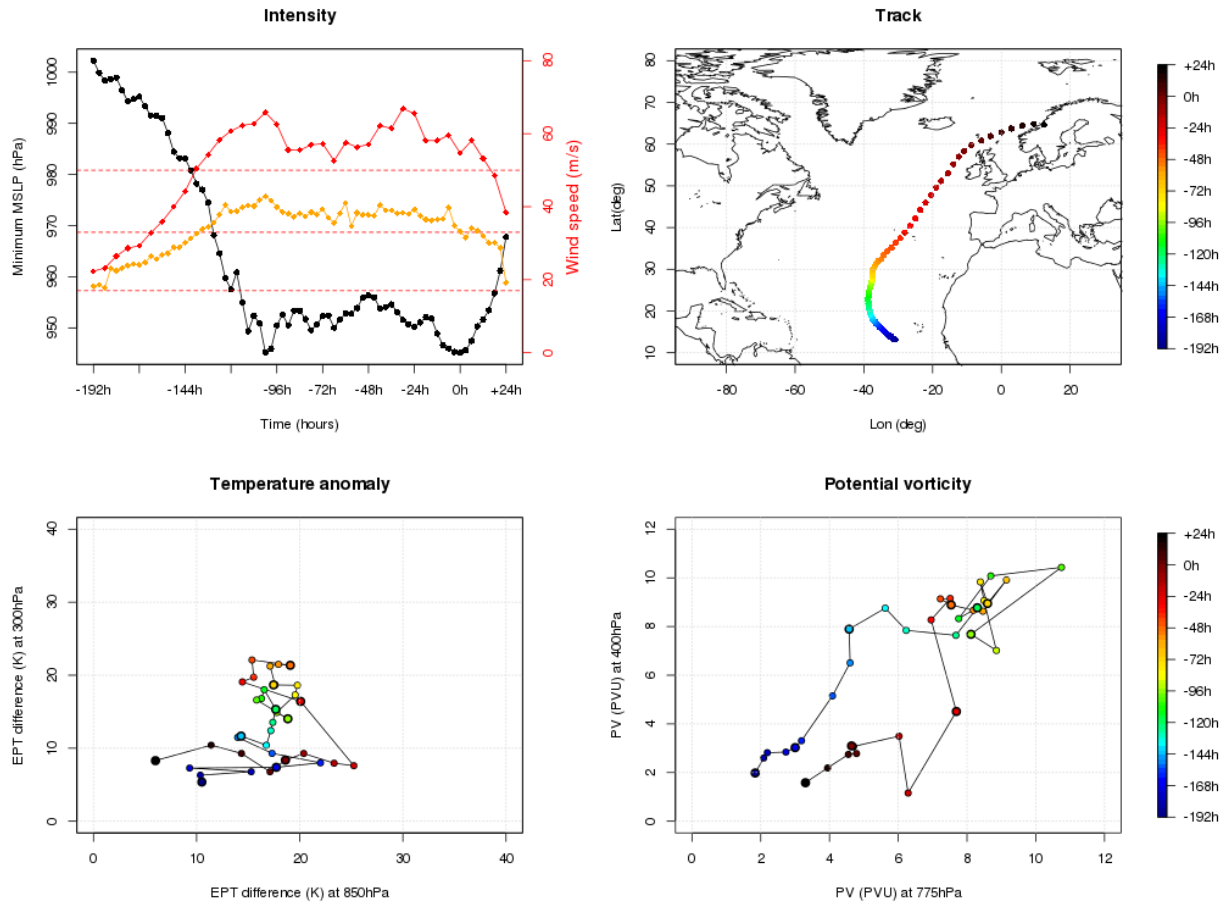

Figure 5.27: Intensity (Minimum MSLP in black, 10m wind speed in orange and 850hPa wind speed in red), track and both parts of the phase space analysis for Amy. Colour fills indicate the time relative to t_0 in hours and in the phase space diagrams thick markers denote 24 hour periods.

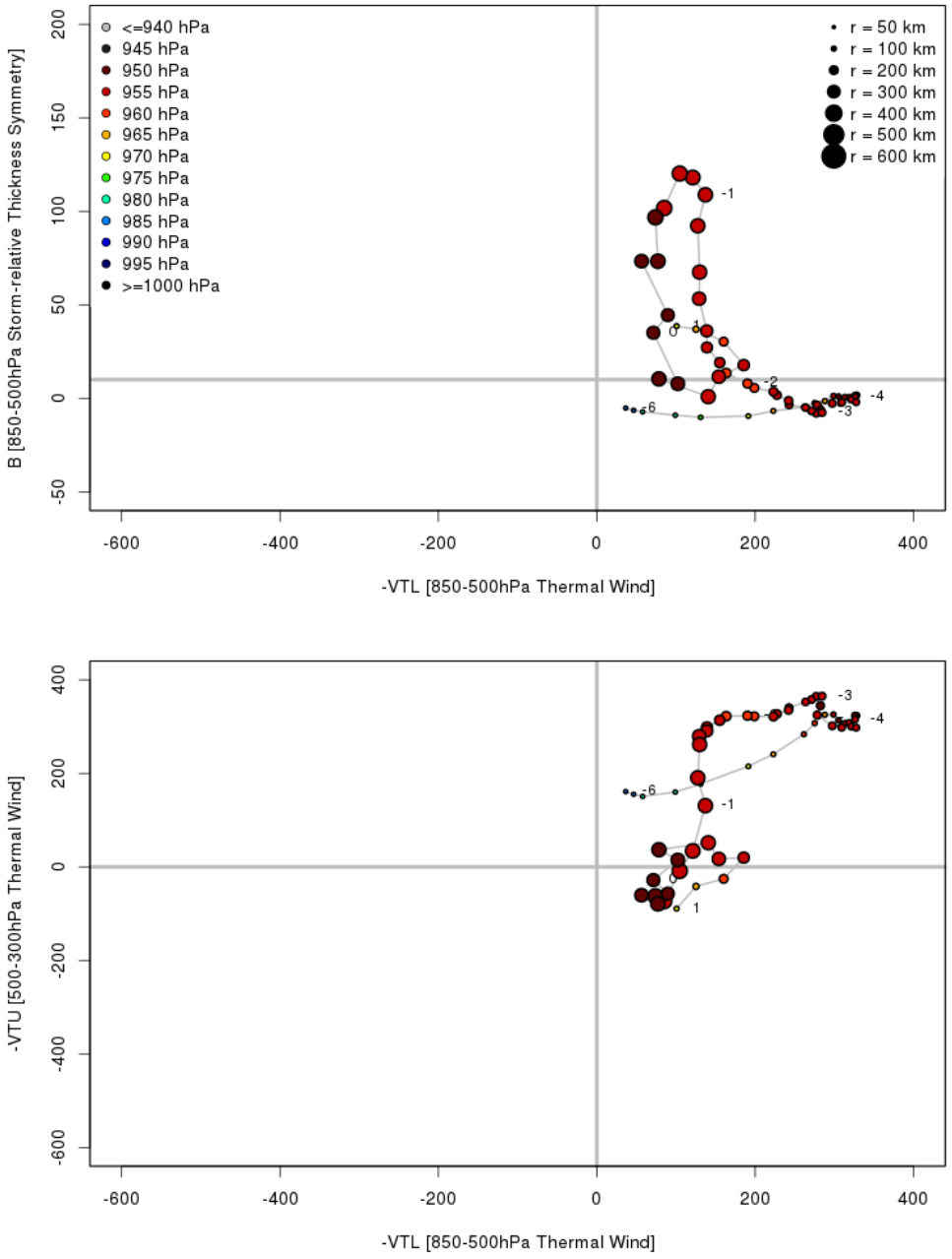

Figure 5.28: Hart diagram of near future storm 5UK, similar to Figure 4.2.

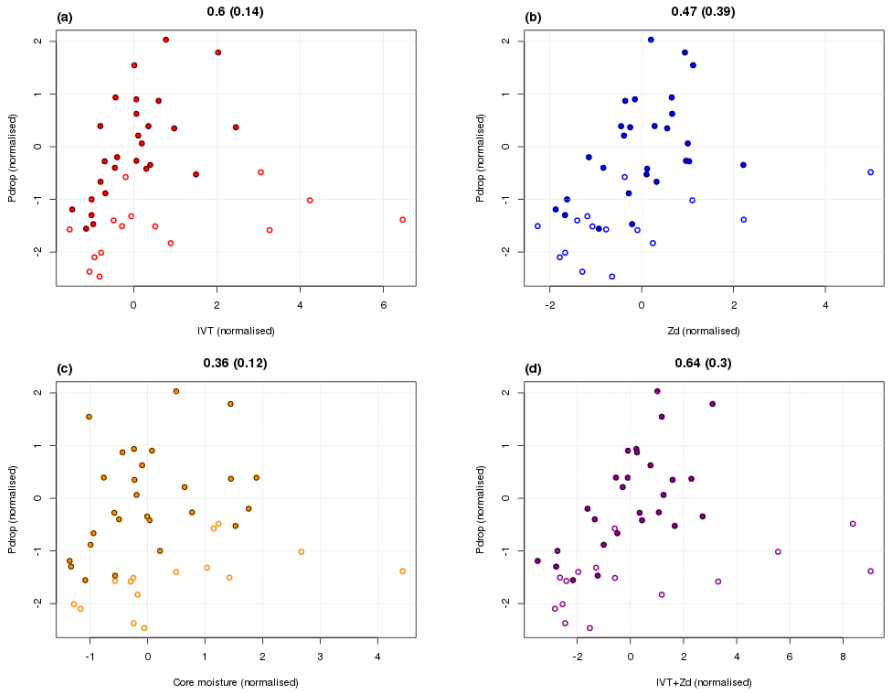

Figure 5.29: Similar to Figure 5.26 but for PT cyclones.

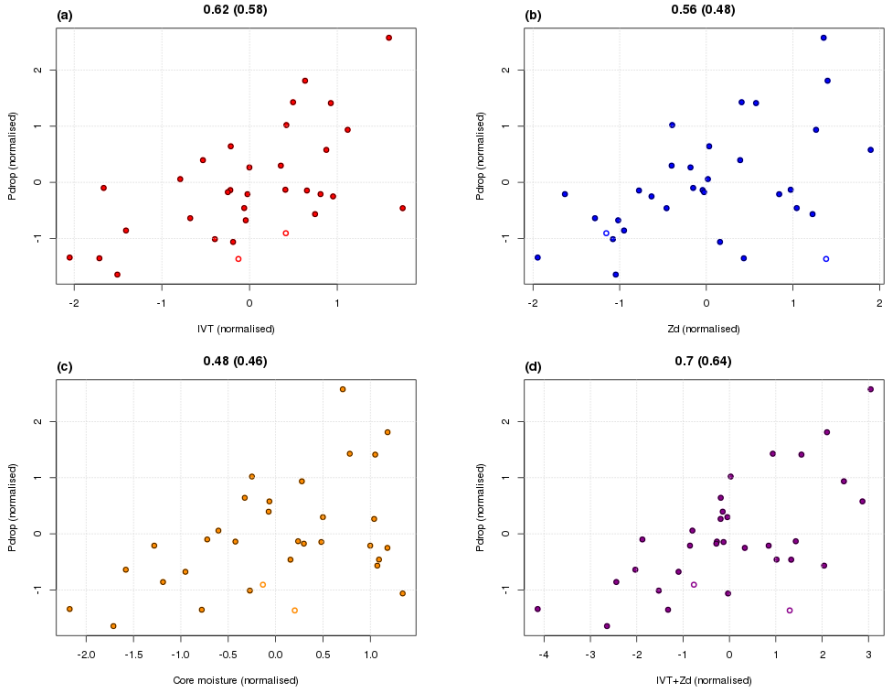

Figure 5.30: Similar to Figure 5.26 but for ET cyclones.

Chapter 6

Observational data

6.1 IBTrACS

The International Best Track Archive for Climate Stewardship (IBTrACS) is an initiative of the NOAA's National Climatic Data Center to generate a freely available data set of international tropical cyclone best track data (http://www.ncdc.noaa.gov/ibtracs/). Among the information for each storm are its track, 10m sustained wind speed, central pressure and some characteristics (such as tropical, subtropical or extratropical). Most storms are ceased to be tracked when they weaken beyond the tropical depression criteria or become extratropical. This poses some limitations on the use of this data but still provides a good indication of how many cyclones reach Europe and how. The same four regions as those used in the previous analyses (Biscay, Norway, North Sea and Western UK) are considered to select tracks of storms impacting Western Europe. This was done to create Figure 1.1 which was given in the introduction, where storms occurring in the 1981-2010 period are indicated by coloured markers. The IBTrACS data set goes back as far as 1851, cyclone tracks entering one of the selection regions before 1981 are represented by the black lines. Prior to the satellite era, the coverage is clearly much worse but the complete set of storms shows that some more easterly tracks are also possible.

When comparing the observed tracks to those selected from the present simulations (Figure 4.1b), the former clearly contains a lot more storms. No considerations have been made so far on the strength of storms when they reach Europe. A major part of them may be dissipating in the final stage so only those systems that have wind speeds of at least 50 knots (storm force) are now selected (6.1). The tracks of the 9 remaining storms agree well to those seen in the present simulations apart from a westward shift. This may simply be inter annual variability but can also be due to the fact that only the last part of the observed period is represented in the simulations. In general, cyclones generated by the model look quite realistic in terms of numbers and tracks (when only considering PTCs).

6.2 MERRA reanalysis

An important finding was the development of a warm seclusion in most of the studied storms. To check whether this is common among observed cyclones as well, their structure using the Modern Era Retrospective-analysis for Research and Applications (MERRA)is investigated. This reanalysis data set is freely available at the NASA Goddard Earth Sciences Data and Information Services Cen-

ter (http://disc.sci.gsfc.nasa.gov/daac-bin/DataHoldings.pl). Data is presented at a relatively high horizontal resolution of 1/2°latitude by 2/3°longitude on 42 pressure levels at 6-hourly intervals. Hourly data is also provided for surface values and several discrete pressure levels such as 850hPa. A set of storms is again generated by checking when a certain wind criterion (10m hourly wind $>$22.5m/s) is met in one of the four European regions (also for the 1981-2010 period). These storms are tracked back in time using 1 hourly MSLP and 10m wind data to consider only those with a tropical origin (Figure 6.2). The number of storms is again comparable to the results for present simulations but tracks in the central Tropical Atlantic are almost non-existent. The resolution of the reanalysis data set is still too coarse to accurately represent tropical cyclones making it hard to trace them back towards the tropics. Nevertheless, the data is very useful to study storms during their final stages and precise tracks can already be found in the IBTrACS database.

To compare the structure of observed storms to those that are simulated, the average EPT, MSLP and wind speed are determined for each storm at the time of minimum central pressure. The results are extrapolated on an equidistant grid and averaged over the 10 strongest storms (out of 15). All of the individual storms develop a warm seclusion (not shown) but when selecting the strongest ones, a familiar picture appears (Figure 6.3). A distinct warm core is almost separated from the warm conveyor belt by a dry intrusion wrapping around it. At the end of the associated back bent front, a maximum of the wind speed is present at 10m and especially at 850hPa. The centre is also located at the left exit region of a jet streak and the presence of a sting jet in some of the storms is suggested. This confirms that also in the present climate, severe Autumn storms with a tropical origin are generally warm seclusion cyclones. In agreement to the model results, their impacts are mainly located away from the European mainland (Figures 4.1b and 6.2).

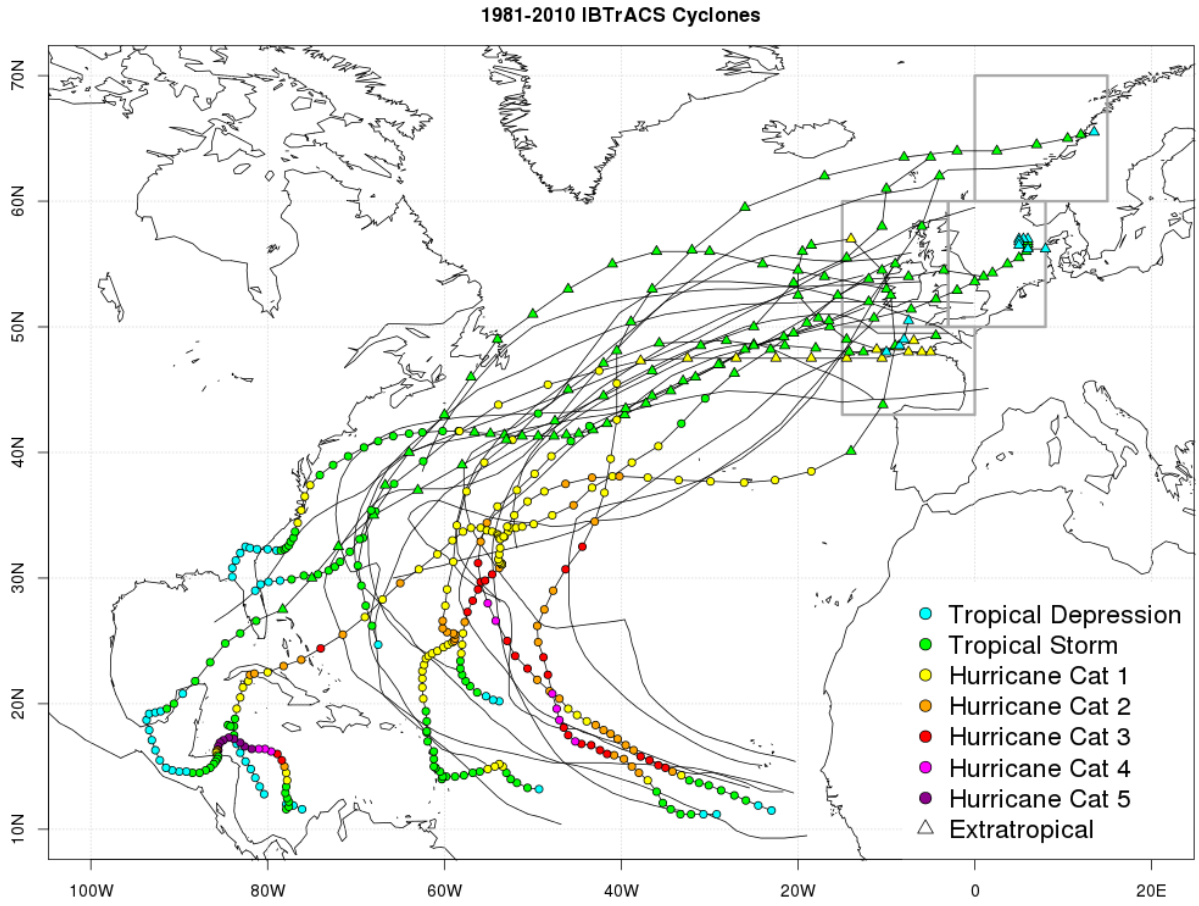

Figure 6.1: Cyclones in the IBTrACS database impacting Western Europe in (markers) and before (lines) the 1981-2010 period and generating at least 50kt wind speeds in the indicated regions.

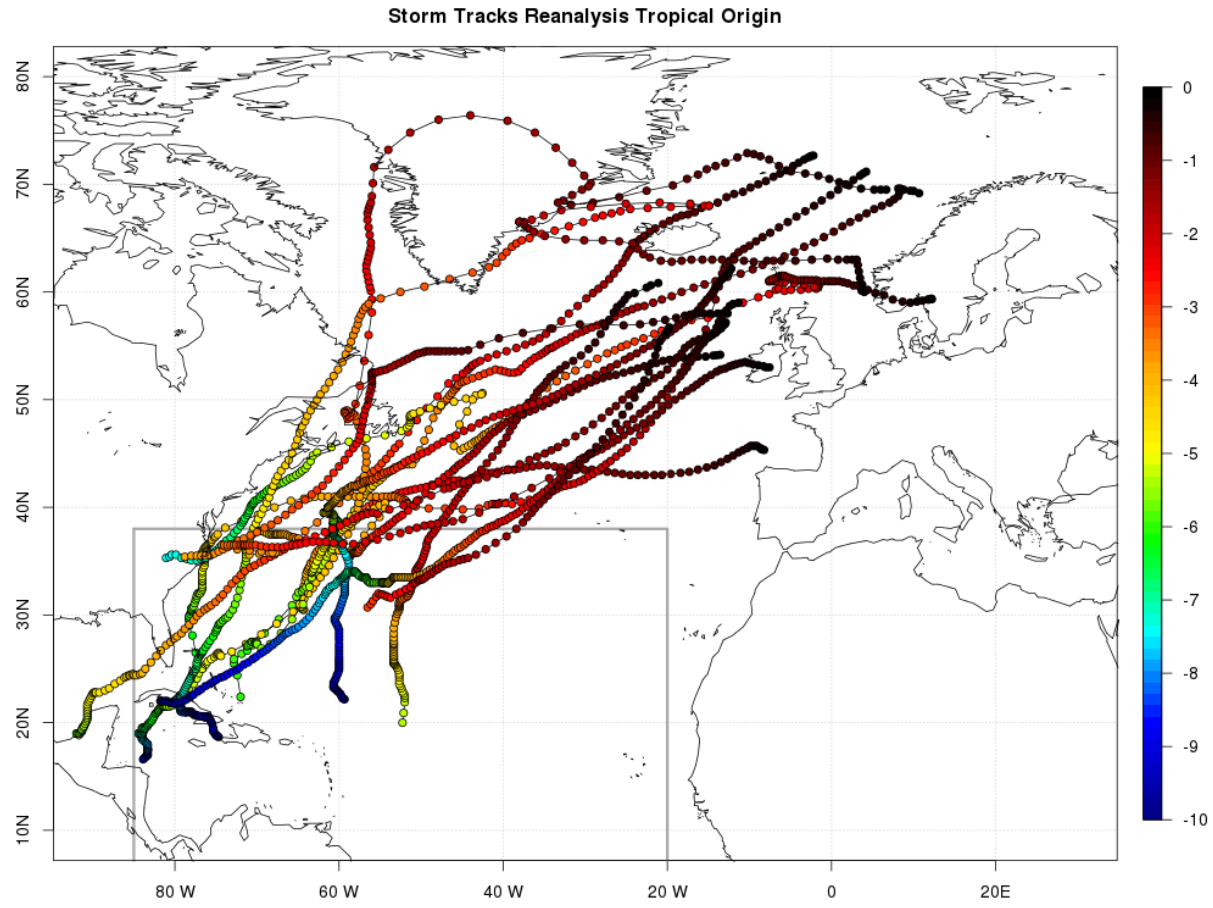

Figure 6.2: Tracks of cyclones originating in the tropics (gray box) and impacting Western Europe in Autumn with at least 22.5m/s hourly 10m wind speeds. The time relative to this wind measurement is indicated by the colour scale in days.

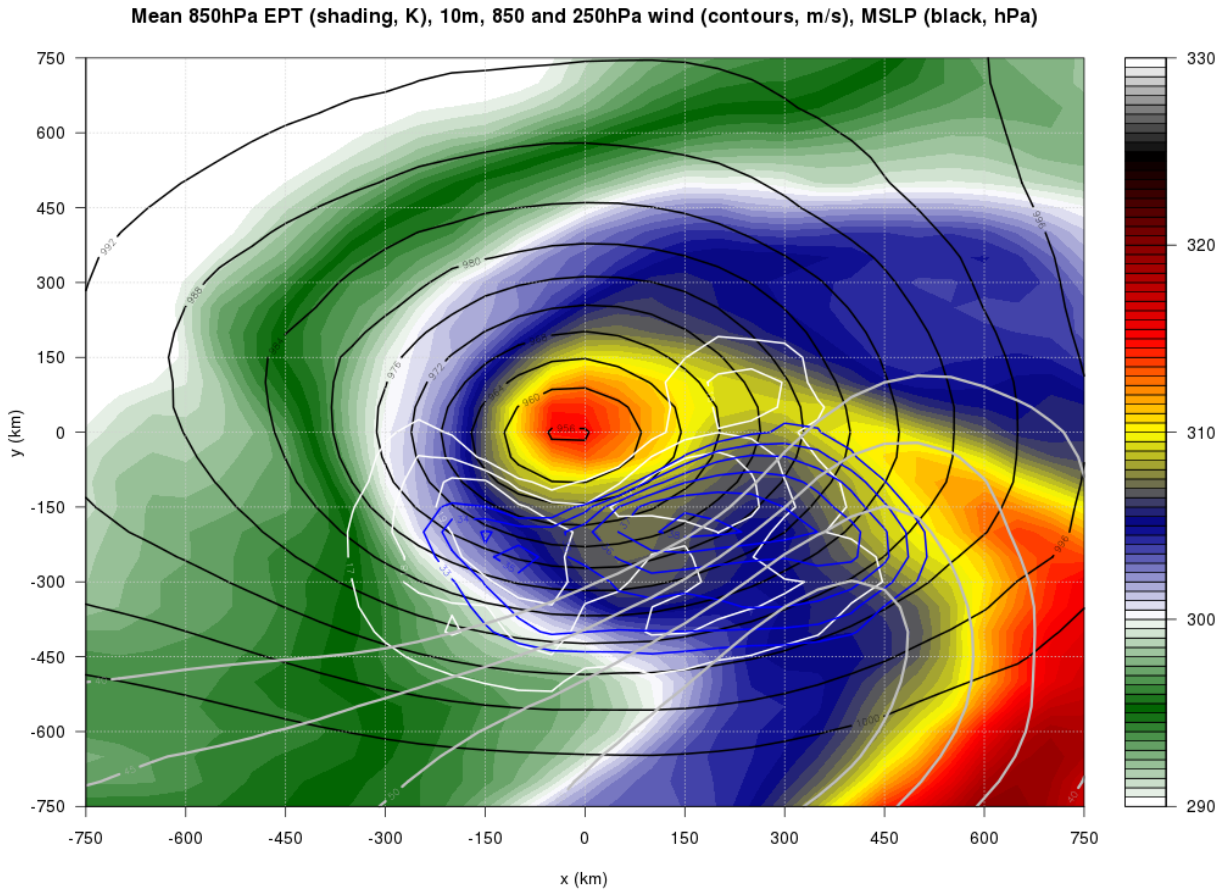

Figure 6.3: Mean 850hPa EPT (shading, K), MSLP (black,hPa) and horizontal wind speed (white: 10m, blue: 850hPa and gray: 250hPa) for the 10 strongest selected storms using MERRA reanalysis data.

Chapter 7

Conclusions

In a warmer future climate, Western Europe will see increased impacts from severe Autumn storms. Not only will they become stronger, they will also occur more frequently while affecting a larger area. The detailed case of Amy is indicative for such intense cyclones, bringing forth high wind speeds and excessive precipitation. An important finding is the fact that most of the studied storms develop a warm seclusion during their final intensification. Common winter storms in the Northern Atlantic are typically occluded systems as described by the Norwegian model and resembling the LC2 cyclone of *Schultz et al.* (1998). Also in observations, the strongest Autumn storms are found to be of the LC1 type forming a warm seclusion. This is confirmed by looking at the average EPT and wind structure of the storms, featuring a warm core that is encircled by cold, dry air and a nearby wind maximum. The latter is located at the end of the back bent front and associated with the formation of a sting jet. The wind maximum is related to parallel flow at higher levels and vertical exchange of momentum. This pattern becomes more pronounced in the future, suggesting sting jets will occur more frequently and/or be more intense.

Not all of the studied storms originate as tropical cyclones that undergo extratropical transition and re-intensify into warm seclusion storms. Some of them form in regions that are only marginally favourable for tropical development and never evolve into a mature tropical cyclone. Some of them are even deep cold core systems forming as a baroclinic wave in the polar jet stream before moving over warm waters. In both observations and simulations of the present climate, most storms are post-tropical systems but this changes in the next few decades. The near future simulations show a large increase in storms with an extratropical origin. This is partly caused by an increase in the temperature gradient between the warm tropical Atlantic and the cold Labrador Current. The northward expansion of the warm pool expands the hurricane genesis region and decreases the area separating it from conditions that are favourable for baroclinic development. This allows more storms to originate in this area but also eases the traverse of weaker systems thus increasing their chance of reaching Europe. These processes wane in the future climate as the polar front moves further north and the Labrador current retreats. A continued warming of the tropics, however, causes the hurricane genesis region to expand considerably and sustain the development of stronger cyclones. Now forming further east, such cyclones can also cross the transit region more easily and have a higher chance of curving towards Europe. In summary, the near future is mainly characterised by an increase of extratropical storms while for the near future more post-tropical cyclones occur and become stronger. The northward and eastward expansion of their genesis region results in a similar shift of the affected area (in both the near future and future climate). The general patterns and changes in storm tracks that are observed for the simulated results

are sketched in Figure 7.1.

Both baroclinic instability and atmospheric rivers are of great importance during the re-intensification of the studied storms. The former initiates the extratropical development while the latter provides warm and moist air that enhances latent heat release in the newly formed warm core thus speeding up the intensification. Especially for tropical cyclones, atmospheric rivers are often already present beforehand, suggesting that they have an important role in the process. Core moisture appears to be unimportant as a cyclone has to loose its warm core to complete the ETT and re-intensify strongly. In fact, some storms sustain their warm core while becoming asymmetric but without much change in strength. These storms are hybrid in nature, exhibiting the dangers of both tropical and extratropical systems just like Hurricane Sandy of 2012. During the ETT, all cyclones have hybrid properties as their warm core becomes embedded into a frontal system. Towards the future, tropical cyclones become more intense resulting in longer transitions during which they can induce very large rainfall amounts. The strength of atmospheric rivers overall increases greatly, resulting in more intense storms that carry more moisture. To conclude, it can be said that tropical air will have a greater impact on future European weather through severe Autumn storms.

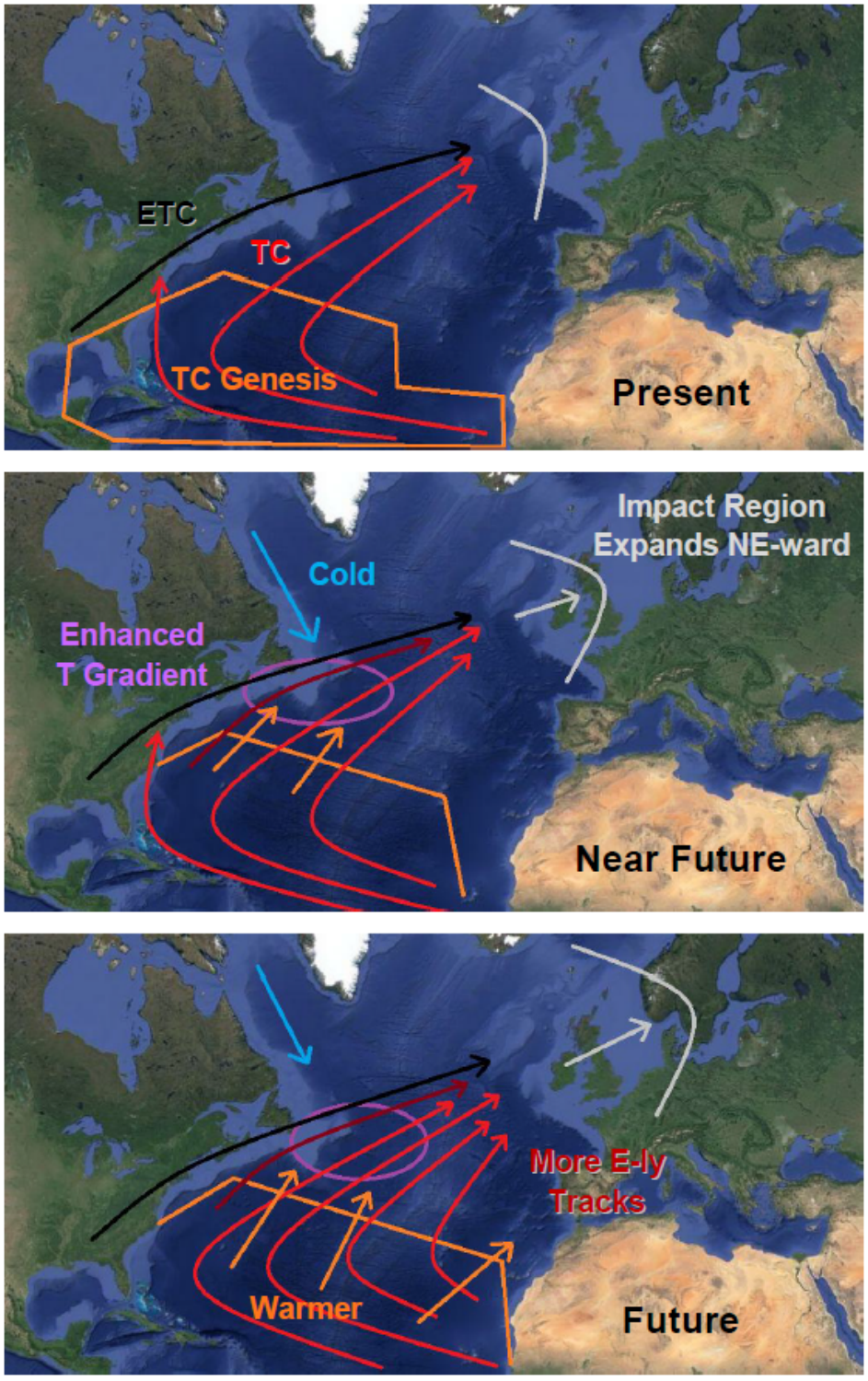

Figure 7.1: Schematic overview of the general changes in severe Autumn storms impacting Western Europe between simulations of the present, near future and future climate.

List of acronyms

- DT: EPT difference between the core and the minimum found in the south-east quadrant of a storm
- $DT_{850,max}$ maximum EPT difference in a cyclone at 850hPa
- EPT: equivalent potential temperature (θ_e)
- EOF: empirical orthogonal function
- ETC: extratropical cyclone
- ETT: extratropical transition
- IVT: integrated vapour transport
- MSLP: mean sea level pressure
- P_{min}: minimum MSLP of a cyclone
- PT: potential temperature (θ)
- PTC: post-tropical cyclone
- PV: potential vorticity
- PVU: potential vorticity units (10^6 Km^2/kgs)
- Q_c: total amount of core moisture in a cyclone
- RV: relative vorticity (ζ)
- SST: sea surface temperature
- TC: tropical cyclone
- $V_{10,max}$: maximum 10m wind speed found within 20 grid boxes of the centre of a storm
- Z_d: storm relative thickness asymmetry of the 850-300hPa layer (750km)

References

Agusti-Panareda, A., C. D. Thorncroft, G. C. Craig, and S. L. Gray (2004), The extratropical transition of hurricane irene: A potential vorticity perspective, *Q. J. R. Met. Soc.*, *130*, 1047–1074.

Baker, L. (2009), Sting jets in severe northern european wind storms, *Weather*, *64*, 143–148.

Bengtsson, L., K. I. Hodges, and E. Roeckner (2006), Storm tracks and climate change, *Journal of Climate*, *19*, 3518–3543.

Bengtsson, L., K. I. Hodges, and N. Keenlyside (2009), Will extratropical storms intensify in a warmer cimate?, *Journal of Climate*, *22*, 2276–2301.

Bjerknes, J. (1919), On the structure of moving cyclones, *Geofys. Publ.*, *1*, 1–8.

Bjerknes, J., and H. Solberg (1922), Life cycle of cyclones and the polar front theory of atmoshperic circulation, *Geofys. Publ.*, *3*, 1–18.

Bolton, D. (1980), The computation of equivalent potential temperature, *Mon. Wea. Rev.*, *108*, 1046–1052.

Browning, K. A. (2004), The sting at the end of the tail: Damaging winds associated with extratropical cyclones, *Q. J. R. Met. Soc.*, *130*, 375–399.

Dorland, C., R. S. J. Tol, and P. Palutikof (1999), Vulnerability of the netherlands and northwest europe to storm damage under climate change, *Climatic Change*, *43*, 513–535.

Gitelman, A. I., J. S. Risbey, R. E. Kass, and R. D. Rosen (1997), Trends in the surface meridional temperature gradient, *Geophys. Res. Lett.*, *24*, 1243–1246.

Haarsma, R. J., W. Hazeleger, C. Severijns, H. de Vries, A. Sterl, R. Bintanja, G. J. van Oldenborgh, and H. W. Van den Brink (2013), More hurricanes to hit western europe due to global warming, *Geophys. Res. Lett.*, *40*, 1–6.

Hart, R. E. (2003), A cyclone phase space analysis derived from thermal wind and thermal asymmetry, *Mon. Wea. Rev.*, *131*, 585–616.

Hazeleger, W. e. a. (2010), Ec-earth: A seamless earth-prediction approach in action, *Bull. Amer. Met. Soc.*, *91*, 1357–1363.

Hoskins, B. J. (1990), *Theory of extratropical cyclones.*, 63-80 pp.

Hoskins, B. J., A. J. Simmons, and D. G. Andrews (1997), Energy dispersion in a barotropic atmosphere, *Q. J. R. Met. Soc.*, *103*, 553–567.

Jones, S. C. e. a. (2003), The extratropical transition of tropical cyclones: Forecast challenges, current understanding, and future directions, *Weather Forecasting*, *18*, 1024–1092.

Lambert, S. J., and J. C. Fyfe (2006), Changes in winter cyclone frequencies and strengths simulated in enhanced greenhouse warming experiments: Results from the models participating in the ipcc diagnostic exercise, *Climate Dynamics*, *26*, 713–728.

Lavers, D. A., R. P. Allen, G. Villarini, B. Lloyd-Hughes, D. J. B. Brayshaw, and A. J. Wade (2013), Future changes in atmospheric rivers and their implications for winter flooding in britain, *Envir. Res. Lett.*, *8*.

Leckebusch, G. C., and U. Ulbrich (2004), On the relationship between cyclones and extreme wind events over europe under climate change, *Glob. Plan. Change*, *44*, 181–193.

Loptien, U., O. Zolina, S. Gulev, M. Latif, and V. Soloviov (2008), Cyclone life cycle characteristics in the northern hemisphere in coupled gcms, *Climate Dynamics*, *31*, 507–532.

Lorentz, D. J., and E. T. De Weaver (2007), Tropopause height and zonal wind response to global warming in the ipcc scenario integrations, *Journal of Geophys. Res.*, *112*.

Maue, R. N. (2010), *Warm Seclusion Extratropical Cyclones*, Florida State University.

Newton, C. W. (1954), Frontogenesis and frontolysis as a three-dimensional process, *Journal of Meteorology*, *11*, 449–461.

Orlanski, I., and J. P. Sheldon (1995), Stages in the energetics of baroclinic systems, *Tellus*, *47*, 605–628.

Schultz, D. M., D. Keyser, and L. F. Bosart (1998), The effect of large-scale flow on low-level frontal structure and evolution in midlatitude cyclones, *Mon. Wea. Rev.*, *126*, 1767–1791.

Schwierz, C., P. Köllner-Heck, E. Z. Mutter, D. N. Bresch, P. Vidale, M. Wild, and C. Schär (2009), Modelling european winter storm losses in current and future climate, *Climatic Change*, *101*, 485–514.

Shapiro, M. A. (1999), *A planetary-scale to mesoscale perspective of the life cycloes of extratropical cyclones*, 139-186 pp., *The life cycles of extratropical cyclones*, M. A. Shapiro and S. Grønås, Eds., Amer. Met. Soc., Boston.

Shapiro, M. A., and D. Keyser (1990), *Fronts, Jet Streams, and the Tropopause*, 167-191 pp., *Extratropical cyclones, the Erik Palmeén Memorial Volume*, C. W. Newton and E. O. Holopainen, Eds., Amer. Met. Soc., Boston.

Sterl, A., et al. (2008), When can we expect extremely high surface temperatures?, *Geophys. Res. Lett.*, *35.14*.

Uccellini, L. W., D. Keyser, K. F. Brill, and C. H. Wash (1985), The president's day cyclone of 18-19 february 1979: influence of upstream trough amplification and associated tropopause folding on rapid cyclogenesis, *Mon. Wea. Rev.*, *113*, 962–988.

Ulbrich, U., J. G. Pinto, H. Kupfer, G. C. Leckebusch, T. Spangehl, and M. Reyers (2008), Changing northern hemisphere storm tracks in an ensemble of ipcc climate change simulations, *Journal of Climate*, *21*, 1669–1679.

van Delden, A. (1989), On the deepening and filling of balanced cyclones by diabatic heating, *Met. Atmos. Phys.*, *41*, 127–145.

van Vuuren, D. P. e. a. (2011), The representative concentration pathways: an overview, *Climatic Change*, *109*, 5–31.

Zhu, Y., and R. E. Newell (1998), A proposed algorithm for moisture fluxes from atmospheric rivers, *Mon. Wea. Rev.*, *126*, 725.